Naval Surface Warfare Center
Carderock Division
West Bethesda, MD 20817-5700

An Examination of a Subsurface Impact on a Floating Ice Sheet

by

Judy A. Conley

19980303 131

DTIC QUALITY INSPECTED 3

DEPARTMENT OF THE NAVY

NAVAL SURFACE WARFARE CENTER, CARDEROCK DIVISION
9500 MACARTHUR BOULEVARD
WEST BETHESDA MD 20817-5700

9020
Ser 65-105
5 Nov 97

From: Commander, Naval Surface Warfare Center, Carderock Division

Subj: SUBMARINE PENETRATION OF ICE FLOES

Encl: (1) NSWCCD-TR-65–97/37, *An Examination of a Subsurface Impact on a Floating Ice Sheet*

1. Enclosure (1) examines the influence that various parameters impose on the structural dynamics of a floating ice sheet due to the initial impact of a submarine.

2. Comments or questions may be referred to the author, Dr. Judy A. Conley, Code 654; telephone (301) 227-1658; e-mail, conleyj@oasys.dt.navy.mil.

J/E. BEACH
By direction

Distribution:

COMNAVSEASYSCOM WASHINGTON DC
  [PEO-USW-ASTO-E4 (Stock), SEA 03P2 (Will),
  SEA 03W14 (Shea)]

COMSUBLANT NORFOLK VA [N019A (Lewis)]

COMSUBPAC PEARL HARBOR HI
  [N3151 (Campbell)]

COMSUBDEVRON FIVE, DET ASL [Bentley]

US ARMY CORPS OF ENGINEERS
COLD REGIONS RESEARCH AND ENGINEERING
  LABORATORY
72 LYME ROAD
HANOVER NEW HAMPSHIRE 03755

DTIC FORT BELVOIR VA

NAVSURFWARCEN CARDEROCKDIV
  BETHESDA MD [Codes 3442 (TIC), 60 (w/o encl),
  65, 65R (2), 651, 652, 653, 654,
  654 (Conley, 5 copies), 655]

DTIC QUALITY INSPECTED 3

Naval Surface Warfare Center
Carderock Division
West Bethesda, MD 20817-5700

An Examination of a Subsurface Impact on a Floating Ice Sheet

by

Judy A. Conley

Enclosure (1)

REPORT DOCUMENTATION PAGE

Public reporting burden for this collection of information is estimated to average 1 hour per response, including the time for reviewing instructions, searching existing data sources, gathering and maintaining the data needed, and completing and reviewing the collection of information. Send comments regarding this burden estimate or any other aspect of this collection of information, including suggestions for reducing this burden, to Washington Headquarters services, Directorate for Information Operations and Reports, 1215 Jefferson Davis Highway, Suite 1204, Arlington, VA 22202-4302, and to the Office of Management and Budget, Paperwork Reduction Project (0704-0188), Washington, DC 20503.

1. AGENCY USE ONLY (Leave blank)	2. REPORT DATE November 1997	3. REPORT TYPE AND DATES COVERED Final

4. TITLE AND SUBTITLE
An Examination of a Subsurface Impact on a Floating Ice Sheet

5. FUNDING NUMBERS
NA

6. AUTHOR(S)
Judy A. Conley

7. PERFORMING ORGANIZATION NAME(S) AND ADDRESS(ES)
Naval Surface Warfare Center
Carderock Division
9500 MacArthur Boulevard
West Bethesda, MD 20817-5700

8. PERFORMING ORGANIZATION REPORT NUMBER
NSWCCD-TR-65–97/37

9. SPONSORING/MONITORING AGENCY NAME(S) AND ADDRESS(ES)
Naval Surface Warfare Center
Carderock Division
9500 MacArthur Boulevard
West Bethesda, MD 20817-5700

10. SPONSORING/MONITORING AGENCY REPORT NUMBER

11. SUPPLEMENTARY NOTES

12a. DISTRIBUTION/AVAILABILITY STATEMENT
Approved for public release; distribution is unlimited.

12b. DISTRIBUTION CODE

13. ABSTRACT (Maximum 200 words)

An examination is made of the influence that various parameters impose upon the structural dynamics of a floating ice sheet due to the initial impact of a large mass. The Ritz method is employed to formulate a simple shape function to approximate a solution of the plate equation, subsequently used to represent the static displacement, obtain bending stiffness, and appropriate the fundamental frequency by the principle of minimum potential energy. Fluid inertia is incorporated by assuming the mass of a hemispherical volume of fluid, associated with the effective radius of the displaced shape, distributed as a function of the displaced shape of the plate.

A dynamic formulation of a two degree-of-freedom system is made and shown equivalent to two separate one degree-of-freedom systems because of the huge disparity between the two masses due to the fluid inertia influence. Each separate system provides solutions for different issues of the study. An inelastic collision represents the global impact loading influencing the general bending of the ice plate. The local crushing deformation on the underside of the ice plate, found using both a Hertz contact solution and linear approximation, depicts the initial impact force. The influence of parameters for each system is quantified.

14. SUBJECT TERMS ice floe penetration submarines		15. NUMBER OF PAGES 89
		16. PRICE CODE

17. SECURITY CLASSIFICATION OF REPORT UNCLASSIFIED	18. SECURITY CLASSIFICATION OF THIS PAGE UNCLASSIFIED	19. SECURITY CLASSIFICATION OF ABSTRACT UNCLASSIFIED	20. LIMITATION OF ABSTRACT SAR

Contents

Chapter *Page*

Figures

Tables

Administrative Information

Acknowledgments

Chapter 1

Summary

This dissertation characterizes the influence that various parameters impose upon the structural dynamics of a floating ice sheet due to the initial impact of a large mass. A static formulation for an infinite plate supported by an elastic foundation was made based on the elastic theory of plates to represent the floating ice sheet and obtain a spring stiffness associated with bending. The Ritz method was employed to formulate a simple shape function to represent a solution of the plate equation. This simple shape function was then used to obtain the fundamental frequency of the plate-fluid system by the principle of minimum potential energy. The fluid inertia was incorporated in the kinetic energy of the system by assuming the mass of a hemispherical volume of fluid, associated with the effective radius of the displaced shape would be distributed as a function of the displaced shape of the plate. The effective mass of the entire plate-fluid system was then obtained by equating the fundamental frequency to the circular frequency of a single degree-of-freedom spring-mass system.

A dynamic formulation of a two degree-of-freedom system was made with a simplification of the local contact subsystem. This simplification involved a linear approximation for the local crushing behavior of underside of the ice plate due to contact with an impact structure. The assumption that the fluid inertia influence will completely dominate the dynamic behavior of the ice plate, creating a huge disparity between the two masses, lead to effectively splitting the proposed 2 degree-of-freedom spring-mass system into two separate 1 degree-of-freedom systems. Each of these two separate systems provided solutions for different issues of the study.

An inelastic collision between the effective plate-fluid mass and that of the impact structure, a submarine in this study, expressed the global impact loading that influences the general bending of the ice plate. The influence of the local crushing deformation on the underside of the ice plate was found by both a Hertz contact solution, the case of a spherical radius contacting a massive plane surface, and the linear approximation for the single degree-of-freedom spring-mass contact where the plate-fluid system is the ground. The linear approximation served a major role, primarily in facilitating a formulation for the 2 degree-of-freedom system, and, secondarily in providing a step in the indirect comparison of that system to the solitary local contact solution. The Hertz contact provides an effectively softer spring than does the linear approximation. Thus, leading to smaller impact loads and larger deformations. However, this effect would not overcome the extreme contrast in the submarine mass to the plate-fluid mass, especially in an ice thickness exceeding 1 ft.

The global impact load on the ice plate was found to be twice the amount of net buoyancy realized to attain an upward velocity and will most likely be a relatively small value. In addition, the time between the impact and maximum response is on the order of hours for an ice thickness exceeding 2 ft. The global impact load on the ice plate would not appear to have an effect on the flexural failure mechanism that may define the requirements to penetrate a floating ice sheet.

The initial impact imparted on the submarine and the deformation to the underside of the ice plate are both influenced by five local parameters:

- the initial velocity,
- the submarine mass,
- local Young's modulus,
- the radius of contact, and
- Poisson's ratio.

The influence of both the initial velocity and submarine mass on the impact load is slightly more than on the deformation, for the Hertz contact, however both directly relate to the increase or decrease of these quantities. The local Young's modulus, E_l, and spherical radius of contact, R_s, provide an opposite effect on the impact load as on the deformation. An increase in either one will increase the impact load, however, that same increase will decrease the deformation. Thus, for the initial impact to cause greater damage to the ice with less load imparted on the submarine, E_l and R_s should both decrease. A change of Poisson's ratio from a value of 0.33 to 0.5 provides a difference of less than 7% to either the impact force or the deformation.

Quantitatively, the impact load appears to be substantial, where an increase in velocity will increase that load by a 6/5 power. The deformation imparted on the ice due to an initial impact does not appear to be substantial, especially when compared to an ice thickness that exceeds 2 ft. All in all, the relative advantage of an initial impact is not ascertained with respect to the range of values used in this study.

Chapter 2

Submarine Ice Penetration

The Arctic Ocean has always been a potentially strategic battleground in the eyes of geopoliticians and is also of great interest to most of the world for environmental and economic reasons. Under-ice submarine cruises in the Arctic offer the unique opportunity to collect data otherwise unobtainable and, in some cases, in areas generally inaccessible by other means [Welsh, et al., 1986]. The Arctic region is an ocean covered with plates of ice that vary greatly in size and thickness. Within this canopy of ice, there are occasional gaps of open water, called polynya, which offer the only surface access for a submarine, unless the capability to penetrate the ice surface exists. Submarines can explore the nooks and crannies of the sea beneath the ice canopy and penetrate that canopy to access the upper surface.

The act of surfacing a submarine through an ice sheet involves some amount of dynamic interaction between the two objects. Dane [1993] described "...a jab from below causes one point on the ice sheet to rise, fall and undulate for a moment like the surface of a shaken waterbed. There is a pause and it rises again, this time more powerfully, splits at the top and crumbles to expose the glistening black sail of the *Puffer*." Or, as described by Gellman [1992], "It looked and felt a bit like an upside-down plane crash. ... The ice pitched and heaved on impact and made unnerving sounds of buckling against the hull." Noted in both these accounts is a vertical rise of 30 feet per minute, and where the former description seems to indicate an elastic type collision and the latter suggests a more inelastic event. However, these are both subjective, anecdotal accounts of the surfacing operation, offering no particular quantification of the event. Whereas, establishing a rational, mathematically based account of the initial velocity effect would help to adjust current practice and assist in future design of Arctic capable submarines.

The history of submarines operating in the Arctic region has produced several claimants on various levels for the title of the first under ice exploration and surfacing. As early as 1903, off Newport, Rhode Island, a lake submarine, *Protector*, was noted as the first to cruise under and surface through ice [McLaren, 1981]. As one would expect, pre-Revolutionary Russia conducted early investigations in winter sailing of submarines, a basic concern for a navy regularly faced with ice at most of its principal operating bases. The *Kafal'*, a submarine designed by the U.S. inventor Simon Lake, was sold to the Russians and tested in December 1908. As described by Lieutenant Merkushev, the boat "commenced the first and only sailing, in the entire world of a submarine beneath a solid ice field;" and further, "At surfacing punched through the ice field, bringing up ice on ourselves." In addition, he noted the demonstrated need for material improvements for these maneuvers, one of which was strengthening the conning tower. Additional Soviet literature, the book *Severniy Flot* (*Northern Fleet*), also contains a claim that, in 1937, the *Dekabrist*-class submarine *Krasnogvardeyets* was the first submarine that

"accomplished a successful under-ice sailing." The authors being apparently unaware of the prior claim of a Tsarist boat to this "first" [Babbitt, 1970].

Even western navies have felt the need to explore the Arctic with a submarine beginning in 1930 when Sir Hubert Wilkins contracted to outfit an obsolete U.S. submarine, the 0-12, for a transpolar crossing [Wilkins, 1931]. However, after installing topside runners with plans to glide along the underside of the ice like an upside-down sled and surface in polynya, the submarine got stuck halfway beneath the ice edge and he was never able to complete his agenda. Despite this failed attempt; there was a continuation of interest in submarine operations in the Arctic Ocean. During World War II, a significant number of German submarines, called U-boats, successfully operated along the Soviet Northern Sea Route [ONI Review, 1951] apparently ducking in and out from under the ice as an evasion tactic. From 1946 to 1951 the U.S. Navy committed several submarines to Arctic and marginal sea ice zone operations [NUC, ASL, 1974].

As noted by the *Kefal'* captain following that early ice cruise, hand in hand with this new operation was a need to address specific loads that occur during Arctic surfacing. The German submarines that operated in the Greenland and Kara Seas from 1942 to 1944 were not equipped to work under ice fields and some had returned to port with buckled bows and bent periscopes [Lyon, 1984]. Following the U.S. Navy's initial investigations, the USS *Redfish* (SS-395) was proposed as an experimental submarine for the study of sea-ice mechanics and Arctic warfare [Lyon, 1952]. As a result, the Bureau of Ships designed a hull modification that would permit collision against the underside of the ice canopy. Even though the submarine force commander did not consent to the modification at that time, in 1955 the Technical Assistant to the Chief of Naval Operations recommended that "a submarine be assigned for experimental under-ice operations, particularly as related to future modifications of submarines for ice operations."

The USS *Nautilus* (SSN-571) was outfitted with special sonar and navigation equipment to operate in the Arctic; however, the sail and superstructure were constructed of aluminum and not designed for upward impact. In 1957 during an attempt to surface vertically into an open-water polynya between ice floes, the sail struck a small block of floating ice, which damaged the periscope and smashed down part of the sail's top surface [Lyon, 1984]. In 1958, modifications were made to make *Nautilus* more Arctic-capable including strengthening and hardening of the sail and deck to permit impact vertically against sea ice. The Nautilus crossed under the North Pole on 3 August 1958.

Next, the USS *Skate* (SSN-578) was given a mission to "develop techniques for surfacing in pack ice areas...if nuclear submarines are to be useful in the Arctic they must have access to the surface" [Calvert, 1959]. While this mission was initially accomplished in the summertime, August 1958, and only through open-water polynya, the need to prove that a submarine could surface in the Arctic during any season drove the *Skate* back the following March. The ice has usually reached its maximum by March, after continued low temperatures in January and February. Even though open water leads may still form when the ice canopy breaks apart under the stress of wind, the exposed surface will freeze six inches thick the first 24 hours with an average winter temperature of about -30°F. However, it was noted that whales had been observed to break ice six or eight inches thick with their backs. With that example, the *Skate*'s "sail" (or conning tower), the protective and streamlining structure surrounding the periscopes and radio masts, was strengthened, and the latest upward-looking fathometers were installed to measure the distance to the underside of the ice and to estimate its thickness [Rockwell, 1992].

In lieu of the vertical-ascent procedure used in summer to surface in the open-water polynya, procedures were devised for locating an acceptably thin lead in the ice canopy, positioning the submarine, and vertically ascending at a controlled rate [Lyon, 1984]. With an externally mounted underwater camera, the first surfacing was observed as allowing "the nearly 3,000-ton mass of the *Skate* to bump against the ice. We rebound gently away....bring her up again, this time a little faster." [Calvert, 1959]. During this winter deployment, the *Skate* attempted several more surfacing maneuvers and even experienced a few failures. As a result of this mission, "the art of routine surfacing through sea ice was devised ... by intuitive engineering, rudimentary knowledge of ice mechanics, and trial" [Lyon, 1992]. A routine surfacing has been described as a stationary, vertical ascent at a specified rate of rise in feet per minute that was calculated to exert a vertical impact force on the sail - assuming the boat did not break through the ice - within the submarine's design strength. However, the conclusions of recent literature implies that the "art" was developed more on trial than a rational basis, especially considering the stated need to "conduct momentum-exchange experiments and impact measurements" [Lyon, 1992].

The U.S. Navy interest in Arctic operations continued during the 1960's with incorporation of special ice-operation features in a submarine design, the *Sturgeon* (SSN-637)-class, beginning it's operations under the ice with *Queenfish* (SSN-651), February 1967. However, interest in these operations waned during the '70's and early '80's, although peaking again with the establishment, in May 1982, of an Arctic Program Steering Committee chaired by then Director of Naval Warfare (Op-95), Vice Admiral Lee Baggett, Jr., to coordinate the development of Arctic capabilities in the Fleet. The committee, at the three-star level, was formed following the initiation of several Arctic-related efforts by then Deputy CNO for Submarine Warfare, Vice Admiral N.R. Thunman, and strong recommendation by the then Oceanographer of the Navy, Rear Admiral Brad Mooney. The then Secretary of the Navy, John Lehman, saw the Arctic as a major area for U.S. naval activity, and called the frigid Kola Peninsula "the most valuable piece of real estate on earth." He said, "The only way you can really keep them [the former Soviet Union] above the GIUK (Greenland, Iceland, and United Kingdom) gap . . . is to be up there . . . forcing them onto the defensive initially because they know they will have to protect their assets" [Getler, 1983]. During that time period, it was noted that the Arctic was an important naval and maritime area for the Soviet Union, beyond ballistic missile submarines. Their building of nuclear icebreakers and reported construction of nuclear merchant ships for Arctic operation demonstrated the importance of the area [Zubrin, 1983].

Even with this renewed U.S. Naval interest in the Arctic, of the submarine classes currently operational by 1990, only the 637-class had conducted surfacings from below ice. The subsequent *Los Angeles* (SSN-688) submarines, the U.S. Navy's largest class of SSN's, do not have under-ice features, thus limiting their Arctic capabilities. However, a later version of this class, designated SSN-688I, was fitted with bow-mounted, retractable diving planes instead of sailplanes, as well as other ice-operation features to make an Arctic capable boat [Polmar, 1984]. The first of this later version, *San Juan* (SSN-751), demonstrated it's operational prowess in the Arctic during 1993 [Dane, 1993]. In addition, the limited edition *Seawolf* (SSN-21) class is also reported as designed with Arctic capabilities.

The former Soviet Union and the United Kingdom are the only other countries that are apparently still operating in the Arctic Ocean. The USSR submarine *Leninskiy Komsomol* made a cruise to the North Pole in June 1962; more recent Arctic cruises have not been publicly

described. However, the ballistic missile submarines of the Northern Fleet are among the few Soviet naval vehicles still operating. As such, the Soviet's most modern nuclear submarine classes, *Typhoon* and *Delta IV*, reportedly hide near and under the polar ice and are capable of punching through to fire their intercontinental ballistic missiles [Gellman, 1992]. Two submarines of the United Kingdom have made cruises to the North Pole, HMS *Dreadnought* (S-101) in 1971 and HMS *Sovereign* (S-108) in 1976. However, the *Trafalgar* is apparently the only current Arctic capable U.K. boat.

The ice thickness that these submarines surface through is not clearly defined. There are very few historical records that detail the state of the ice and those that do are quite vague, such as the description given during the 1908 *Kefal'* effort of the ice field "spreading out in the horizontal as far as one could see." The ice thickness was related as being only one inch and during part of the short journey the periscope was held three feet above the surface, cutting through the ice. However, a single flagstaff also was high enough to cut through the ice and at some point was bent over, demonstrating the strength of the ice [Babbitt, 1970]. One reported surfacing of the *Skate* was in an ice skylite about 1 ft thick - a narrow lead 100 yards wide lying between rugged, high hummocks [Lyon, 1984]. *Sargo*, of the same class of submarine as the *Skate*, was noted to have surfaced through ice, 3 ft thick at the North Pole. The remaining accounts are even more vague when relating the ice thickness, such as referring to "thick ice" surfacing as major accomplishments for the USS *Whale* and USS *Pargo* during cruises in April-May 1969 [McLaren, 1981]. More recent reports of Arctic operations [Dane, 1993] have indicated that a typical surfacing has evolved to include penetration of an "ice slab, several feet thick." As for the Russian *Typhoon*, conjecture has been made for a surfacing capability through ice of up to 3 m (9.8 ft.) thick due to the sail configuration [Jane, 1989/90].

Reports on ice forecasting have proved very useful in bracketing the ice thickness to be addressed in this study. The major source of ice thickness statistics available to date in the public domain for the entire Arctic Ocean and virtually the only source for the Siberian segment of the Arctic Ocean is from submarine sonar profiling. A detailed analysis of ice thickness distribution in the entire Arctic Ocean has been made based on 17 cruises of U.S. and British submarines between 1960 and 1982 [Bourke and Garrett, 1987]. A summary of several reports [Tunik, 1994] shows that the values of the mean ice thickness range from 3 to 13 feet, with large standard deviations that range from 41 to 91 percent. However, one study [McLaren, 1989] using submarine sonar under-ice thickness profiles, specifically categorized refrozen leads and/or polynya into "surfaceable areas" which involved up to and including 200 cm (approximately 6.5 feet) thick ice. In the same study, the mean thickness of level ice, defined as areas that vary less than 1 ft within a 33 ft radius, was up to 9 ft with a standard deviation of 2 ft in some sections.

Sea stories are entertaining and provide great fodder for historical lore; however, these anecdotal accounts do not accurately quantify ice and submarine characteristics and, consequently cannot provide a true basis for design guidelines. Assessing the structural dynamics of a floating ice sheet due to an initial impact will be useful in rationally quantifying the relative importance of a submarine ramming the ice during the surfacing maneuver. This part of the surfacing evolution is likely the most uncontrolled and thus undesirable portion, considering the inherent conservatism found in the nuclear navy. These dynamics also contribute another negative aspect in the additional forces occurring due to the inertial effects of water coupled with the ice sheet motion.

The following study will mathematically describe the structural dynamics of a floating ice sheet due to an initial impact. The main parameters appearing to affect these dynamics are the ice thickness, initial velocity, and impacting mass (submarine). Secondarily, it would seem that variation of the ice sheet material properties (most notably the Young's modulus, E) will affect the phenomena, although the inclusion is typically in the form of a fourth root value which would tend to lessen the effect. Using the closed-form solution of a simple spring-mass system, this study will determine how a range of initial velocity magnitudes affects the peak impact force, on both the ice sheet and the submarine, resulting from contact through a range of ice thickness. The effect that this initial impact has on the ice sheet will be quantified through observation of the maximum displacement relative to the ice thickness.

Chapter 3

Theoretical Background

This effort is intended to quantify the effect of the various parameters on the structural dynamics of a floating ice sheet due to a low-velocity, large-mass initial impact, specifically, that experienced during submarine Arctic surfacing maneuvers. To formulate a solution, it is prudent to understand previous work in this area.

Theoretical treatment of submarine ice penetration operations, noted as a process based largely upon trial and error, was addressed in connection with the first successful U.S. Naval attempts to surface submarines through ice [Assur 1962]. One consideration within that treatment was whether the submarine applies a force "topping" at rest against the ice or whether it approaches the ice sheet with a vertical velocity. Both of these cases were addressed with a focus on the failure point of the ice sheet. The first case involved computing the force required to penetrate the ice sheet under static loading, whereas the energy required under impact load was computed for the second.

The basic formulation for solutions in this early study involved a combination of both cylindrical bending of a plate with a finite line load, as well as circular bending at each end to represent the sail as a long, roughly elliptical load. Using a plastic moment, $M_p = \sigma h^2/4$ as the failure criteria, the maximum deflection, w_{max}, was derived. With the load formulated as a function of displacement, $P(w)$, the work (or kinetic energy) to achieve failure was found by;

$$W = \int_0^{w_{max}} P(w)dw \qquad (3\text{-}1)$$

The conclusions obtained concerning the kinetic energy required to break through the ice by impacting or "bouncing" were twofold:

1. that the value "increased rapidly" with the ice thickness (h) apparently by a power of 5/2, and

2. it is proportional to the square of the flexural strength of the ice (σ).

However, this early treatment does not take into account two very important aspects of the dynamic problem:

1. the strain energy for both the plate and that owing to the deformation of the elastic foundation, and

2. the inertial effects of each of the components (ice sheet, fluid foundation, and submarine).

In the case of forced vibrations or dynamic loading, the water imparts an additional bottom-surface pressure as the water mass is accelerated. However, as noted about the aforementioned

study and earlier efforts [Holl, 1950], the consideration of forced vibrations of thin plates resting on elastic foundations does not include the inertial effects of the water. Additional literature [Ross, 1969][Likhomanov and Kheisin, 1971][Kennedy and Iyengar, 1981][Timco and Frederking, 1993] is directed towards much higher velocities, on the order of 6 to 1000 times the rate of 30 fpm cited in the introduction literature. Each completely ignores the inertial effects of the foundation, as well as the ice. In most cases, the main concern was with contact pressures and shear plug expulsion.

Treatment of the inertia due to the elastic foundation has been made by applying Lagrange's principle of virtual displacements within a generalized study of beams, plates, and shells on elastic foundations [Vlasov and Leont'ev, 1960]. The assumptions are that no horizontal displacements occur in the elastic foundation and that the z-distribution of the vertical displacements is given by a known dimensionless linearly independent function, $\varphi(z)$. This function is selected in such a way that $\varphi(0) = 1$. However, these formulations are geared mainly toward soil as the foundation and, as such, that layer is considered compressible.

Incompressible potential flow theory has been used to treat the hydrodynamic reaction when analyzing the initial vertical motion of a floating ice sheet [Kheisin, 1967] along with assuming elastic plate behavior and small deflections. This approach was followed in later studies [Nevel, 1970] to provide solutions for the case of free vibration upon sudden removal of a static load and for forced sinusoidal vibration. A more recent finite element analysis [McGilvary et al., 1990] used incompressible potential flow to assess the validity of a coupled model to predict loads from a series of small-scale tests [Sodhi, 1989] involving constant velocity, vertical penetration of floating urea model ice sheets by cylindrical indentors. Even though the analysis required material property manipulation to agree with the experimental test data, the relative model results clearly demonstrated the predominance of fluid inertia over the ice inertia for the case studied.

These small-scale tests also motivated another study [Dempsey and Zhao, 1992] in which the ice sheet is modeled as an infinite thin plate undergoing small deflections with the supporting fluid modeled using incompressible potential flow theory. Closed-form solutions are used and the conclusions are in complete agreement with the earlier finite element effort in that the inclusion of the hydrodynamic reaction is of major importance. Thin plate theory supported by a Winkler foundation, described later, has been shown by use of Mindlin plate theory [Reismann and Lee, 1968] to be highly accurate, even if the effects of shear deformation and rotatory inertia are excluded. Other comparisons have been made [Zhao and Dempsey, 1990][Dempsey et al., 1991] between thin plate and layer solutions showing that the thin plate theory can accurately be used if the ratio of the characteristic length, l, (see equation 3-5), to layer depth is greater than 8. This will be evaluated within Chapter 6 of this study. Basically, these results indicate that the transverse deformation and shear deformation of the layer become less significant for $l/h \geq 8$. When specifically evaluating impact force, it was noted that, for relatively thick ice sheets, the influence of water depth, fluid inertia and characteristic length is unimportant, whereas, thinner ice sheet impact is significantly influenced by the bending deformation, as well as the dynamic water reaction.

The theory of plates on a continuous elastic foundation [Winkler, 1867] was formulated by assuming that the intensity of the reaction of the elastic foundation at any point is proportional to the deflection of the plate, w, at that point. This formulation is referred to as a Winkler foundation. This intensity is then given by the expression kw, where the constant k, expressed in

force per area per deflection, is called the modulus of the foundation. The response of a homogeneous, isotropic, elastic plate that rests on an elastic foundation and is subjected to a static vertical load, q, is described by the partial differential equation;

$$D\nabla^2\nabla^2 w + kw = q \tag{3-2}$$

where, ∇^2 is the Laplace operator, which for axisymetric cases is $\left(\dfrac{d^2}{dr^2} + \dfrac{1}{r}\dfrac{d}{dr}\right)$, and

$$D = Eh^3/[12(1-v^2)] \tag{3-3}$$

is the flexural rigidity of the plate, in which E is Young's modulus and v is Poisson's ratio.

The specific problem of a floating plate loaded at the center with a concentrated load, P, was later addressed [Hertz, 1884] in which k is regarded as the unit weight of the liquid (64.1 lb/ft^3 for seawater at 32°F). Bessel functions have been used [Timoshenko and Woinowsky-Krieger, 1959] to obtain an expression for the general deflections of the plate. Where in the case of an infinite plate, the solution is in the form [Wyman, 1950]:

$$w = -\frac{Pl^2}{2\pi D}\,\mathrm{kei}\,x \tag{3-4}$$

where x is the distance from P, and l is the characteristic length of the plate is defined by

$$l = \sqrt[4]{\frac{D}{k}} \tag{3-5}$$

The modified Bessel function, kei, may be represented for small values as follows;

$$\mathrm{kei}\,x = -\left(x^2/4\right)\ln x - \pi/4 + \left(1 + \ln 2 - \gamma\right)x^2/4 + \cdots \tag{3-6}$$

In which $\gamma = 0.5772157\cdots$ is Euler's constant. Thus, at the center $\mathrm{kei}\,x = -\pi/4$ where the deflection under the load becomes,

$$w_{max} = \frac{Pl^2}{8D} \tag{3-7}$$

The behavior of floating ice sheets subjected to static and moving loads has been examined by several investigators through the decades, and a survey of these efforts [Kerr, 1976] has shown that most of those treatments have used plate theory. Concern about the bearing capacity of floating ice sheets which are subjected to static or quasi-static loads has focused on the static loads of platforms (for storage in logging operations, construction of river structures, or offshore drilling) or moving loads (for ice roads or aircraft runways). One of the basic revelations of earlier studies was that the plate response may be considered elastic up until failure for the case when a small and relatively heavy vehicle breaks through the ice immediately after placement. Note that the current study is aimed at characterizing the immediate response of the ice plate and is thus supported by consistent conclusions of early efforts in the sole use of elastic deformation.

An aforementioned critical survey [Kerr, 1976] of the literature on the bearing capacity of floating ice plates was specifically aimed toward predictions of $P_f(t_f)$ for both the magnitude of

the "break-through load", P_f, and the corresponding "time to failure", t_f. This survey found that a majority of papers on the bearing capacity of ice plates deal with the determination of the special case of $P_f(0)$, the load which is just sufficient to break through the ice immediately after it is placed on the ice cover. There were five different procedures cited for the determination of $P_f(0)$; three were based on elasticity analyses and two were based on plasticity analyses.

The three procedures found based on elasticity analyses were:

1. An analogy method for determination of P_a, the allowable load, based on the failure moment in cylindrical bending, $M_a = \dfrac{\sigma_f h^2}{6}$, which assumes a linear stress distribution across the plate thickness. The final relationship, $P_a = Ah^2$, requires determining the coefficient, $A = P/h^2$, empirically.

2. Based on the elastic theory of plates and solutions for an infinite plate subjected to a load uniformly distributed over a circular area. The load at which the first crack occurs, P_{cr}, is determined with the criterion $\sigma_{max} = \sigma_f$, where σ_{max} is found empirically.

3. Using the elastic theory for the analysis of a cracked ice plate to determine $P_f(0)$ directly by assuming that the value is reached when the radial cracked wedges break at the base. Again, σ_f is obtained empirically.

The two approaches for the determination of $P_f(0)$, based on plasticity theories, use the yield-line and limit-load analysis, respectively. These theories are conceptually related to the elastic-based approach that analyzes the cracked plate, using yield lines instead of cracks and plastic moments instead of wedge-in moments. It was noted, however, the assumption that the ice plate can resist a full plastic moment M without cracking may not be realistic, since its formation was not observed in the field.

The consistent criticism for all the procedures examined in the survey was the use of a linear distribution of bending stresses to determine the maximum stress. The material parameters of a floating ice plate vary throughout the thickness [Kerr and Palmer, 1972], especially Young's modulus E. However, this survey cited that, according to several other papers [Newman and Forray, 1962] [Panfilov, 1966] [Assur, 1967], when E varies through the plate thickness h, and Poisson's ratio υ is assumed to be constant, the homogeneous partial differential equation is still valid if the flexural rigidity is

$$D = \frac{1}{1-v^2} \int_{-z_0}^{h-z_0} z^2 E(z)\,dz \tag{3-8}$$

and the position of the reference plane is determined from the condition

$$\int_{-z_0}^{h-z_0} z^2 E(z)\,dz = 0 \tag{3-9}$$

Systematic formulation of this problem [Kerr and Palmer, 1972] using Hamilton's principle in conjunction with the three-dimensional theory of elasticity, has shown that using this

nonhomogeneous definition, $E = E(z)$, still allows for the same corresponding boundary conditions as for homogeneous plates.

Two very important items for the current study resulted from the study of the Kerr survey:

1. As was surmised from field observations, the ice plate response to a loading of short duration may be considered elastic and as such formulation of solutions based on the elastic theory, including Kirchhoff's hypothesis, is justified.

2. 2. A proposed failure criterion [Zubov, 1942] [Kobeko *et al*, 1946] resulting from test data, for loads of short and long duration, was found based on a critical deflection, w_f. Specific empirical data [Panfilov, 1961], with ice plate thickness from 1 to 6 cm and temperatures form -3°C to -8.5°C, found the following relationship:

$$w_f = 2.2\sqrt{h}$$

This relationship indicates that the resulting ratio, $w/\sqrt{h}$, may be used to compare the effect of the parameter variations.

In the mid-1980's the current state and future needs of ice cover research was again addressed [Kerr and Frankenstein, 1986] with no new revelations bearing on this study. With the exception of a widely agreed upon failure criteria, use of the basic differential equation for homogeneous thin elastic plates, while incorporating a through thickness variable Young's modulus E, continues to be an acceptable method for analyzing floating ice covers. However, within another survey [Kerr, 1996] of analyses and tests of the bearing capacity of floating ice covers conducted another decade later, there is a note that for the determination of the deflection surface, bending moments, and shearing forces, the use of an averaged Young's modulus, E_{av}, is admissible. This E_{av} value is determined by equating the flexural rigidity expressions (3-3) and (3-8), which yields

$$E_{av} = \frac{12}{h^3} \int_{-z_0}^{h-z_0} z^2 E(z)\,dz \tag{3-10}$$

In addition, this latest survey noted that an investigation [Hutter, 1974] of the effect of brine on Poisson's ratio found negligible results and, thus concluded that the assumption of $v \approx$ constant is sufficient for many engineering ice cover analyses.

Chapter 4

Static Formulation

The dense ice cover floating on the ocean surface will be regarded as a plate supported by an elastic foundation. An acceptable formulation of the static solution for an axisymmetric plate with a concentrated load is required as an initial step in the overall study. Initial observations will be made with the simpler solutions for beams on elastic foundations to observe the effects of expanse and boundary conditions on the various aspects of the problem. The aim is to use only an infinite plate solution while addressing the more complex issues in the following dynamic formulation, with a caveat on the minimum expanse issues that arise in the finite beam observations.

Classic plate theory will be briefly reviewed before making the next step into the specific formulation for an axisymmetric plate supported by an elastic foundation. The exact solution for the infinite plate on an elastic foundation involves functions that will be difficult to mathematically manage during the dynamic formulation. Therefore, the Ritz method, a convenient procedure for determining solutions by the principle of minimum potential energy, will be used to obtain an acceptable approximation of this solution.

Beams on an Elastic Foundation

Thorough observation of a simple beam supported by an elastic foundation will illustrate the effect of length expansion and boundary conditions on various aspects of the problem, such as, maximum deflection and moment. These results support the next step where an infinite axisymmetric plate will be used on an elastic foundation with the knowledge of the limiting length expansion.

The support that an elastic foundation gives to a structure, beam or plate, is assumed to be proportional to the deflection due to loads [Winkler, 1867]. When a concentrated lateral load, P, causes the beam to deflect and displace the elastic foundation, the foundation's resistance to this displacement produces a laterally distributed force, q (force per unit length), on the beam. See Figure 4-1. When the x-axis coincides with the axis of the beam, and the y-axis is normal to the elastic foundation, this force may be described by $q = ky$, where k is the proportional constant of the supporting medium, referred to as the modulus of the foundation. When the foundation medium is a fluid, then k is simply the unit weight of the liquid [Hertz, 1884].
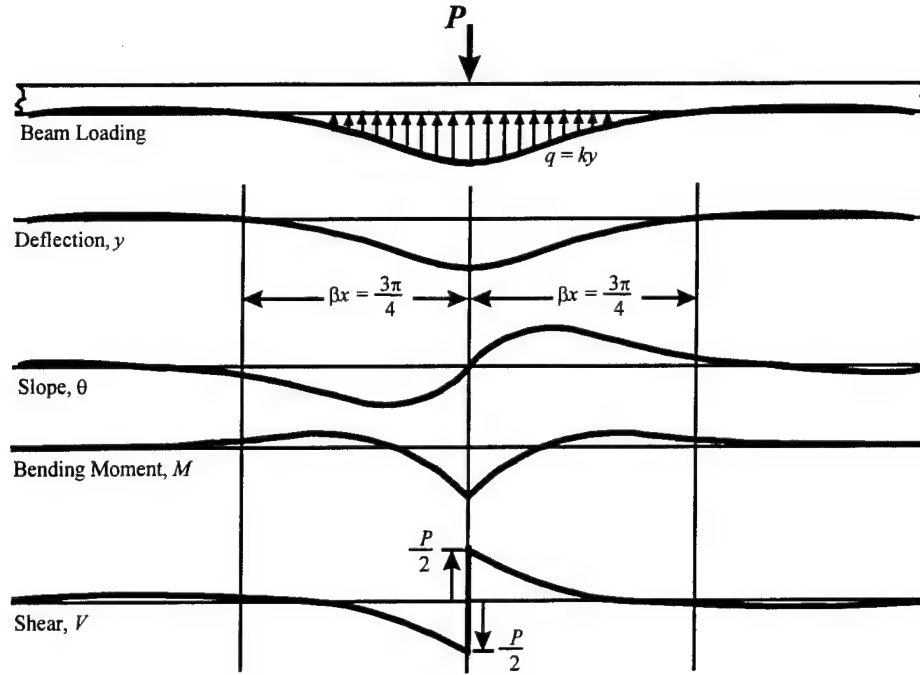
Figure 4-1. Infinite Beam on an Elastic Foundation with Concentrated Load at Origin.

There are certain regions where the deflection of the beam may be negative within the solution of this deflection problem. The basic formulation of a Winkler foundation assumes that the beam is attached to the foundation, which may, in certain regions, exert a tensile force on the beam. Note that in the case of a floating beam there is initial foundation pressure already on the beam resulting from beam weight which creates an initial constant deflection. This initial pressure is added to the laterally distributed force created by the loading. Thus, if a load is tending to lift the beam from the fluid, the combined laterally distributed force will be entirely compressive until the beam has been lifted clear of the fluid, at which point the foundation does not exist and this solution is no longer valid.

The general solution for the deflection, y, starts by obtaining the differential equation of the bending axis of the beam on an elastic foundation [Hentényi, 1946]:

$$EI\frac{d^4y}{dx^4} = -ky \qquad (4\text{-}1)$$

The general solution of (y) may be expressed as:

$$y = e^{\beta x}\left(A\sin\beta x + B\cos\beta x\right) + e^{-\beta x}\left(C\sin\beta x + D\cos\beta x\right) \qquad (4\text{-}2)$$

where

$$\beta = \sqrt[4]{\frac{k}{4EI}} \qquad (4\text{-}3)$$

Note that β includes the flexural rigidity of the beam as well as the elasticity of the supporting medium and this is referred to as the characteristic of the system. Since β's dimension is length^{-1}, the inverse, $1/\beta$, is known as the characteristic length. This quantity is similar to the characteristic length defined previously in the background for a plate. Thus, the separate solutions, for beams and plates, may be addressed with respect to the characteristic length in general.

The constants found in (4-2) are determined due to the boundary conditions, as well as, employing symmetry conditions where:

1. the slope of the beam remains zero under the load,

$$\frac{dy}{dx} = 0 \ @ \, x = 0 \tag{4-4}$$

2. half of the load P must be supported by the elastic foundation under the half of the beam specified by positive values of x,

$$2 \int_0^\infty kydx = P \ @ \, x \geq 0 \tag{4-5}$$

For infinite beams, the deflection of the beam converges toward zero for large positive values of x. Consequently, since the positively powered exponential $\left(e^{\beta x}\right)$ continuously increases as x increases, the constants A and B must be set equal to zero and (4-2) reduces to:

$$y = e^{-\beta x}\left(C \sin \beta x + D \cos \beta x\right) \ @ \, x \geq 0 \tag{4-6}$$

The remaining constants, C and D, are found by applying the symmetry conditions. First solving for the slope:

$$\frac{dy}{dx} = \beta e^{-\beta x}\left[(C - D)\cos \beta x - (C + D)\sin \beta x\right] \tag{4-7}$$

where $@ \, x = 0$, $\dfrac{dy}{dx} = 0 = \beta(C - D) \Rightarrow C = D$, thus:

$$y = C e^{-\beta x}\left(\sin \beta x + \cos \beta x\right) \tag{4-8}$$

Next equating the half of the load to half of the foundation support:

$$P = 2 \int_0^\infty kC e^{-\beta x}\left(\sin \beta x + \cos \beta x\right)dx \tag{4-9}$$

where integration results in the following:

$$P = 2kC\left[\frac{e^{-\beta x}}{2\beta^2}\left(-\beta\sin\beta x - \beta\cos\beta x - \beta\cos\beta x + \beta\sin\beta x\right)\right]_0^\infty \tag{4-10}$$

where applying the limits results in:

$$P = -\frac{2kC}{\beta} \Rightarrow C = -\frac{P\beta}{2k} \tag{4-11}$$

The deflection of an infinite beam, supported by an elastic foundation with a concentrated load (P) applied at the origin, may be expressed as:

$$y = -\frac{P\beta}{2k}e^{-\beta x}\left(\sin\beta x + \cos\beta x\right) \tag{4-12}$$

The resulting shape may be drawn with respect to βx, as shown in Figure 4-2. Note that by the distance $\beta x = 2\pi$ the deflection is less than 0.2% of the central maximum deflection, hence essentially zero. Discussion on the implications of the distance βx is found later within the observations of finite to infinite beam results.
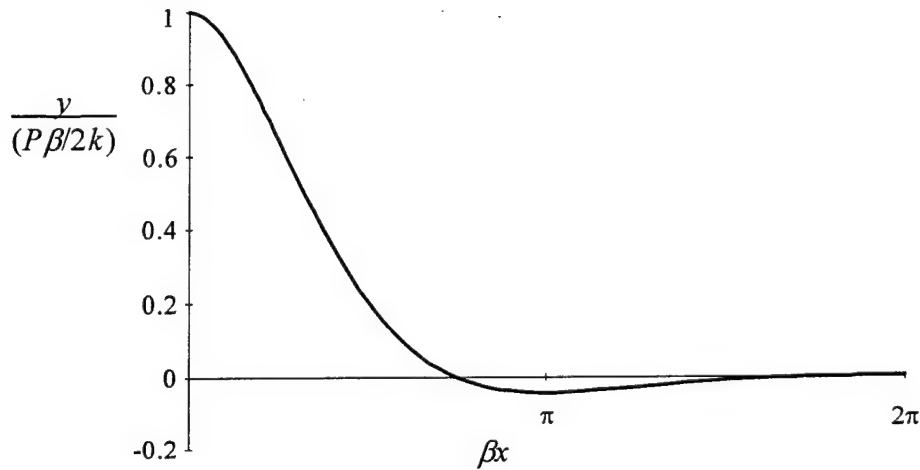
Figure 4- 2. Deflection Shape of an Infinite Beam on an Elastic Foundation.

A finite length beam on elastic foundation solution involves solving four simultaneous equations for the four unknowns. Two of the equations have already been given in all cases that involve symmetric loading and end conditions. These are the symmetry conditions addressed earlier in (4-4) and (4-5). However, the condition in (4-5) will be modified somewhat by addressing the following shear condition found at, just right of, the origin:

$$EI\frac{d^3y}{dx^3} = -\frac{P}{2} \quad @ x = 0 \tag{4-13}$$

where the negative sign is introduced because of the shear sign convention.

The deflection equation was derived for three sets of finite length beams where the end conditions are (a) fixed-fixed, (b) simply supported, and (c) free-free. The beams were considered of length equal to $2L$ and the coordinate system, as with the infinite beam, has the origin at the center where the load is applied. The boundary conditions, at $x = \pm L$, for each case of finite length beam considered are:

1. Fixed - Fixed: $y = 0$ and $\dfrac{dy}{dx} = 0$

2. Simple Supports: $y = 0$ and $\dfrac{d^2 y}{dx^2} = 0$

3. Free - Free: $\dfrac{d^2 y}{dx^2} = 0$ 3 and $\dfrac{d^3 y}{dx^3} = 0$

The solution for each of these finite length beam cases is of the following form:

$$y = -\frac{P\beta}{2k\alpha}\left[e^{\beta x}\left(A \sin \beta x + B \cos \beta x\right) + e^{-\beta x}\left(C \sin \beta x + D \cos \beta x\right)\right] \tag{4-14}$$

The constants for each end condition are as follows;

1. Fixed - Fixed:

$$\alpha = e^{4\beta L} + 2 e^{2\beta L} \sin 2\beta L - 1 \tag{4-15a}$$

$$A = e^{2\beta L}\left(\cos 2\beta L + \sin 2\beta L\right) - 1 \tag{4-15b}$$

$$B = e^{2\beta L}\left(\cos 2\beta L - \sin 2\beta L - 2\right) + 1 \tag{4-15c}$$

$$C = e^{2\beta L}\left(e^{2\beta L} - \cos 2\beta L + \sin 2\beta L\right) \tag{4-15d}$$

$$D = e^{2\beta L}\left(e^{2\beta L} + \cos 2\beta L + \sin 2\beta L - 2\right) \tag{4-15e}$$

2. Simple Supports:

$$\alpha = e^{4\beta L} + 2 e^{2\beta L} \cos 2\beta L + 1 \tag{4-15f}$$

$$A = e^{2\beta L}\left(\cos 2\beta L - \sin 2\beta L\right) + 1 \tag{4-15g}$$

$$B = e^{2\beta L}\left(\cos 2\beta L - \sin 2\beta L\right) - 1 \tag{4-15h}$$

$$C = e^{2\beta L}\left(e^{2\beta L} + \cos 2\beta L + \sin 2\beta L\right) \tag{4-15i}$$

$$D = e^{2\beta L}\left(e^{2\beta L} + \cos 2\beta L - \sin 2\beta L\right) \tag{4-15j}$$

3. Free - Free:

$$\alpha = e^{4\beta L} + 2 e^{2\beta L} \sin 2\beta L - 1 \tag{4-15k}$$

$$A = e^{2\beta L}\left(\cos 2\beta L + \sin 2\beta L\right) - 1 \tag{4-15l}$$

$$B = e^{2\beta L}\left(\cos 2\beta L - \sin 2\beta L + 2\right) + 1 \tag{4-15m}$$

$$C = e^{2\beta L}\left(e^{2\beta L} - \cos 2\beta L + \sin 2\beta L\right) \tag{4-15n}$$

$$D = e^{2\beta L}\left(e^{2\beta L} + \cos 2\beta L + \sin 2\beta L + 2\right) \tag{4-15o}$$

Observations of the range at which the beam conditions may be approximated more easily by the infinite solution are made by comparing plots of the various results; deflection, moment, and shear. See Figures 4-3 through 4-7. These results are normalized by the particular value found for an infinite beam at the origin and plotted along a horizontal axis delineated by βL, which correlates to a given finite beam expanse. Values, resulting at the origin for both deflection and moment are compared in Figures 4-3 and 4-5, respectively. Shear values are defined at the origin for all cases as -P/2, which, of course, leaves no comparison. Note that these plots of finite beam origin results are compared to unity, 1, because of the infinite beam normalization value, which defines the infinite beam as unity regardless of the finite beam expanse, βL. Deflection, moment, and shear are all compared for values occurring at the end of the finite beam expanse, βL. These plots, Figures 4-4, 4-6, and 4-7 for deflection, moment, and shear respectively, are mapped against the continuous normalized infinite beam results, as found at a distance βL from the origin.
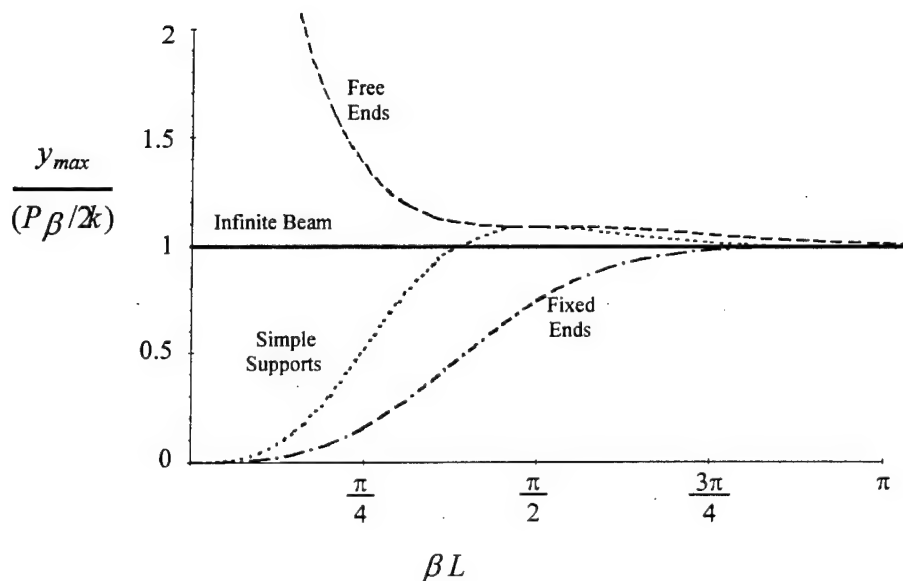

Figure 4- 3. Maximum Central Deflections of Finite Beams.
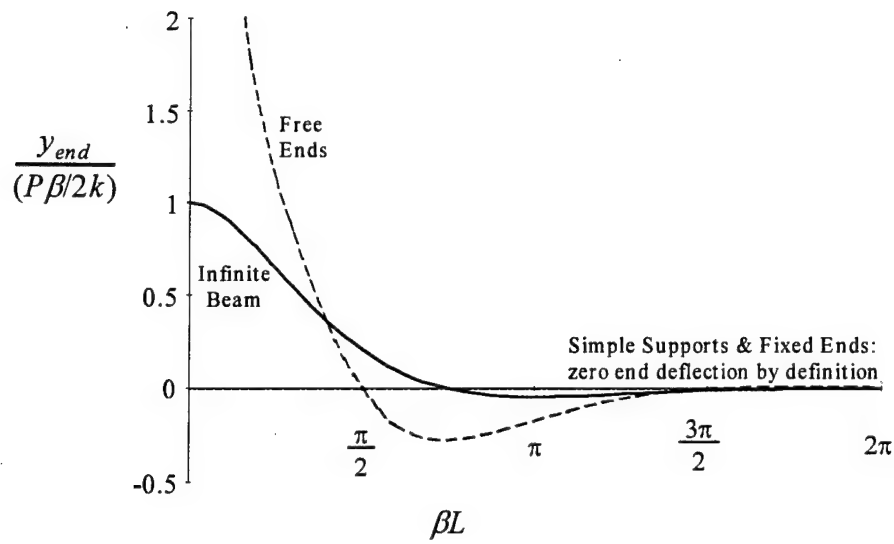
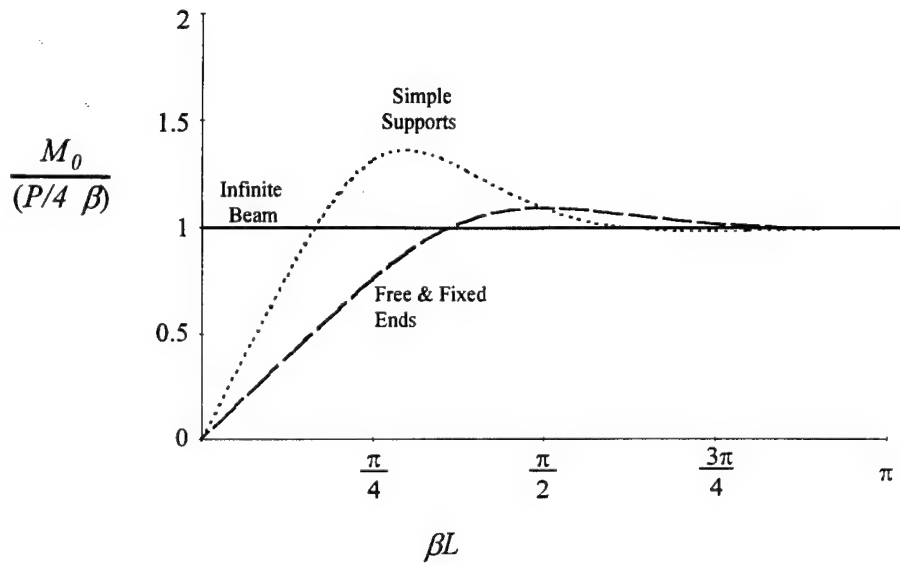**Figure 4- 4. End Deflection for Finite Beams.**

Figure 4- 5. Central Moments for Finite Beams.
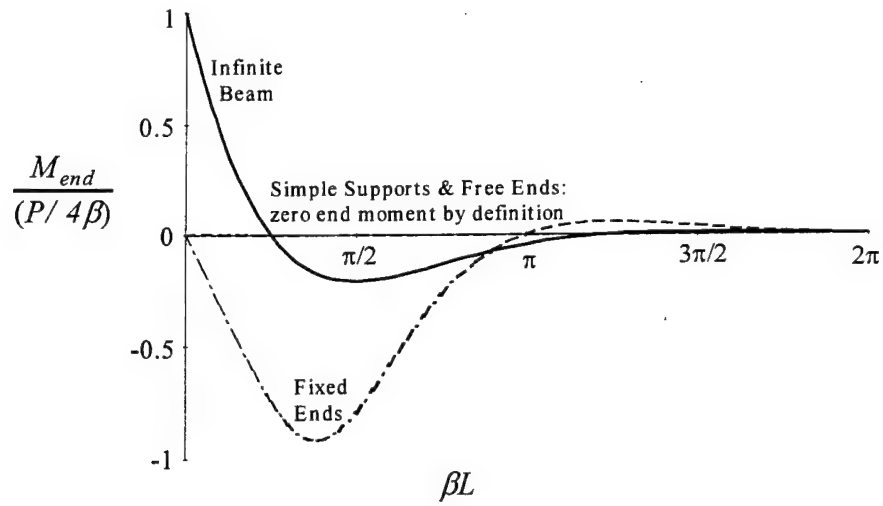
Figure 4- 6. End Moments for Finite Beams.
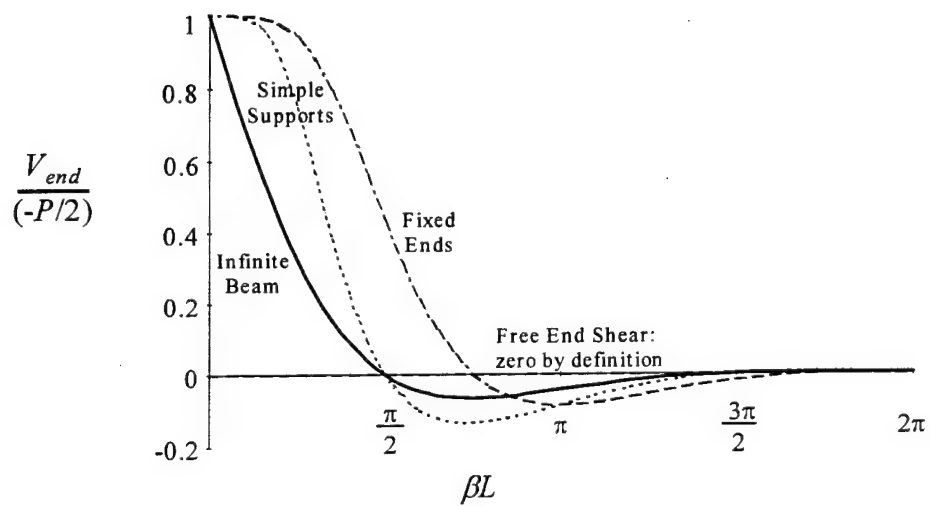
Figure 4- 7. End Shear for Finite Beams.

Comparing these plots shows that the origin results for finite beams converge within almost half the distance it takes for the end conditions to converge to the infinite beam values. This trend is not surprising, since the end conditions are the differences to overcome in the finite beams and region furthest from these areas, the origin, will be the least affected by those conditions. Quantitative comparison of the beam expanse effect is as follows:

1. origin results converge almost completely, within 1.1%, by the time $\beta L = \pi$, as well as within 5.5% by the time $\beta L = 3\pi/4$, and

2. finite beam end results converge almost completely, within 0.7%, by the time $\beta L = 2\pi$, as well as within 3.6% by the time $\beta L = 3\pi/2$.

Classic Plate Theory

A flat plate is often described as a structural element or member whose middle surface lies in a flat plane [Boresi, et al., 1978]. The dimension of a flat plate in a direction normal to the plane of its middle surface is called the thickness of the plate. A plate is characterized by the fact that its lateral dimension, the thickness, is relatively small compared to the plate dimensions in the plane of the middle surface. As a consequence, the bending behavior of a plate depends strongly on the plate thickness, as compared to the in-plane dimensions of the plate.

The fundamental assumptions of the classic plate theory, or the small-deflection theory of bending for isotropic, homogeneous, elastic, thin plates, is based on the geometry of deformations [Ugural, 1981]. Known as the Kirchhoff hypotheses, these assumptions are analogous to those associated with the simple bending theory of beams and serve to reduce the three-dimensional problem to a more tractable two-dimensional problem. The following is a short description of these assumptions:

1. The deflection of the midsurface is small compared with the thickness of the plate. The slope of the deflected surface is therefore very small and the square of the slope is a negligible quantity compared to unity.

2. The midplane remains undeformed subsequent to bending.

3. Plane sections initially normal to the midsurface remain plane and normal to that surface after the bending. The deflection of the plate is thus associated principally with bending strains. It is deduced therefore that the normal strain resulting from transverse loading may also be omitted.

4. The stress normal to the midplane is small compared with the other stress components and may be ignored.

The equations of equilibrium for a plate may be derived, using these assumptions, by several methods such as:

1. considering the equilibrium requirements for an infinitesimal plate element [Marguerre and Woernle, 1969],

2. by integrating the pointwise equilibrium equations through the plate thickness and employing the definitions for the stress resultants [Boresi, *et al,* 1978], or

3. by a direct application of the principle of virtual work [Marguerre and Woernle, 1969].

The combination of these equilibrium equations with the derivations for moments in terms of the curvatures and deflection, reveals one of the main results of classic plate theory, the plate equation:

$$\nabla^2 \nabla^2 w = \frac{q}{D} \qquad (4\text{-}16)$$

where:

w is the transverse deflection of the plate,

q is the lateral load per unit area,

∇^2 is the Laplace operator, which for axisymmetric, polar coordinates is:

$$\nabla^2 = \frac{\partial^2}{\partial r^2} + \frac{1}{r}\frac{\partial}{\partial r} \qquad (4\text{-}17)$$

D is the flexural rigidity of the plate, which is expressed as:

$$\frac{Eh^3}{12\left(1 - v^2\right)} \qquad (4\text{-}18)$$

h is the plate thickness.

To determine w, (4-16) must be integrated where the resulting constants depend on the appropriate boundary conditions.

Axisymmetric Plate Bending on an Elastic Foundation

In the case of a plate supported continuously along its bottom surface by a foundation, the intensity of the foundation reaction is proportional to the deflection, w, of the plate. As described earlier in formulating the beam solutions, this intensity is given by the expression kw, where w is used to designate the transverse deflection for plates, as opposed to y for beams. As denoted earlier for beams, the constant k, expressed in pounds per square inch per inch of deflection, is called the modulus of the foundation. Which follows that for the specific problem of a floating plate [Hertz, 1884] k is regarded as the unit weight of the liquid.

Formulation of the solution for this case may be initiated by adding the load -kw, due to the foundation reaction, to the lateral load q [Timoshenko and Woinowsky-Krieger, 1959] of the plate equation. This results in the following differential equation for the bent plate:

$$\left(\frac{d^2}{dr^2} + \frac{1}{r}\frac{d}{dr}\right)\left(\frac{d^2w}{dr^2} + \frac{1}{r}\frac{dw}{dr}\right) = \frac{q - kw}{D} \qquad (4\text{-}19)$$

In the particular case of a plate loaded at the center with a load P, q becomes zero over the entire surface of the plate except at the center. Thus (4-19) becomes:

$$l^4\left(\frac{d^2}{dr^2} + \frac{1}{r}\frac{d}{dr}\right)\left(\frac{d^2w}{dr^2} + \frac{1}{r}\frac{dw}{dr}\right) + w = 0 \qquad (4\text{-}20)$$

where the following notation is introduced:

$$l^4 = \frac{D}{k} \tag{4-21}$$

Often referred to as the characteristic length of the plate, l, having dimensions of length, is comparable to the inverse of β that was found in the beam cases. As an aside, a direct comparison of these two characteristic length terms reveals that the plate value is nearly 1.5 times less than that of the beam, depending on Poisson's ratio. This is not surprising since the plate case involves bending in two dimensions and, hence, less flexible than a beam which involves only cylindrical bending. Continuing with the plate solution, dimensionless quantities are introduced to simplify the solution process, these are: $\frac{w}{l} = \bar{z}$ and $\frac{r}{l} = \bar{x}$. Using these substitutions (4-20) becomes:

$$\left(\frac{d^2}{d\bar{x}^2} + \frac{1}{\bar{x}}\frac{d}{d\bar{x}}\right)\left(\frac{d^2\bar{z}}{d\bar{x}^2} + \frac{1}{\bar{x}}\frac{d\bar{z}}{d\bar{x}}\right) + \bar{z} = 0 \tag{4-22a}$$

Using the symbol Δ for $\left(\frac{d^2}{d\bar{x}^2} + \frac{1}{\bar{x}}\frac{d}{d\bar{x}}\right)$, (4-20) may be expressed finally as:

$$\Delta\Delta\bar{z} + \bar{z} = 0 \tag{4-22b}$$

This is a linear differential equation of the fourth order and may be solved with a general solution of the form:

$$\bar{z} = c_1 f_1(\bar{x}) + c_2 f_2(\bar{x}) + c_3 f_3(\bar{x}) + c_4 f_4(\bar{x}) \tag{4-23}$$

where $c_1, \ldots, c_4$ are constants of integration and the functions $f_1(\bar{x}), \ldots, f_4(\bar{x})$ are four independent solutions of (4-22).

One successful manner of representing (4-23) to solve (4-22) is with the application of Bessel functions [Timoshenko and Woinowsky-Krieger, 1959]. In the particular case of an infinite plate with a central concentrated load, P, the complete solution is in the form

$$w(r) = -\frac{Pl^2}{2\pi D}\text{kei}\left(\frac{r}{l}\right) \tag{4-24}$$

where kei(x) is a modified Bessel function of the form:

$$\text{kei}(x) = \frac{\pi}{2}\text{Im}\left[Y_0\left(xe^{i\pi/4}\right)\right] - \frac{\pi}{2}\text{Re}\left[J_0\left(xe^{i\pi/4}\right)\right] \tag{4-25}$$

which is essentially the imaginary portion of $K_0\left(x\sqrt{\pm i}\right)$, a Bessel function of the second kind sometimes referred to as a Kelvin function. At the origin $\text{kei}(0) = -\frac{\pi}{4}$, which gives a maximum deflection of:

$$w_{max} = -\frac{Pl^2}{8D}$$

(4-26)

Using the form (4-24) will be mathematically cumbersome with the continuation of this study into the dynamic solutions. There are approximations for kei(x), however, these are dependent on whether x is small, $x < 1$, where the following may be used

$$\text{kei}(x) \approx -\left(\frac{x^2}{4}\right)\ln x - \frac{\pi}{4} + \left(1 + \ln 2 - \gamma\right)\frac{x^2}{4}$$

(4-27a)

in which γ is Euler's constant (0.5772157…). Where for larger values, the following asymptotic expression holds:

$$\text{kei}(x) \approx -\frac{e^{-\sigma}}{\sqrt{2x/\pi}}\sin\left(\vartheta + \frac{\pi}{8}\right)$$

(4-27b)

in which $\vartheta = x/\sqrt{2}$. Neither one of these approximations provides a valid continuous function that represents the overall displacement of the plate, see Figure 4-8. Thus another means of approximating the solution for an infinite plate supported by an elastic foundation with a central concentrated load is required.
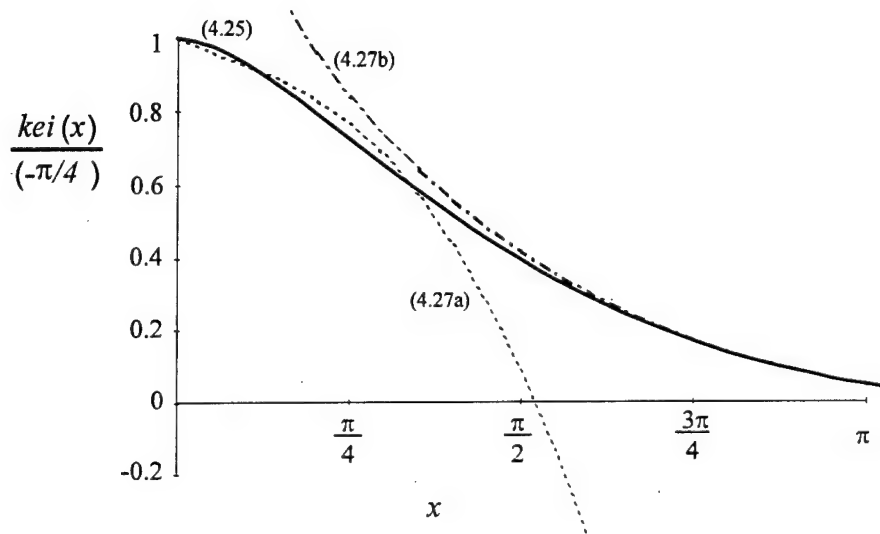
Figure 4- 8. Approximations for kei(x).

Strain Energy Method Solutions

The plate equation, (4-16) is solved for deflections with considerable difficulty, or, even for as simple a case as the axisymmetric loaded circular plate, results in unwieldy mathematical forms. As an alternative to the equilibrium methods, the analysis of deformation and stress in an elastic body can be accomplished by employing energy methods. These two techniques are, respectively, the Newtonian and Lagrangian approaches to mechanics. While the former is governed by the conditions of equilibrium of statics, the latter is predicated upon the fact that the governing equation of a deformed elastic body is derived by minimizing the energy associated with the deformation and loading.

The Ritz method is a convenient procedure for determining solutions by the principle of minimum potential energy [Ugural, 1981]. This principle is based on the fact that, for stable equilibrium, the potential energy is a minimum. For all displacements satisfying given boundary conditions and the equilibrium conditions, the potential energy will assume a minimum value.

To employ the Ritz method, a form of the solution for the deflection, w, is selected to satisfy the geometric boundary conditions. It is desirable, to assume an expression which is nearly identical to the true bent surface of the plate. Note that the static boundary conditions need not be fulfilled. This solution form will contain one or more undetermined parameters, C_n, which will govern the variation of the potential energy.

The potential energy of a system is the difference between the strain energy that is stored in an elastic body and the work done by external loads. In the case of axisymmetric bending, with infinite boundaries, the expression for strain energy in the plate is:

$$U_p = \pi D \int_0^\infty \left[\left(\frac{d^2w}{dr^2} + \frac{1}{r}\frac{dw}{dr} \right)^2 - \frac{2(1-v)}{r}\frac{dw}{dr}\frac{d^2w}{dr^2} \right] r\,dr \qquad (4\text{-}28)$$

In addition, the strain energy owing to the deformation of the elastic foundation is:

$$U_f = \pi k \int_0^\infty w^2 r\,dr \qquad (4\text{-}29)$$

The work done by the load is given by:

$$W = P(w)_{r=0} = Pw_0 \qquad (4\text{-}30)$$

The potential energy is a result of:

$$E_P = U_p + U_f - W \qquad (4\text{-}31)$$

The constants in the chosen solution form are then found by the minimizing condition. This condition is defined by equating the partial derivative of the potential energy with respect to each individual constant to zero

$$\frac{\partial E_P}{\partial C_n} = 0 \qquad (4\text{-}32)$$

The resulting system of algebraic equations is solved to yield the parameters, C_n, which in turn are used in the originally assumed expression for calculating the deflection.

Several assumed solutions were initially made for the deflection, w. These solutions are, ostensibly, in the form of a series, allowing improved approximation with retention of more terms. However, singular term functions may serve as good assumptions if the contents are chosen carefully to imitate the actual deflected shape. In addition, the typical series does not hold for infinite boundary conditions.

Several singular term functions were therefore initially formulated with the Ritz method to estimate the deflected shape of an infinite, axisymmetric plate on an elastic foundation with a concentrated load, P. A partial list of the attempted functions is as follows:

$$w_0 e^{-cr}[\sin cr + \cos cr] \tag{4-33a}$$

$$w_0 e^{-(cr)^2} \tag{4-33b}$$

$$\frac{w_0}{1+(cr)^2} \tag{4-33c}$$

$$w_0 e^{-(cr)^2} \cos(cr)^2 \tag{4-33d}$$

$$\frac{w_0}{1+(cr)^4} \tag{4-33e}$$

$$w_0 e^{-(cr)^2}\left[\sin(cr)^2 + \cos(cr)^2\right] \tag{4-33f}$$

Note that several other combinations of the exponential, e, sine, and cosine functions were attempted, but complications arose when integrating the energy terms. Thus, these shape functions were not used.

After minimizing the potential energy to complete the formulations of these shape functions (4-33) by obtaining the w_0 and c parameters, a graphic comparison was initially made to the Timoshenko Bessel function solution (4-24), see Figure 4-9. These functions have all been nondimensionalized by the maximum deflection (4-26) of (4-24). As a consequence of this view, the last three shape functions (4-33d-f) were eliminated from further evaluation. A comparison was then made of the maximum (origin) deflection, as well as, the effective radius for each of the three remaining shape functions (4-33a-c) and these values are listed in Table 4-1 along with those found for (4-24). A glaring difference is found in the effective radius of the third shape function (4-33c) and, as such, this one is eliminated as well.
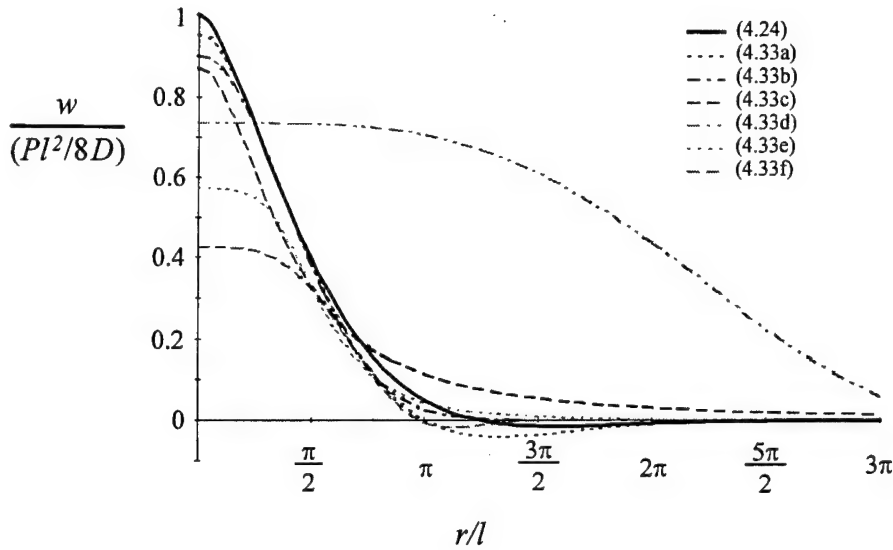
Figure 4- 9. Comparison of the Shape Functions.

An uncluttered view of the two remaining shape functions is provided in Figure 4-10. Notice that the first shape (4-33a) better approximates the maximum deflection, whereas the second shape (4-33b) provides a closer estimate in the region of the effective radius. Thus both shapes are carried on to the next step of evaluation.

Table 4-1. Comparison of Various Shape Functions.

Shape Function $w(r)$	$w_0 / \left(Pl^2 / 8D \right)$	c	Effective Radius* (r/l)
$-\dfrac{P}{2\pi k l^2}\,\mathrm{kei}\dfrac{r}{l}$	1	---	3.915
$w_0 e^{-\left(cr/l\right)}\left[\sin\left(cr/l\right) + \cos\left(cr/l\right)\right]$	0.95	$\sqrt[4]{\dfrac{3}{4(1+2\ln 2)}}$	3.147
$w_0\, e^{-\left(cr/l\right)^2}$	0.90	$\sqrt[4]{\dfrac{1}{8}}$	3.609
$\dfrac{w_0}{1+\left(cr/l\right)^2}$	0.87	$\sqrt[4]{\dfrac{15}{32}}$	12.025

*   The effective radius for the first two functions is the distance to the first instance where the deflection is zero and for the last two it is where the radius is a deflection of 1% w_0.
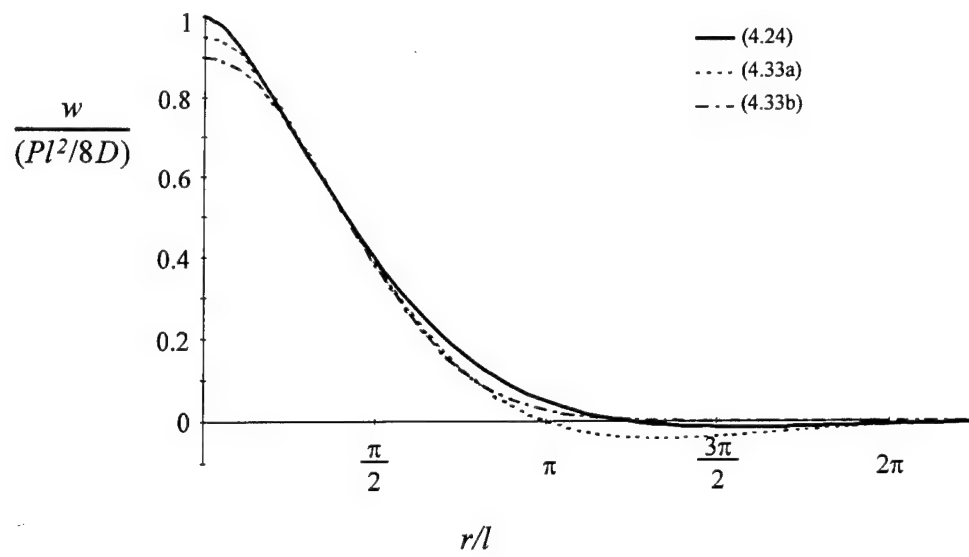
Figure 4- 10. Best Two Shape Functions.

Chapter 5

Dynamic Formulation

The dynamic phenomena of a submarine impacting the underside of an ice floe will be modeled as a simple spring-mass system, see Figure 5-1. The components within this system are as follows:
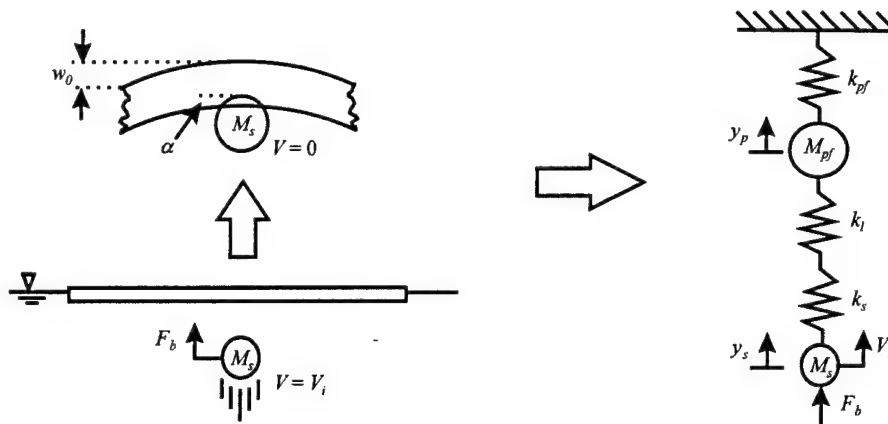
Figure 5-1. Spring-Mass System Representation of Impact.

α - local crushing deformation at the contact point,

F_b - buoyancy force of impact structure,

k_l - spring stiffness associated with the local crushing deformation,

k_{pf} - spring stiffness associated with the plate and fluid together,

k_s - spring stiffness associated with the impacting structure,

M_{pf} - mass of the plate and fluid together,

M_s - mass of the impacting structure,

V_i - initial velocity of the impacting structure at contact with the plate

w_o - maximum plate deformation at the origin,

y_p - displacement of the plate-fluid system, and

y_s - displacement of the impact structure.

Damping, due to fluid interaction or otherwise, is ignored in this model. Observation of the system for this study will be limited to the time required to achieve the maximum force. This event should occur within a relatively short time. This study will only address the initial velocity

and buoyancy force as the external forcing functions applied to obtain a maximum deflection, thus the long-term effect of damping does not come into play.

The spring stiffness associated with the combined plate and fluid is determined from the origin deflection, w_o, due to a concentrated load, P. This component has already been resolved from the static formulation and may be found in Table 4-1. The value in the second column may be multiplied by $(l^2/8D)$ and inverted to determine k_{pf} for the particular shape function.

The other two springs found in series, k_l and k_s, must be determined and combined into one effective stiffness value using the following:

$$k_{ls} = \frac{1}{1/k_l + 1/k_s} \qquad (5\text{-}1)$$

The stiffnesses of each of these two springs are likely to be vastly different in magnitude. It is assumed that $k_l \ll k_s$, and, as such, the $1/k_s$ term on the left hand side of (5-1) will essentially equal zero with respect to $1/k_l$. This being the case, the spring stiffness between the two masses, $k_{ls} \equiv k_l$, will depend on the local crushing due to contact between the impacting structure and the underside of the plate.

The effective mass of the plate and fluid together, M_{pf}, will be determined via the fundamental, or natural frequency, ω_n, of the axisymmetric plate on elastic foundation solutions. The fundamental frequency will be found from the principle of conservation of energy. The mass of the impacting vehicle, M_s, as well as an initial velocity, v_i, are both values that will be given. The effects of both may be observed through a range of expected magnitudes.

The buoyancy force, F_b, may be determined in general as the fraction of the submarine's displacement required to achieve a typical terminal velocity within a typical rise height. This fraction may be found by using the following basic physics relationship for velocity of a dropped object from a height, h_t:

$$V = \sqrt{2gh_t} \qquad (5\text{-}2)$$

Where a description of the Arctic surfacing evolution [Dane, 1993] has noted that the submarine was "...80 ft down and rising at 30 ft per minute." The 30 fpm was achieved after having risen 20 ft. Thus, (5-2) may be used by replacing the acceleration due to gravity, g, by acceleration in general, which, in turn, may be equated to the initial buoyant force per mass of the entire structure:

$$g \Rightarrow \frac{F_b}{M_s} \qquad (5\text{-}3)$$

Then, h may be replaced by the 20 ft cited as the distance traveled to achieve the velocity of 30 fpm. After rearranging (5-2) and substituting (5-3) and these values for V, g, and h_t, the initial buoyant force may be equated to a fraction of the mass as follows:

$$F_b = 0.00625M_s \qquad (5\text{-}4a)$$

However, (5-4) is specific to a gravity acceleration of 32.174 ft/s². A nondimensional form may be achieved by the following:

$$F_b = 0.000194gM_s \qquad (5\text{-}4b)$$

Note that this formulation neglects the friction of the fluid against the structure. Calculations that include friction have been made [Bedel and Feldman, 1991] for the net buoyancy required for the USS *San Juan* to achieve a vertical velocity of 30 fpm over a given distance. Utilizing 6927 tons as the submerged displacement [Polmar, 1993] and 3 tons net buoyancy over a 21 ft distance, the fraction becomes:

$$F_b = 0.000433 g M_s \tag{5-5}$$

where friction is included. This value is 2.23 times (5-4). However, the buoyancy force is still a very small fraction of the entire mass of the impact structure. It shall be denoted in most equations as F_b, unless a comparison with M_s is required.

The dynamic formulation will produce equations for the system displacements, y_p and y_s or α, which, in turn, will be used with the appropriate spring stiffness to determine the impact load imparted on both the plate in general and the impact structure. These formulations will be used in the next chapter to illustrate the effect that given parameter ranges will have on both impact loads.

Fundamental Frequency of the Plate-Fluid System

Obtaining the fundamental or natural frequency for an axisymmetric plate on an elastic foundation will not only assist in further evaluation of the two remaining shape functions (4-33a&b), but also provide the effective mass, M_{pf}, of the system. The energy method will be used to obtain the natural frequency [Thomson, 1981].

In a conservative system, the total energy is constant. The free vibration of an undamped system has a total energy that is a combination of kinetic and potential. The kinetic energy, E_K, is stored in the mass by virtue of its velocity; whereas, the potential energy, E_P, is stored in the form of strain energy in elastic deformation or work done in a force field such as gravity. Since the total energy is constant, the change with respect to time is zero as demonstrated by the following:

$$E_K + E_P = \text{constant} \quad \therefore \quad \frac{d}{dt}\left(E_K + E_P\right) = 0 \tag{5-6}$$

Due to the principle of conservation of energy, the total energy from two instances of time may be equated. These two specific times will be chosen as follows:

1. when the mass is passing through its static equilibrium position which is where E_K, is maximum and E_P, is zero, and

2. corresponding to the maximum displacement of the mass which is also where the velocity of the mass is zero and, as such, where E_K, is zero and E_P, is maximum.

Therefore, equating these two instances of time it follows that:

$$E_{K(max)} = E_{P(max)} \tag{5-7}$$

In distributed mass systems such as a plate on an elastic foundation, knowledge of the distribution of the vibration amplitude is necessary to formulate the kinetic energy. Rayleigh showed that with a reasonable assumption for the shape of the vibration amplitude, it is possible to take into account previously ignored masses and arrive at a better estimate for the fundamental

frequency [Strutt, 1937]. Rayleigh also observed that, for undamped free vibration, the motion may be represented as a simple harmonic shape [Craig, 1981], therefore, the fundamental system dynamics of an axisymmetric plate may be defined by the following:

$$w(r,t) = w \cos(\omega_{Rn}t) \tag{5-8}$$

where ω_{Rn} designates the Rayleigh approximation to the fundamental frequency, and $w = w(r)$ is the same assumed shape function found for the static solution.

The maximum potential energy, $E_{P(max)}$, occurs at $t = 0$ and, as such, from (5-8) the transient term, $\cos(\omega_{Rn}t) = 1$, is maximized. Note that this static strain energy has already been established during the previous effort in the static formulation of the shape functions using the Ritz method. Therefore, combining (4-28) and (4-29) may produce an expression for the maximum potential energy from the previous chapter, which gives the following:

$$E_{p(max)} = \pi \int_0^\infty \left\{ D\left[\left(\frac{d^2w}{dr^2} + \frac{1}{r}\frac{dw}{dr} \right)^2 - \frac{2(1-v)}{r}\frac{dw}{dr}\frac{d^2w}{dr^2} \right] + kw^2 \right\} r\,dr \tag{5-9}$$

The maximum kinetic energy, $E_{K(max)}$, occurs when the system velocity, the first derivative of (5-8) with respect to time, denoted by the following:

$$\dot{w}(r,t) = -w\,\omega_{Rn} \sin(\omega_{Rn}t) \tag{5-10}$$

is maximum. The maximum velocity occurs when the transient term of (5-10) is maximized, or $\sin(\omega_{Rn}t) = 1$. Given the basic expression for kinetic energy as:

$$E_K = \tfrac{1}{2}mv^2 \tag{5-11}$$

where m is mass and v is velocity. The maximum kinetic energy for the plate is formulated as:

$$E_{Kp(max)} = \tfrac{1}{2} \int_0^{2\pi}\int_0^\infty (\rho_p h)(\omega_{Rn}w)^2 r\,dr\,d\theta \tag{5-12a}$$

which may be simplified as:

$$E_{Kp(max)} = \rho_p h \pi \omega_{Rn}^2 \int_0^\infty w^2 r\,dr \tag{5-12b}$$

where ρ_p is the mass density and h is the thickness, each associated with the plate.

To make a quick comparison of the two remaining shape functions (4-33a&b), the fundamental frequency was determined initially without considering the additional foundation kinetic energy, essentially assuming the foundation to be without mass. However, no comparison was available, since the fundamental frequency evaluated for both shape functions was exactly the same as follows:

$$\omega_{Rn}^{\cdot} = \sqrt{\frac{2k}{\rho_p h}} \tag{5-13}$$

where ω_{Rn}^{*} is designated as neglecting the additional foundation kinetic energy. This phenomena was determined to exist because of the basic manner in which the shape functions were chosen. The function, $w(r)$ may be more accurately thought of in the form $w(cr)$, in that the parameter c and the variable r do not appear in w except together as (cr). As a result of this form, three situations occur:

1. The kinetic energy of the plate (5-12) is related to the strain energy due to the foundation (4-29) by a factor of $\left(\rho_p h \, \omega_{Rn}^2 \, / \, k\right)$, or basically:

$$E_{Kp(max)} = \left(\rho_p h \, \omega_{Rn}^2 \, / \, k\right) U_f \tag{5-14}$$

2. Obtaining c on the basis of minimum potential energy achieves a result that equates the strain energy of the plate to that due to the foundation, or $U_p = U_f$, by default.

3. Using the principle of conservation of energy to choose ω_{Rn} from $E_{P(max)} = E_{Kp(max)}$ with these last two relationships will automatically give (5-13) when the foundation kinetic energy is neglected.

Nonetheless, this frequency will be an accurate gauge to compare the influence that the foundation has on the system dynamics.

Fluid coupling under dynamic conditions creates an additional field of pressure in the foundation beyond the buoyancy or stiffness that was already taken into account for the static solution. This additional pressure can be thought of as an inertial effect due to the additional mass of fluid essentially riding the dynamic wave action of the plate. The structural motion at any point accelerates the entire fluid mass, thus developing a pressure field at all locations along the structure/fluid interface.

This additional fluid "mass" always decreases the natural frequency of the structure from that which would be measured in a vacuum. The importance of this additional "mass" in the dynamic analysis of a structure can be estimated from the ratio of the density of the surrounding fluid to the average density of the structure. When this ratio is small, such as most structures in air, the additional "mass" effects are ordinarily negligible in the dynamic results. However, the density ratio of seawater to the floating ice is very close to 1:1, thus, the additional "mass" plays a large role in the dynamic analysis.

The additional "mass" can either be measured experimentally or calculated theoretically. Experiments have generally shown that the added mass of a structure vibrating in a still fluid is a function of:

1. the geometry of the surface of the structure, including the location of the free surface,

2. the amplitude and direction of vibration, and

3. a Reynolds-number-like parameter.

This additional "mass", unlike fluid drag or fluid damping, can exist in an incompressible, inviscid, irrotational fluid (i.e., density is constant and kinematic viscosity is zero). With this assumption, the third parameter may be dropped and the added mass may be expressed as follows:

$$M_f = \rho_f \, \mathrm{F}\left(geometry, \frac{A}{r_{eff}}\right) \tag{5-15}$$

where ρ_f is the density of the fluid, A is the amplitude of vibration in a given direction relative to the structure, and r_{eff} is an effective radius.

It is possible to evaluate this additional "mass" through the application of potential flow theory. When predicted by potential flow theory, the additional "mass" is depends only on the geometry of the surface of the structure. Comparison of experimental and theoretical results [McConnell and Young, 1965] [Ackermann and Arbhabhirama, 1964] suggests that the potential flow theory prediction is within about 10% of the experimentally measured value when the following conditions are found:

1. The vibration frequency is much smaller than the speed of sound in the fluid.

2. The amplitude of vibration is small compared with a characteristic diameter of the structure.

3. The Reynolds-number-like parameter is large.

Potential flow theory has been used by many authors [Lamb, 1921] [Kheisin, 1967] [Zhao and Dempsey, 1990] for this particular problem as well. However, application of this theory essentially requires that the potential function of the fluid, ϕ, must satisfy the Laplace equation:

$$\nabla^2 \phi = 0 \tag{5-16}$$

as well as, the appropriate boundary conditions. The hydrodynamic pressure is then found by Bernoulli's equation [Streeter and Wylie, 1979]:

$$p_f = \rho_f g w - \tfrac{1}{2}\rho_p \dot{w}^2 - \rho_f \frac{\partial \phi}{\partial t} \tag{5-17}$$

Note here that $\rho_f g$ is equivalent to k for the fluid.

However, the solution for the potential function requires the same sort of complicated mathematics (Bessel functions, Fourier transforms, etc.) that was avoided earlier in the static solution. Thus, this approach would defeat the purpose of using the earlier static product, which also could not be used within the potential function, since none of these earlier solutions satisfied the Laplace equation.

It has been shown that, if a body moves at a velocity, v, in an ideal, incompressible fluid, of infinite extent, and in irrotational motion, the total kinetic energy of the fluid, E_{Kf}, is:

$$E_{Kf} = \tfrac{1}{2} c \dot{w}^2 \tag{5-18}$$

where c is a constant that depends only on the density of the fluid, the size and shape of the body, and the direction of motion [Birkhoff, 1950]. Results of experiments [Stelson and Mavis, 1955] conducted to measure added masses of various shaped and sized bodies have shown that rectangular plates with length to width ratios of infinite extent will have added masses that are nearly equivalent to a cylindrical mass of fluid with diameter equal to the width of the plate. This same type of phenomena is found in at least two other places:

1. [Wendel, 1959] analytical results of ellipses of different aspect ratios, a:b, with motion in the direction of a varying axis, a, where the other axis, b, is held constant. The hydrodynamic mass for each ellipse is found to be equivalent to the fluid density times a circular area with radius b/2.

2. [Blevins, 1979] tabulated theoretical results of a floating plate in a channel, resulting in an added mass per unit length equivalent to a semi-circular area times the fluid density.

This suggests that the magnitude of added mass for axisymmetric plates in the fundamental mode is of the same order as the fluid contained by the volume which is generated by rotating the plate about the axis of symmetry, giving a spherical volume when surrounded by fluid and a hemispherical volume when only one side of the plate is exposed. However, note that these results have been for rigid plates, where theoretical results show that the added mass is a function of the plate boundary conditions and generally declines with increasing mode number.

Tabulated formulas [Blevins, 1979] for the added masses of circular plates with one side exposed to a fluid have been collected from various sources [Lamb, 1921] [McLachlan, 1932] [Peake and Thurston, 1954]. For a plate with radius a, the following added mass formulas have been found for the specific boundary conditions and mode listed:

1. Free edges with one nodal circle (see Figure 5-2):

$$\tfrac{24}{35}\rho_f a^3 \approx 0.6857\rho_f a^3 \qquad\qquad (5\text{-}19)$$

2. Free edges with central point support and in axisymmetric mode:

$$\tfrac{120}{63}\rho_f a^3 \approx 1.905\rho_f a^3 \qquad\qquad (5\text{-}20)$$

3. Simply supported edges in fundamental mode:

$$1.045\pi\rho_f a^3 \approx 3.283\rho_f a^3 \qquad\qquad (5\text{-}21)$$

4. Fixed edges in fundamental mode:

$$0.6689\pi\rho_f a^3 \approx 2.101\rho_f a^3 \qquad\qquad (5\text{-}22)$$

where a hemispherical volume with radius a is equivalent to:

$$\tfrac{2}{3}\pi a^3 \approx 2.09 a^3 \qquad\qquad (5\text{-}23)$$
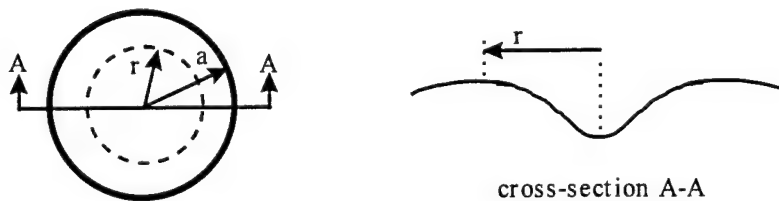

cross-section A-A

Figure 5-2. Example of Mode with One Nodal Circle.

The greatest deviation from a basic hemispherical volume occurs in two of these cases, where there are free edges with one nodal circle (5-19) and with simply supported edges (5-21). The first case involves essentially a circle within a circle due to the mode shape, where the radius of the inner circle is $r = 0.68a$. When this inner circle radius is used to calculate the hemisphere volume, a value is found equivalent to $0.6585a^3$ which is less than 4% from the analytical value (5-19) listed. The difference found for the simply supported edges (5-21) is most likely due to the difference in displaced shape from the other cases. Considering the inner circle of the free edge case and the fixed edge case, the shapes are most likely comparable, since the inner circle of the free edge case actually has the outer ring as a boundary condition that will be more rigid (like a fixed edge) than a simple support. Thus, on the whole, considering a finite radius, a, the displaced shape of the simply supported case creates a greater displaced volume than that of the fixed edge and, relatively, the inner circle of the free edge case. This observation leads to the assumption that the volume due to the displace shape is directly related to the added mass.

Considering the infinite axisymmetric plate, the resulting displaced shape, shown in the previous chapter in Figure 4-10, may be interpreted as a free edge case in a mode with one nodal circle that has a radius equivalent to the effective radius listed in Table 4-1. This leads to the assumption that the fluid inertia will essentially contribute an added mass equivalent to:

$$m_f = \tfrac{2}{3}\pi\rho_f r_{eff}^3 \tag{5-24}$$

This assumption takes care of the total magnitude of this mass but distribution has not been addressed. The most likely application would be to distribute this mass in kind with the displaced shape, especially since this relates directly to the relative amount of fluid being moved at any one place.

The volume distributed by the shape function will be equivalent to that associated with a hemisphere of radius, r_{eff}. Thus, the unit shape function volume must be multiplied by an amplitude which will equate the total volume to the hemisphere as follows:

$$A_s r_{eff} \int_0^{2\pi}\int_0^\infty \frac{w(r)}{w_0} r\,dr\,d\theta = \tfrac{2}{3}\pi\, r_{eff}^3 \tag{5-25}$$

where $A_s r_{eff}$ is the amplitude required. Solving the above integral for both remaining shapes (4-33 a&b) gives the following definition for A:

$$A_s = \tfrac{2}{3}\frac{c^2}{l^2}r_{eff}^2 \tag{5-26}$$

where c, as well as r_{eff}, is defined for each shape function in Table 4-1. The amplitude, $A_s r_{eff}$, to apply for the shape functions individually is for (4-33a):

$$\tfrac{9}{32}\pi^3 l\sqrt[4]{\frac{4(1+2\ln 2)}{3}} \approx 11.65\, l \tag{5-27a}$$

and for (4-33b):

$$\tfrac{2}{3}(-\ln 0.01)^{3/2} l\sqrt[4]{8} \approx 11.08\, l \tag{5-27b}$$

Note that this amplitude is a function of the characteristic length of the plate. Distribution of the added mass due to the fluid inertia, M_f, with respect to the plate mass, M_p, for both shape

functions is demonstrated in Figure 5-3 with a range of plots covering the possible span of l/h values. Also note that, as mentioned earlier, the density ratio of seawater to floating ice is very near 1:1, thus, the multiplier $\rho_f/\rho_p \approx 1$ and may essentially be ignored for comparative purposes.
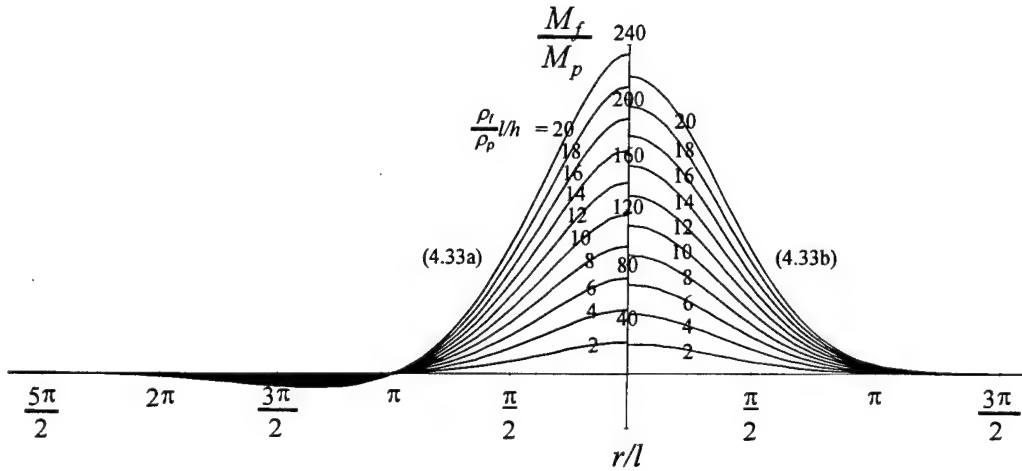
Figure 5-3. Distribution of the Mass Ratio (fluid to plate) for Two Shape Functions.

It is significant to note at this point that additional inertia from fluid interaction will also be applied to the impacting structure. Assuming a strict cylindrical cross section, the additional mass would be essentially equal to the actual mass, therefore giving an effective mass of $2M_s$. However, the point of impact is rarely at the mass center of the structure, depending on the location of the sail. Therefore, this new effective mass, $2M_s$, will be lessened because of the rotational effect of an eccentric loading. The acceleration at the impact point is equal to the tranlational plus rotational effect on the central mass, as follows:

$$\text{acceleration} = \frac{P}{M_{eff}} = \frac{P}{2M_s}\left(1 + \frac{e_c^2}{r_p^2}\right) \tag{5-28}$$

Where, e_c is the distance from the mass center to the impact point, which varies from submarine to submarine. However, for the purpose of this study, it appears that this distance can be estimated between 1/6 to 1/4 of the total length. Now r_p is the rotational radius of the submarine and is equivalent to 1/4 of the total length. Thus, with these two values, (5-28) gives an effective mass at the impact point of:

$$M_{eff} = \frac{2M_s}{1 + \frac{e_c^2}{r_p^2}} \quad \Rightarrow \quad M_{eff} = 1.38M_s \text{ to } M_s \tag{5-29}$$

Therefore, the effective mass of the submarine is essentially equal to the original mass, M_s, and will thus be used as such for the remainder of the study.

The kinetic energy due to the foundation may be obtained with the use of (5-11) and the assumptions made for the added mass due to fluid inertia. Therefore, the foundation kinetic energy may be expressed as follows:

$$E_{Kf(max)} = \tfrac{1}{2} \int_0^{2\pi}\int_0^{\infty}\left(\rho_f A_s r_{eff}\,\frac{w(r)}{w_0}\right)\left(\omega_{Rn}w(r)\right)^2 r\,dr\,d\theta \tag{5-30a}$$

which may be simplified as:

$$E_{Kf(max)} = \rho_f \pi\,\frac{A_s r_{eff}}{w_0}\,\omega_{Rn}^2 \int_0^{\infty} w^3(r)r\,dr \tag{5-30b}$$

A comparison of the kinetic energy due to the fluid inertia, E_{Kf}, and the plate inertia, E_{Kp}, is shown in Figure 5-4 for both shape functions (4-33a&b) with respect to the possible span of l/h values. Although there is a noticeable difference in the mass magnitude and distribution for each shape function, very little difference is found in the kinetic energy comparison. Thus, the effect of the specific application of the added mass is lessened when integrated over the infinite expanse of the plate.
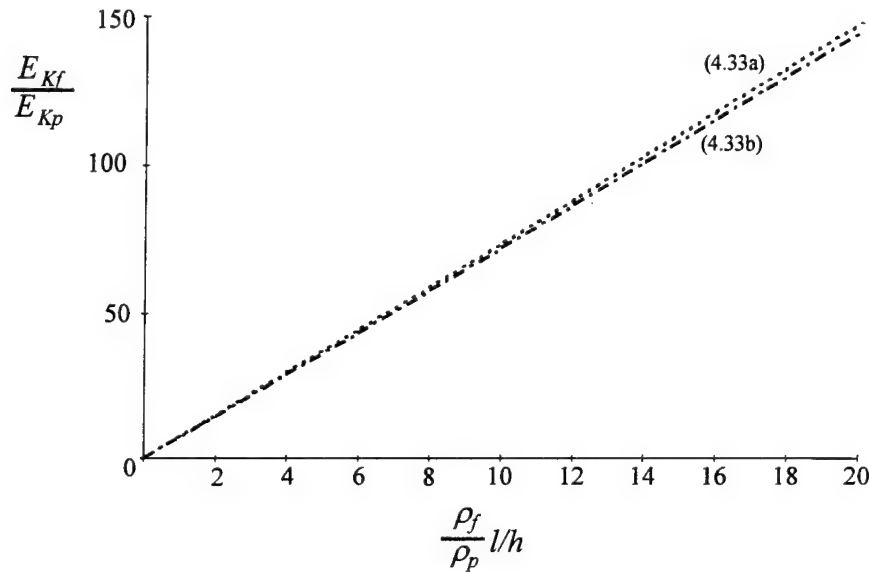
Figure 5-4. Comparison of the Kinetic Energy Contribution (fluid to plate).

The system fundamental frequency can now be obtained by using the principle of conservation of energy (5-7) and equating the maximum potential energy (5-9) to the maximum kinetic energy, found by combining both (5-12) and (5-30). This results in the following:

$$\omega_{Rn} = \sqrt{\frac{2k}{\left(\rho_p h + B_s \rho_f l\right)}} \tag{5-31}$$

where B_s is a constant determined by the amplitude, (5-27), applied individually for each of the shape functions within the integration of (5-30). However, the difference in B_s between the two shape functions is found to be negligible, where, for (4-33a), $B_s \approx 7.385$, and, for (4-33b), $B_s \approx 7.387$. Thus, the fundamental frequency values found, with incorporation of the fluid inertia for each of the shape functions, are essentially equal.

A comparison of the total system fundamental frequency (5-31) to that found without considering the inertial effects of the fluid (5-13), is shown in Figure 5-5 with respect to the range of l/h. As expected, the fluid inertia lowers the fundamental frequency considerably, where larger l/h values correspond to a larger disparity between the mass contribution of the fluid and that of the plate.
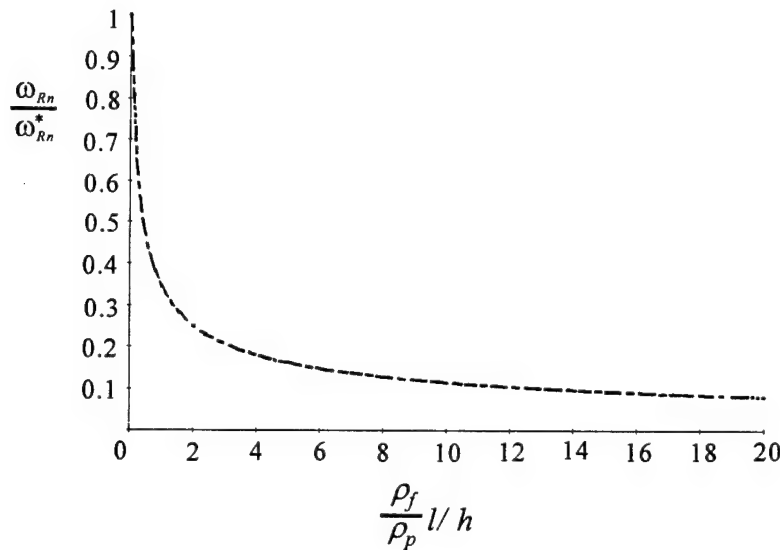
Figure 5-5. Comparison of Fundamental Frequency with and without Fluid Inertia.

Spring-Mass System Representation

The fundamental frequency (5-31) of the plate-fluid system obtained with the principle of conservation of energy may be equated to the circular frequency, ω_n, of the upper spring and mass found in Figure 5-1. This circular frequency, ω_n, may be defined by the equation [Craig, 1981]:

$$\omega_n = \sqrt{\frac{k_{pf}}{M_{pf}}} \tag{5-32}$$

Where k_{pf} may be defined by the static deformation as follows:

$$k_{pf} = \frac{P}{w_0} \tag{5-33}$$

Since the plate-fluid system has mass distributed along the radius, the effective mass value designated by M_{pf} will most likely be different than the total mass of the system. This value may be found by incorporating the fundamental frequency (5-31) and static spring stiffness (5-33) into the circular frequency equation (5-32), thus giving:

$$M_{pf} = \frac{k_{pf}}{\omega_n^2} = \frac{P\left(\rho_p h + B_s \rho_f l\right)}{2kw_0} \tag{5-34}$$

However, for comparative purposes, the effective mass may also be assumed equal to the mass of the hemispherical volume of fluid that was used as the added mass value for the kinetic energy. Thus equating M_{pf} to m_f from (5-20) and neglecting the plate mass because of its relatively small contribution. A comparison is shown in Figure 5-6 between the effective mass (5-34) found knowing stiffness and frequency and the fluid mass from the hemispherical volume (5-24).
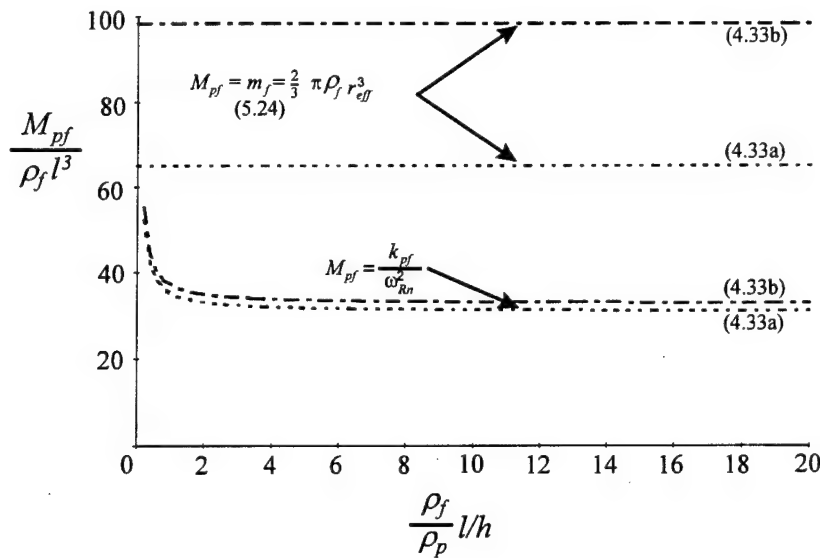
Figure 5-6. Comparison of Two Definitions for the Effective Plate-fluid Mass.

The mass, M_{pf} has been nondimensionalized with respect to the quantity $\rho_f l^3$ to facilitate the comparison. The figure also includes values found for both shape functions (4-33a&b). Use of these two different shape functions illustrates the sensitivity that exists between the two possible definitions for the effective mass. There exists a great disparity between the values when the lumped hemispherical fluid volume mass is used. This big contrast is due to the variance of the effective radius between the two shape functions. However, when this volume is distributed for the kinetic energy and then found with the resulting natural frequency, the values are much more consistent regardless of the shape function. There is less than a 6% difference between the effective mass for each of the shape functions found from the circular frequency. The consistency between these shape functions supports the argument that the static solution from (4-24) would be within a 10% range of these two shape functions.

A comparison may also be made between two methods of defining the stiffness, k_{pf}, for the plate-fluid system. The stiffness will most likely be defined as in (5-33). However, if the mass were assumed to be lumped and equal to the value of (5-24), then the stiffness could be found from the circular frequency equation (5-32) with that mass and the system natural frequency (5-31). These two definitions for stiffness are shown in Figure 5-7, where k_{pf} is nondimensionalized by the value kl^2. With the use of both shape functions (4-33a&b), the effect of lumping the mass from a hemispherical volume of fluid is again found to create a much greater disparity. The static stiffness values (5-33) for each shape function (4-33a&b) are only 5% and 11% different from that found for static solution (4-24).
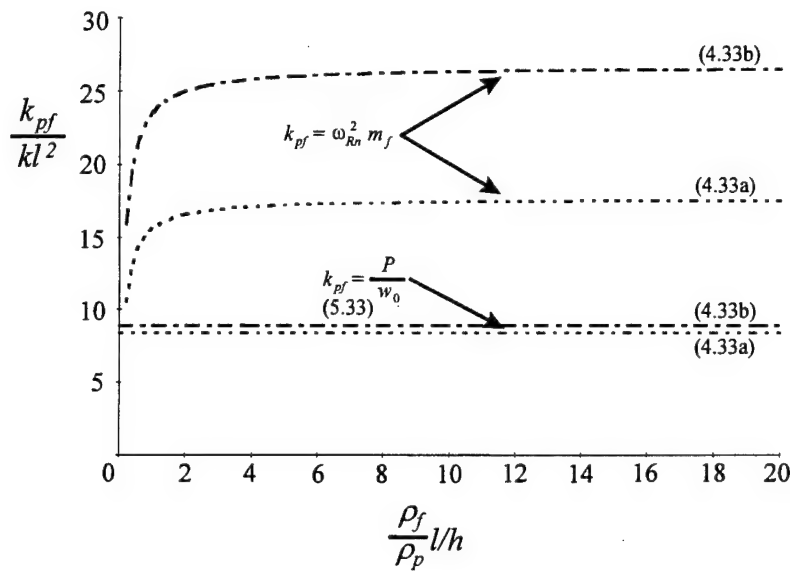
Figure 5-7. Comparison of Two Definitions for the Plate-fluid Stiffness.

A comparison similar to that for mass and stiffness may also be shown for the natural frequency, ω_{Rn}, of the plate-fluid system. The frequency found by the principle of conservation of energy (5-31) may be compared to values found using the circular frequency equation (5-32) incorporating the static stiffness (5-33) and lumped mass (5-24). The comparison of these two definitions is shown in Figure 5-8. The square of the system natural frequency, ω_{Rn}^2, is nondimensionalized by the value, $2g/l$, in which g denotes the acceleration due to gravity. The effect of the lumped mass is again clearly demonstrated by a wide margin between the results of the two different shape functions. The values found from (5-31) for each shape function are indistinguishable.
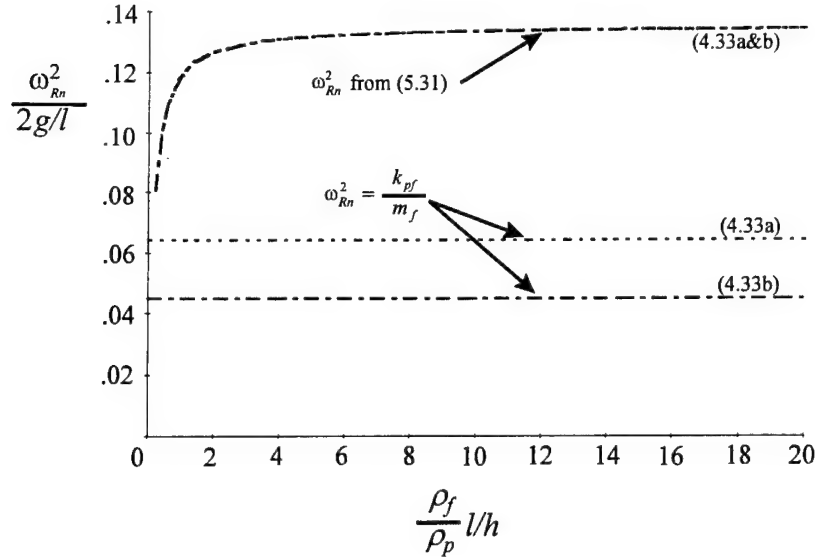
Figure 5-8. Comparison of Two Definitions for the Plate-fluid Fundamental Frequency.

These extensive comparisons for the plate-fluid elements of the spring-mass system lead firmly to the conclusion that (5-33) and (5-34) should define the stiffness, k_{pf}, and mass, M_{pf}, respectively. Recall that the stiffness, k_s, shown in Figure 5-1 associated with the impact structure, will be neglected as a result of the quick assessment made early in this chapter. Essentially, the series combination (5-1) of the two springs, k_l and k_s, may be estimated with $k_{ls} \approx k_l$, because of the assumption that $k_l \ll k_s$. Thus, the remaining element of the spring-mass system to be determined is the stiffness, k_l, associated with the local plate deformation.

The impact force, P, and contact deformation, α, relationship during impact of two bodies of revolution is given by the Hertz law [Goldsmith, 1960]:

$$P = \eta \alpha^{3/2} \tag{5-35}$$

where η is the contact stiffness parameter, which depends on material and geometrical properties of the plate and the impact structure. The expression for η, for a spherical isotropic impact structure and isotropic plate is given by [Conway, 1956]:

$$\eta = \frac{4\sqrt{R_s}}{3\pi\left(K_s + K_l\right)} \tag{5-36}$$

where

$$K = \frac{1 - v^2}{\pi E} \tag{5-37}$$

and R_s is the radius of the spherical contact area of the impact structure. The equation for K in (5-37) corresponds to the impact structure, K_s, and the local plate area, K_l, with incorporation of their respective constants E and v.

The contact stiffness parameter, η, may be simplified further by comparing the two values for K. Since the Poisson's ratio values will be essentially the same for both participants, the comparison falls to that of the Young's modulus, where E values for the bottom of the plate will be on the order of 200 times less than that found for the potential impact material. As such, $K_l \gg K_s$, which allows the impact structure value, K_s, to be neglected in (5-36).

With a nonlinear local displacement relationship (5-35), the solution for the displacement as a function of time with coupled equations of motion will be difficult. A numerical integration technique, such as Adam's, will be required; as well as actual values for most, if not all, of the parameters involved. Thus, a simple nondimensional parametric view will be impossible. Two alternatives to the current situation are:

1. approximate the local deformation with a linear relationship and continue with the two degree of freedom spring-mass system, or

2. determine the maximum displacement response with an energy-balance method that maintains the nonlinear local displacement relationship [Shivakumar et al., 1985].

Each of these alternatives will be performed such that the effect of the linear approximation utilized in the first may be compared to the accepted nonlinear relationship of the second.

An approximate linear relationship for local deformation may be borrowed from the example of an absolutely rigid die in the form of a circular cylinder pressed against the plane boundary of a semi-infinite elastic solid [Timoshenko and Goodier, 1970]. In such a case, the displacement, w, is constant over the circular base of the die and is given by:

$$w = \frac{P(1 - v^2)}{2a_d E_l} \tag{5-38}$$

in which P is the total load on the die, a_d is the radius of the die, and E_l is the local modulus of the plate. Using this behavior, the local stiffness, k_l, may be obtained from the ratio of the total load to displacement as follows:

$$k_l = \frac{2a_d E_l}{(1 - v^2)} \tag{5-39}$$

With this linear relationship, the couple equations of motion for the plate-impact structure system may be solved very simply.
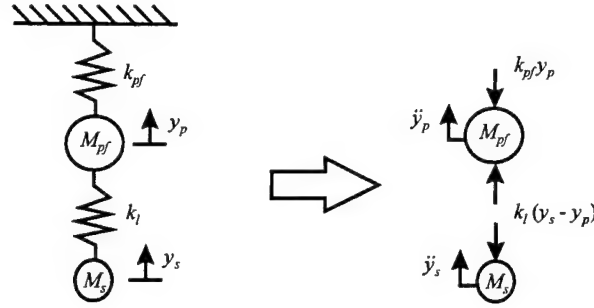
Figure 5-9. Force Equilibrium of Masses for a Two Degree-of-Freedom System.

Equations of motion for a two degree-of-freedom spring-mass system may now be derived and solved with the linear local deflection stiffness (5-39). To obtain the solution for free vibrations, the force equilibrium of masses, as shown in Figure 5-9, must be satisfied. The applicable coupled equations of motion are:

$$M_{pf}\ddot{y}_p + k_{pf}y_p - k_l(y_s - y_p) = 0$$
$$M_s\ddot{y}_s + k_l(y_s - y_p) = 0$$

(5-40)

With an assumed harmonic solution of the form:

$$y_p = Y_p \cos(\omega t - \theta)$$
$$y_s = Y_s \cos(\omega t - \theta)$$

(5-41)

and substitution of (5-41) into (5-40) gives the algebraic eigenvalue problem:

$$-\omega^2 Y_p M_{pf} + Y_p k_{pf} - k_l(Y_s - Y_p) = 0$$
$$-\omega^2 Y_s M_s + k_l(Y_s - Y_p) = 0$$

(5-42a)

These coupled equations may also be arranged in matrix form:

$$\begin{bmatrix} -\omega^2 M_{pf} + k_{pf} + k_l & -k_l \\ -k_l & -\omega^2 M_s + k_l \end{bmatrix} \begin{bmatrix} Y_p \\ Y_s \end{bmatrix} = \begin{bmatrix} 0 \\ 0 \end{bmatrix}$$

(5-42b)

The only nontrivial solution of this set of homogeneous linear algebraic equations corresponds to the values of ω^2, which satisfy the characteristic equation; that is, for which the determinant of the first matrix is equal to zero. Therefore, the resulting two roots of this polynomial equation of order two in ω^2 determines the squares of the plate-impact structure system natural frequencies:

$$\omega_{1\&2}^2 = \frac{k_l M_{pf} + M_s(k_l + k_{pf}) \pm \sqrt{(k_l M_{pf} + M_s(k_l + k_{pf}))^2 - 4k_l k_{pf} M_{pf} M_s}}{2M_{pf} M_s}$$

(5-43)

The natural mode, or mode shape, corresponding to each value of (5-43) may be found by substitution of these values back into the original equations (5-42) and solving for the ratio of the deflections:

$$\frac{Y_s}{Y_p} = \beta_{1\&2} = \tfrac{1}{2}\left[1 + \frac{k_{pf}}{k_I} - \frac{M_{pf}}{M_s} \mp \sqrt{1 + 2\left(\frac{M_{pf}}{M_s} + \frac{k_{pf}}{k_I}\right) + \left(\frac{M_{pf}}{M_s} - \frac{k_{pf}}{k_I}\right)^2}\,\right] \quad (5\text{-}44)$$

Where this is the basic result, note that mode shapes are highly dependent on the ratios of the participant stiffnesses and masses. It will be shown in the next chapter that the extremes, zero and infinity, of these ratios greatly simplified the results.

The general solution for the plate-impact structure system is a linear combination of the free vibrations that occur at the two natural frequencies (5-43) with each respective mode shape ratio (5-44). Using an alternate form of the general solution:

$$y_p = A_1 \cos \omega_1 t + B_1 \sin \omega_1 t + A_2 \cos \omega_2 t + B_2 \sin \omega_2 t + C_p$$
$$y_s = \beta_1 A_1 \cos \omega_1 t + \beta_1 B_1 \sin \omega_1 t + \beta_2 A_2 \cos \omega_2 t + \beta_2 B_2 \sin \omega_2 t + C_s \quad (5\text{-}45)$$

The initial conditions of the system determine the constants; A_1, B_1, A_2, B_2. A system with an initial velocity acting on the impact structure, where all other aspects are zero, have initial conditions that correspond to:

$$y_p(0) = 0 \qquad\qquad y_s(0) = 0$$
$$\dot{y}_p(0) = 0 \qquad\qquad \dot{y}_s(0) = V_i \qquad\qquad (5\text{-}46)$$
$$\ddot{y}_p(0) = 0 \qquad\qquad \ddot{y}_s(0) = \frac{F_b}{M_s}$$

The solution of the resulting four equations from these initial conditions (5-46) gives the following values for the constants of the general equation (5-45):

$$A_1 = \frac{F_b}{M_s \omega_1^2 (\beta_2 - \beta_1)} \qquad\qquad B_1 = \frac{V_i}{\omega_1 (\beta_1 - \beta_2)}$$
$$A_2 = \frac{F_b}{M_s \omega_2^2 (\beta_1 - \beta_2)} \qquad\qquad B_2 = \frac{V_i}{\omega_2 (\beta_2 - \beta_1)} \qquad (5\text{-}47)$$
$$C_p = \frac{F_b (\omega_2^2 - \omega_1^2)}{M_s \omega_1^2 \omega_2^2 (\beta_1 - \beta_2)} \qquad\qquad C_s = \frac{F_b (\omega_2^2 \beta_1 - \omega_1^2 \beta_2)}{M_s \omega_1^2 \omega_2^2 (\beta_1 - \beta_2)}$$

The displacements of each mass may now be defined as a function of time:

$$y_p = \frac{F_b}{M_s}\left[\frac{\omega_2^2(1 - \cos \omega_1 t) - \omega_1^2(1 - \cos \omega_2 t)}{\omega_1^2 \omega_2^2 (\beta_1 - \beta_2)}\right] + V_i\left[\frac{\omega_2 \sin \omega_1 t - \omega_1 \sin \omega_2 t}{\omega_1 \omega_2 (\beta_1 - \beta_2)}\right]$$
$$y_s = \frac{F_b}{M_s}\left[\frac{\omega_2^2 \beta_1(1 - \cos \omega_1 t) - \omega_1^2 \beta_2(1 - \cos \omega_2 t)}{\omega_1^2 \omega_2^2 (\beta_1 - \beta_2)}\right] + V_i\left[\frac{\omega_2 \beta_1 \sin \omega_1 t - \omega_1 \beta_2 \sin \omega_2 t}{\omega_1 \omega_2 (\beta_1 - \beta_2)}\right] \quad (5\text{-}48)$$

The impact force that is imparted globally on the plate-fluid system and the local force on the impact structure may each be found through the following relationships:

$$P_{pf} = k_{pf} y_p$$
$$P_s = k_l \left(y_s - y_p \right)$$

$$(5\text{-}49)$$

However, this formulation ignores the nonlinear effect of the local crushing, which should be evaluated in some manner to check the feasibility of using the linear approximation.

An energy-balance method is an alternate straightforward approach to determine the maximum displacement response for the given system with an initial velocity. Based on the principle of conservation of total energy of the plate-impact structure system, the kinetic and potential energy of the impacting mass is equated to the sum of the energies due to contact and bending deformations. Shear and membrane deformations will be neglected, as well as, the energy losses from material damping, surface friction, and higher mode vibrations [Rayleigh, 1906].

The maximum kinetic energy of the impact structure before contact, at t = 0, is:

$$E_{Ks} = \tfrac{1}{2} M_s V_i^2 \qquad (5\text{-}50)$$

The initial potential energy corresponds to the buoyant force of impact structure and the maximum distance traveled to the peak plate deflection, y_m:

$$E_{Ps} = F_b \left(y_{pm} + \alpha \right) \qquad (5\text{-}51\text{a})$$

Substitution for F_b as a fraction of M_s (5-5), as well as, α as a function of P from (5-35), gives:

$$E_{Ps} = 0.000433\, g M_s \left[y_{pm} + \left(\frac{P}{\eta} \right)^{2/3} \right] \qquad (5\text{-}51\text{b})$$

After t = 0, the plate-impact structure system undergoes contact and bending deformations, where the corresponding stored deformation energies are E_c and E_b, respectively. The contact energy, E_c, is the integral of the product of the impact force and contact deformation:

$$E_c = \int_0^\alpha P\, d\alpha \qquad (5\text{-}52\text{a})$$

The impact force, P, is replaced by the function α from (5-35). Following integration and simplification, the contact energy, E_c, becomes:

$$E_c = \frac{2 P^{5/3}}{5 \eta^{2/3}} \qquad (5\text{-}52\text{b})$$

The energy due to bending deformation is the integral of the impact force with respect to the plate deflection:

$$E_b = \int_0^{y_{pm}} P\, dy_p \qquad (5\text{-}53\text{a})$$

where P may be substituted with $k_{pf}y_p$. Integration then leads to the following expression for bending energy:

$$E_b = \tfrac{1}{2} k_{pf} y_{pm}^2 \qquad (5\text{-}53b)$$

Applying the principle of conservation of total energy, the energy-balance equation of the plate-impact structure system equates the sum of (5-50) and (5-51) with (5-52) and (5-53). When the impact load, P, is replaced with $k_{pf}y_{pm}$ in all places, the energy-balance equation becomes:

$$\tfrac{1}{2} M_s V_i^2 + 0.00625 M_s \left[y_{pm} + \left(\frac{k_{pf} y_{pm}}{\eta} \right)^{2/3} \right] = \frac{2 k_{pf}^{5/3} y_{pm}^{5/3}}{5 \eta^{2/3}} + \tfrac{1}{2} k_{pf} y_{pm}^2 \qquad (5\text{-}54)$$

The deflection, y_{pm}, may be found by solving (5-52), using a numerical technique like Newton-Raphson [Carnahan et al., 1969]. Then the impact force, P, is calculated by multiplying the value of y_{pm} by the stiffness of the plate-fluid system.

However, this solution method assumes that both the masses are in phase with each other until the maximum displacement is obtained and also ignores the inertial effects of the plate and fluid. In an attempt to rectify the inertial omission, a completely inelastic impact may be assumed, wherein both the impact structure and the plate-fluid system impulsively attain the same velocity immediately after contact. This will give a global impact force for the plate-fluid system.

This inelastic collision will, however, ignore the local crushing that occurs. Where the inertial effects will highly influence the maximum force on the plate-fluid system, the effect of local crushing will likely define the impact load applied to the impact structure. This will specifically be the case when there is a large discrepancy between the two masses, as will be shown in chapter five. Thus, this particular problem may be split into the two separate one-degree-of-freedom systems, shown in Figure 5-10, as follows:

1. Inelastic collision, addressing the maximum force applied to the plate-fluid system, and

2. Local crushing, addressing the maximum force applied to the impact structure.

a. Inelastic collision   b. Local crushing
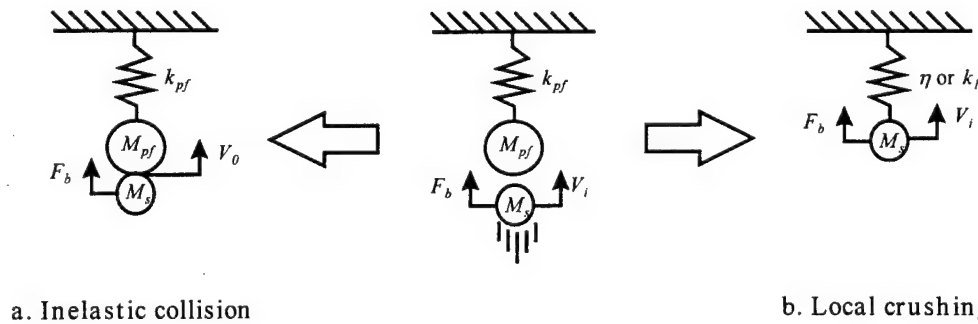
Figure 5-10. Separation into: a. Inelastic Collision and b. Local Crushing.

An inelastic collision occurs when the impacting bodies stick together and move as a unit after contact, Figure 5-10a. This occurrence is one extreme of a process based on the conservation of momentum, Newton's third law. This principle maintains that whenever there is a force of interaction between two particles, the momentum of each particle is changed as a result of the force exerted on it by the other. The vector change in momentum of either particle is equal in magnitude and opposite in direction to the vector change in momentum of the other. Hence, the net change in momentum of the system is zero. As such, the conservation of momentum is given as:

$$m_a v_{a1} + m_b v_{b1} = m_a v_{a2} + m_b v_{b2} \qquad (5\text{-}55)$$

In the extreme case of an inelastic collision, the effective mass becomes a sum of the two colliding bodies, $M_{pf} + M_s$, and the resulting velocities, v_{a2} and v_{b2}, of (5-55) are equal. For the additional special circumstance in which one mass, M_{pf}, is initially at rest, the resulting velocity is defined as follows:

$$V_0 = \frac{M_s V_i}{M_{pf} + M_s} \qquad (5\text{-}56)$$

This will be used as the initial velocity condition for the inelastic formulation.

The equation of motion for the inelastic system is as follows:

$$\left(M_{pf} + M_s \right) \ddot{y}_p + k_{pf} y_p = 0 \qquad (5\text{-}57)$$

The solution of (5-57) for y_{ps} is accomplished by assuming the following form:

$$y_{ps} = C_1 + C_2 \cos \omega_{pfs} t + C_3 \sin \omega_{pfs} t \qquad (5\text{-}58)$$

where the system fundamental frequency, ω_{pfs}, may be defined by:

$$\omega_{pfs} = \sqrt{\frac{k_{pf}}{M_{pf} + M_s}} \qquad (5\text{-}59)$$

and applying the initial conditions:

$$y_{ps}(0) = 0$$
$$\dot{y}_{ps}(0) = V_0 \qquad (5\text{-}60)$$
$$\ddot{y}_{ps}(0) = \frac{F_b}{M_{pf} + M_s}$$

defines the constants, C_1, C_2, and C_3 as follows:

$$C_1 = -C_2 = \frac{F_b}{k_{pf}},$$
$$C_3 = \frac{V_0}{\omega} = \frac{V_i M_s}{\sqrt{k_{pf} \left(M_{pf} + M_s \right)}} \qquad (5\text{-}61)$$

Thus, the inelastic formulation for y_p is achieved from incorporating the definitions for the constants (5-61), as well as, the fundamental frequency (5-59) into (5-58), giving:

$$y_{ps} = \frac{F_b}{k_{pf}}\left(1 - \cos\sqrt{\frac{k_{pf}}{M_{pf} + M_s}}t\right) + \frac{V_i M_s}{\sqrt{k_{pf}\left(M_{pf} + M_s\right)}}\sin\sqrt{\frac{k_{pf}}{M_{pf} + M_s}}t \qquad (5\text{-}62)$$

The impact force, P_{pfs}, imparted on the inelastic system may be obtained by multiplying this formulation by k_{pf}.

Local crushing effects may be addressed by assuming the plate-fluid system is so massive compared to the impact structure that it essentially acts as the fixed ground. See Figure 5-10b. There are two cases that may be addressed for this scenario with respect to the crushing stiffness; Hertz contact (5-35&36) and linear approximation (5-38&39).

The Hertz contact case of a sphere against a massive plane of contact has been solved [Goldsmith, 1960] where the maximum deflection, $\alpha_{H(max)}$, is defined as:

$$\alpha_{H(max)} = \left(\frac{15\pi V_i^2 K_l M_s}{16\sqrt{R_s}}\right)^{2/5} \qquad (5\text{-}63)$$

The maximum impact force can then be formulated by substituting (5-63) into (5-35), which gives:

$$P_{sH(max)} = \left(\frac{125 V_i^6 M_s^3 R_s}{36\pi^2 K_l^2}\right)^{1/5} \qquad (5\text{-}64)$$

Note that this formulation neglects the buoyant force of the impacting structure.

The linear approximation for local deformation (5-38&39) used in the earlier two degree-of-freedom system may be applied for this one degree-of-freedom system as well. The solution of this local crushing one degree-of-freedom system follows the same general steps as for the inelastic collision. The equation of motion for the system in Figure 5-10b may be expressed as:

$$M_x \ddot{\alpha}_l + k_l \alpha_l = 0 \qquad (5\text{-}65)$$

The assumed form for α_l is the same as for y_{ps} in (5-60) as follows:

$$\alpha_l = C_1 + C_2 \cos\omega_{lc}t + C_3 \sin\omega_{lc}t \qquad (5\text{-}66)$$

where the local crushing system's fundamental frequency is defined by:

$$\omega_{lc} = \sqrt{\frac{k_l}{M_s}} \qquad (5\text{-}67)$$

The constants in (5-66) are determined by the initial conditions, which are:

$$\alpha_l(0) = 0$$
$$\dot{\alpha}_l(0) = V_i \qquad (5\text{-}68)$$
$$\ddot{\alpha}_l(0) = \frac{F_b}{M_s}$$

Thus the constants for (5-66) become:

$$C_1 = -C_2 = \frac{F_b}{k_l}, \quad C_3 = \frac{V_i}{\omega_{lc}} = V_i \sqrt{\frac{M_s}{k_l}} \tag{5-69}$$

Therefore, assembling the following definition for α_l assuming linear deformation:

$$\alpha_l = \frac{F_b}{k_l}\left(1 - \cos\sqrt{\frac{k_l}{M_s}}t\right) + V_i\sqrt{\frac{M_s}{k_l}}\sin\sqrt{\frac{k_l}{M_s}}t \tag{5-70}$$

where the force imparted on the impact structure may be found by the following:

$$P_{sl} = k_l\alpha_l = F_b\left(1 - \cos\sqrt{\frac{k_l}{M_s}}t\right) + V_i\sqrt{k_l M_s}\sin\sqrt{\frac{k_l}{M_s}}t \tag{5-71}$$

The maximum values for both the linear deformation (5-70) and impact force (5-71) may then be compared to the respective values found by the nonlinear Hertz contact solution (5-63&4) to evaluate the effect that this linear approximation has on the two degree-of-freedom system.

The conclusion of the dynamic formulation is highlighted by proposing two separate sets of equations to model a submarine impacting the underside of an ice floe. The first set of equations is the result of a two degree-of-freedom spring-mass system that incorporates an approximation for linear local deformation. The maximum impact forces will be found from (5-49) with the appropriate substitution for the displacements (5-48), which in turn requires the natural frequencies (5-43) and mode shapes (5-44).

The second set of equations evolved from splitting the original spring-mass system into two separate one degree-of-freedom systems as shown in Figure 5-10, with the caveat that there will be a huge disparity between the masses and springs of the system. One of these separate systems models the impact force imparted globally upon the plate-fluid system as an inelastic collision with the impact structure. The deflection of this inelastic system is found with (5-62), which may be multiplied by the plate-fluid stiffness, k_{pf}, to obtain the global impact force.

The other one degree-of-freedom system assumes the plate-fluid system is so massive that it becomes the ground against which the local crushing completely influences the impact force imparted upon the impact structure. This local crushing is modeled by both a nonlinear Hertzian contact, which ignores the buoyancy force of the impacting structure, and by using the linear local deformation approximation incorporated in the two degree-of-freedom spring-mass system which does include the buoyancy force. The maximum impact force acting on the impact structure may be found from both these models and compared to evaluate the difference between the Hertz contact solution (5-64) and the linear approximation (5-71). The maximum deformation imparted on the underside of the ice plate may also be compared between the Hertz contact solution (5-63) and the linear approximation (5-70).

Chapter 6

Parametric Effects

The formulations that have been made in the past two chapters have included a number of parameters that vary a great deal. The significance of the variation for each of these parameters is important to note, such that future attention to detail may be placed in the appropriate channels. This chapter begins with a review of the formulations to extract the system components, each of which will then be broken down into the most basic parameters to study.

After listing the range for each basic parameter, another review of the formulations will be required to discern how the basic interaction and/or comparison of each of these parameters may simplify the proceedings. Following simplification, each formulation will be broken down into the various sinusoidal parts. The amplitude and frequency of each of these parts will be observed to distinguish the leading contributor and determine the maximum impact force from each set of equations.

The parameters contributing to this maximum impact force will be highlighted and the effect that the range of variation for each will be quantified. This quantification will help to qualify the significance of each of the parameters to the maximum impact force, such that future design or maneuvers may be adjusted accordingly.

Parametric Breakdown of the Proposed Formulations

The two separate sets of dynamic formulations that have been proposed for modeling a submarine impacting the underside of an ice floe are listed in Table 6-1. The first set is the result of modeling the entire phenomena by a two degree-of-freedom spring-mass system. Expressions are listed for both impact forces imparted each on a separate spring-mass subsystem. These forces represent the global loading on the plate-fluid subsystem, P_{pf}, and the general loading on the impact structure, P_s, which may also be thought of as a localized load on the underside of the plate. Each of these forces is a simple function of the applicable spring stiffness and a deflection. The two different springs are represented; one by the stiffness of the infinite plate on an elastic foundation, k_{pf}, and the other associated with crushing due to contact, k_l, which is a stiffness obtained by a linear approximation for this model.

Table 6-1. Formulations for the Impact Model.

2 degree-of-freedom system: $P_{pf} = k_{pf} y_p$ & $P_s = k_l(y_s - y_p)$

$$y_p = \frac{F_b}{M_s}\left[\frac{\omega_2^2(1 - \cos\omega_1 t) - \omega_1^2(1 - \cos\omega_2 t)}{\omega_1^2\omega_2^2(\beta_1 - \beta_2)}\right] + V_i\left[\frac{\omega_2 \sin\omega_1 t - \omega_1 \sin\omega_2 t}{\omega_1\omega_2(\beta_1 - \beta_2)}\right]$$

$$y_s = \frac{F_b}{M_s}\left[\frac{\omega_2^2\beta_1(1 - \cos\omega_1 t) - \omega_1^2\beta_2(1 - \cos\omega_2 t)}{\omega_1^2\omega_2^2(\beta_1 - \beta_2)}\right] + V_i\left[\frac{\omega_2\beta_1 \sin\omega_1 t - \omega_1\beta_2 \sin\omega_2 t}{\omega_1\omega_2(\beta_1 - \beta_2)}\right]$$

$$\omega_{1\&2}^2 = \frac{k_l M_{pf} + M_s(k_l + k_{pf}) \pm \sqrt{(k_l M_{pf} + M_s(k_l + k_{pf}))^2 - 4k_l k_{pf} M_{pf} M_s}}{2M_{pf} M_s}$$

$$\frac{Y_s}{Y_p} = \beta_{\&2} = \tfrac{1}{2}\left[1 + \frac{k_{pf}}{k_l} - \frac{M_{pf}}{M_s} \mp \sqrt{1 + 2\left(\frac{M_{pf}}{M_s} + \frac{k_{pf}}{k_l}\right) + \left(\frac{M_{pf}}{M_s} - \frac{k_{pf}}{k_l}\right)^2}\right]$$

Inelastic collision: $P_{pfs} = k_{pf} y_{ps}$

$$y_{ps} = \frac{F_b}{k_{pf}}\left(1 - \cos\sqrt{\frac{k_{pf}}{M_{pf} + M_s}}t\right) + \frac{V_i M_s}{\sqrt{k_{pf}(M_{pf} + M_s)}}\sin\sqrt{\frac{k_{pf}}{M_{pf} + M_s}}t$$

Local Crushing:

Hertz contact   Linear approximation

$$P_{sH(max)} = \left(\frac{125 V_i^6 M_s^3 R_s}{36\pi^2 K_l^2}\right)^{1/5} \qquad P_{sl} = k_l\alpha_l = F_b\left(1 - \cos\sqrt{\frac{k_l}{M_s}}t\right) + V_i\sqrt{k_l M_s}\sin\sqrt{\frac{k_l}{M_s}}t$$

$$\alpha_{H(max)} = \left(\frac{15\pi V_i^2 K_l M_s}{16\sqrt{R_s}}\right)^{2/5} \qquad \alpha_l = \frac{F_b}{k_l}\left(1 - \cos\sqrt{\frac{k_l}{M_s}}t\right) + V_i\sqrt{\frac{M_s}{k_l}}\sin\sqrt{\frac{k_l}{M_s}}t$$

There is a separate transient expression for the deflection of each spring-mass combination. The central deflection of the infinite plate on an elastic foundation is represented by y_p and the vertical movement of the impact structure with respect to the initial contact point in space is represented by y_s. The local deformation into the bottom of the plate is represented by the difference between y_s and y_p. It is important to note that the expression for y_s, and subsequently P_s, is limited to the time required to achieve the maximum deformation due to crushing, since k_l is only valid for the initial crushing action.

The two natural frequencies of the system, ω_1 and ω_2, are basic components of the transient deflection expressions. The squares of each of these two values are linked by the same general expression with the difference being the addition or subtraction of the term found within the

square root. The addition of this term is associated with ω_1 and the subtraction with ω_2. It is important to keep this association straight since the shape functions, β_1 and β_2, are tied directly to a particular frequency. These values are also linked in the same general fashion of the frequencies. However, in this instance, β_1 is calculated by subtracting the associated square root term. The addition of the square root term determines the value for β_2.

The second set of equations evolved from splitting the original spring-mass system into two separate one degree-of-freedom systems with the caveat that there will be a huge disparity between the masses and springs within the model. One of these separate systems obtains the impact force imparted globally upon the plate-fluid system through an inelastic collision with the impact structure, thus ignoring the local contact effect on this global load. This force, P_{pfs}, is determined in the same general fashion as P_{pf} from the two degree-of-freedom system. However, while the spring stiffness, k_{pf}, is the same quantity, the deflection of the plate-submarine mass amalgam, y_{ps}, has a different expression. There is only one natural frequency associated with this system, thus simplifying the equation for the deflection.

The other one degree-of-freedom system assumes the plate-fluid subsystem is so massive that it becomes the ground against which the local crushing completely influences the impact force imparted upon the impact structure. Two sets of results are found for this system, representing two separate models of the local crushing phenomena. One set incorporates a nonlinear Hertzian contact representation of the local crushing effect. An expression is given for the maximum value of the impact force, $P_{sH(max)}$, as well as the maximum local deformation, $\alpha_{H(max)}$, due to the contact. The local contact was also modeled again by assuming a linear stiffness, k_l, associated with the local deformation. The force imparted on the impact structure, P_{sl}, obtained by the local deformation, α_l, and k_l for this model, may be more directly compared to the result of the two degree-of-freedom system, as well as the Hertz contact, thus, providing the link for an indirect comparison of the Hertz contact and the two degree-of-freedom system.

Table 6-2. Formulation Components.

$k_{pf} = 8Xkl^2$	$M_{pf} = 4Xl^2\left(\rho_p h + B\rho_f l\right)$
$k_l = \dfrac{2a_d E_l}{\left(1 - v^2\right)}$	$K_l = \dfrac{1 - v^2}{\pi E_l}$
$M_s = \dfrac{\Delta}{g}$	$V_i = 0 \Rightarrow 30 fpm \Leftrightarrow 120 fpm$
$F_b = 0.000433 g M_s$	$l = \sqrt[4]{\dfrac{Eh^3}{12k\left(1 - v^2\right)}}$
$X_a = \dfrac{\pi}{8}\sqrt{3(1 + 2\ln 2)} = 1.05$	$X_b = \dfrac{\pi}{\sqrt{8}} = 1.11$
$B_a = \dfrac{107\pi^3}{600}\sqrt[4]{\dfrac{4(1 + 2\ln 2)}{3}} = 7.385$	$B_b = 2^{3/4}\dfrac{4}{9}(-\ln 0.01)^{3/2} = 7.387$

The components of the formulations include the four basic items that compose the systems, two masses and the stiffness of each of the two springs, as well as the two externally acting components, the initial velocity and the buoyancy force of the impacting structure. These components are listed in Table 6-2 along with their equivalent parametric composition.

Both k_{pf} and M_{pf} contain the parameter X, which is representative of a constant associated with a specific shape function obtained in the static formulation. The composition of M_{pf} also includes B, which is another constant associated with a specific shape function. The constant quantities connected to the two shape functions that provided the best representation (3.33a&b), are both listed for each function with a subscript of a or b to indicate the appropriate association. Notice that there is vary little difference in each of the constants between the two functions. Therefore, the value associated with (3.33b) was used in the numerical evaluation to provide a simple and consistent approach in the upcoming comparisons.

Note that, since two different local crushing schemes were addressed, there is a difference between the K_l of the Hertz contact and k_l of the linear approximation. Each incorporates a localized value for Young's modulus, E_l, and the general Poisson's ratio, ν. However, where k_l is a stiffness, the value for K_l is associated only as a portion of the Hertz contact formulation.

The mass associated with a submarine, M_s, is not given directly. Thus, this component is obtained by the displacement value, Δ, given for a particular platform. The buoyancy force, F_b, may then be found either indirectly through M_s or directly from Δ.

The initial velocity component is a basic parameter by itself. The only specific value that has been found in open literature is 30 feet per minute. There is no indication how representative this particular value is for any specific platform, or for Arctic surfacing maneuvers in general. Therefore, some liberty will be taken, with this value in mind, to provide a more comprehensive comparison of the effect that an initial velocity has on the resulting loads and displacements. Thus, a range will be used in the upcoming comparison, beginning with essentially no initial velocity up to 120 fpm.

The characteristic length, l, is another parameter found in both k_{pf} and M_{pf}. However, this parameter is an item that represents the plate-fluid system in general, disregarding any specific shape function. The composition of this constituent may be further broken down into more basic parameters, as shown in Table 6-2.

The parameters that form the basis for the components, and in turn the formulations, are listed in Table 6-3. These specific values have been extracted from a variety of sources. A few of these parameters may be practically thought of as constants and have been assigned one value for the continued evaluation. There may exist some variation associated with these parameters, however the range is so small and/or the application insensitive enough that these particular quantities have been assigned just one value in this study. Two of these parameters are the foundation bulk modulus, k, which is represented in this study as the fluid specific weight, and the fluid density, ρ_f, each given values associated with seawater at 10°C and 3.3% salinity [Roberson and Crowe, 1980]. The value used for acceleration due to gravity is associated with the *standard station* [Sears, et al., 1977]. The plate density, ρ_p, is an average value used for sea ice that is found in many different sources and was also computed from available ice core data [Garrison, *et al*, 1987] [Wen, *et al*, 1989] [Wen, *et al*, 1992].

Table 6-3. Parameter Ranges.

$k = 64.1\,\mathrm{lbf/ft^3}$	$g = 32.174\,\mathrm{ft/s^2}$
$\rho_f = 1.99\,\mathrm{lbf}/\left(\mathrm{ft^3 - ft/s^2}\right)$	$\rho_p = 1.78\,\mathrm{lbf}/\left(\mathrm{ft^3 - ft/s^2}\right)$
$E_{\mathit{eff}} = 1\mathrm{GPa} \Leftrightarrow 5\mathrm{GPa}$	$E_l = 1\mathrm{GPa} \Leftrightarrow 0.01\mathrm{GPa}$
$h = 1\mathrm{ft} \Leftrightarrow 10\mathrm{ft}$	$v = 0.33,\,0.5$
$\Delta = 5,10,\,\mathrm{or}\,26\,\mathrm{kton}$	Beam $= 31, 40,\,\mathrm{or}\,79\,\mathrm{ft}$
$R_s = \frac{1}{2}\mathrm{Beam} \Rightarrow 15,\,20,\,\mathrm{or}\,40\,\mathrm{ft}$	$a_d = \frac{1}{10}\mathrm{Beam} \Rightarrow 3,\,4,\,\mathrm{or}\,8\,\mathrm{ft}$
$1\,\mathrm{kton} = 2240\,\mathrm{lbf}$	$1\mathrm{GPa} = 20.866\mathrm{x}10^6\,\mathrm{lbf/ft^2}$

Parametric values that are assigned ranges in the continued evaluation, relating specifically to the ice plate, are two different Young's moduli, E and E_l, thickness, h, and Poisson's ratio, v. In situ seismic determinations of E have been found [Weeks and Assur, 1967] to vary from 1.7 to 6-7 GPa when measured by flexural waves and from 1.7 to 9.1 GPa when determined by in situ body wave velocities. The smaller range measured by flexural waves are more applicable to this study, since the measurement style is controlled by the overall properties of the ice and the static formulation is based on the flexural deformation of the infinite plate in general.

There is variation in E throughout the thickness of ice. Although it has been determined acceptable to use an averaged value for the determination of the deflection surface, the value used for the general overall behavior of the plate does not do justice to the localized underside crushing that dominates the contact formulation. Profile properties of first-year sea ice [Cox and Weeks, 1986], as well as core sample measurements [Wen, et al, 1989], show distinctly that the last small percent of thickness, on the order of 10%, has drastically decreased property values. This is due to the occurrence of brine drainage channels [Lake and Lewis, 1970] [Niedrauer and Martin, 1979] that have been found on a horizontal spacing of 15 to 20 cm with a diameter of approximately 1 cm near the bottom of thick annual ice. Such features obviously affect the mechanical properties of the ice, as they are gross macroscopic flaws. Thus, a local Young's modulus, E_l, is used for the contact stiffness with values ranging from 1 GPa to 0.01 GPa.

Reports on ice forecasting have proved very useful in bracketing the ice thickness addressed in this study. The major source of ice thickness statistics available to date in the public domain for the entire Arctic Ocean and virtually the only source for the Siberian segment of the Arctic Ocean are from submarine sonar profiling. A detailed analysis of ice thickness distribution in the entire Arctic Ocean has been made based on 17 cruises of U.S. and British submarines between 1960 and 1982 [Bourke and Garrett, 1987]. A summary of several reports [Tunik, 1994] shows that the values of the mean ice thickness range from 3 to 13 feet with large standard deviations that range from 41 to 91 percent.

One particular study which used submarine sonar under-ice thickness profiles [McLaren, 1989], specifically categorized refrozen leads and/or polynya into "surfaceable areas" which involved up to and included 200 cm (approximately 6.5 ft) thick ice. In the same study, the mean thickness of level ice, defined as areas that vary less than 1 ft within a 33 ft radius, was up to 9 ft with a standard deviation of 2 ft in some sections. On the basis of these reports, a neat range of 0 to 10 ft was chosen for this study. However, when the thickness is plotted against a

log scale, the low end is limited to 1 ft, since values below that are most likely trivial in the interest of this study.

The specific range of the ratio of the plate characteristic length, l, to thickness, h, is an important quantity in qualifying the accurate application of thin plate theory, as mentioned in Chapter 2. The limitation was set for $l/h \geq 8$, where smaller values would suggest the need to include transverse and shear deformation when evaluating the plate reactions to transverse loads. Figure 6-1 shows the span of l/h with respect to the proposed ranges for both h and E. The Figure clearly shows that thin plate theory cannot be used for $h > 3$ ft. The effect on the results of this study will be addressed in the next chapter.

The effective Poisson's ratio, ν, for sea ice [Murat and Lainey, 1982] has been found to decrease with increasing stress rate and decreasing temperature. At very low stress rates the ratio tended to be the expected limit of 0.5 and at high stress rates the ratio tended to be 0.33, the dynamic or seismic value of Poisson's ratio for sea ice. A detailed examination of the theoretical effects of the vertical variation of ν through floating ice on the mechanical response of the sheet [Hutter, 1975] has indicated that, for many real problems, it is not necessary to consider such variations. Therefore, 0.33 will be used throughout the evaluation with an aside relating the percentage effect that a value of 0.5 would have on those results.
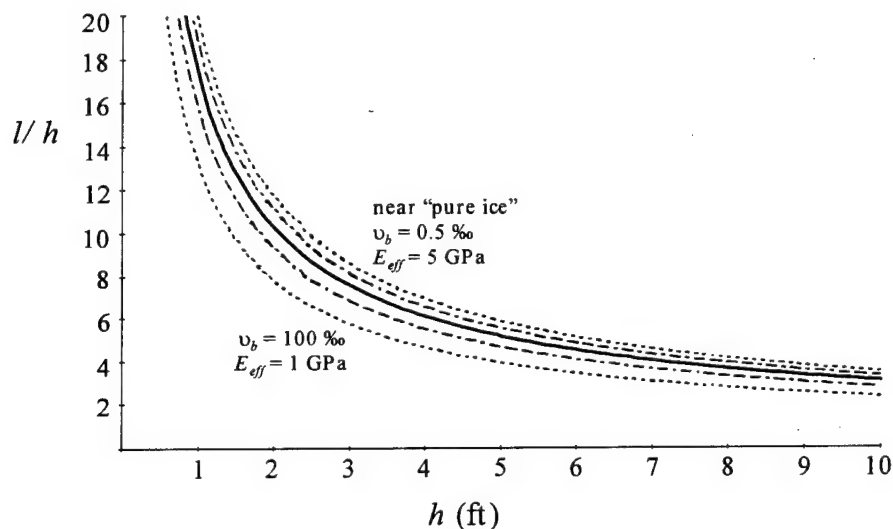
Figure 6-1. Ratio of the Plate's Characteristic Length to Thickness.

The impact structure, specifically a submarine in this study, has a few parameters that are associated with more discrete values. These values come from the various classes of submarines that have been cited in the literature as operating in the Arctic region. Of the specific classes cited as Arctic operational, three are from the U.S. Navy [Polmar, 1993], two are Russian [Jordan, 1989], and one is British [Jane, 1989-90]. The quantities for the displacement, beam, and overall length are listed in Table 6-4.

The Russian submarine, *Typhoon*, stands out distinctly within this group as the largest. The specific quantities for this particular submarine are therefore used to represent the high end of discrete values. Two other sets of discrete values are used in the ensuing evaluation, where each set generally represents a subgroup of the five remaining submarines. The low end of the

spectrum represents the improved *Los Angeles*, *Sturgeon*, and *Trafalgar*. The third set is geared more toward representation of the *Seawolf* and *Delta IV*.

Each submarine parameter is divided into small, medium, and large value that are also directly associated with each other. For example, the small Δ is associated with the small beam value that is used to estimate values for the local contact. Where the representative spherical radius for the Hertz contact solution, R_s, is estimated by a value associated with one-half of the beam quantity. The beam is a measure of the width of the submarine and, for most, is the diameter of the main cylindrical portion. Thus, the radius associated with this cylinder was used for R_s. The radius value, a_d, associated with k_l for the linear approximation is associated with the beam in an entirely different sense. This radius represents a flat circular area of contact, which is dependent on the width and length of the sail. These structures generally appear to be about a fifth of the overall beam; thus a_d was assigned the value of a tenth of the beam for each set of submarine parameters.

Table 6-4. Descriptive Quantities of Arctic Operational Submarines.

Submarine Class	Displacement (ton)	Beam (ft.)	Overall length (ft.)
Seawolf	9150	40	350
Los Angeles (improved)	6927	33	360
Sturgeon	4780 & 4960	31	292 & 302
Typhoon	26000	79	558
Delta IV	13500	39	538
Trafalgar	5208	32	280

Note that the use of *ton* in all values in this study is associated with a "long" ton that is equivalent to 2240 lbs. Although it is inconsistent, the range of both E values for the ice are designated in metric units, GPa, because these are the units used in the community that studies these values. Therefore, it is more cognizant to represent the range in metric units, although all the calculations were done in foot-ton-second units.

Simplification of the Proposed Formulations

Comparison of actual values associated with the four basic items that compose the two degree-of-freedom system, k_{pf}, M_{pf}, k_l, and M_s, will demonstrate that the specific quantities of the particular application within this study turn it into a special case. The result of being a special case, where there are vast differences between the comparative components, is the extreme simplification of the fundamental frequencies, as well as the mode shapes.

The stiffness associated with the plate-fluid system, k_{pf}, is influenced by the ice thickness, h, to the 1.5 power and only by the square root of E, see Figure 6-2. The comparison of this stiffness to the local contact, k_l, shows a large contrast in values at the lower range of ice thickness, where, k_{pf} is less than 10% of k_l for $h < 4$ ft. See Figure 6-3. The largest value for this ratio is a little over $\frac{1}{3}$. Note that this comparison is for a local value of Young's modulus, E_l, of 0.1 GPa, which is slightly on the conservative end of the range available. Where $E_l = 1$ GPa, the values in Figure 6-3 would all be lowered by a factor of ten.
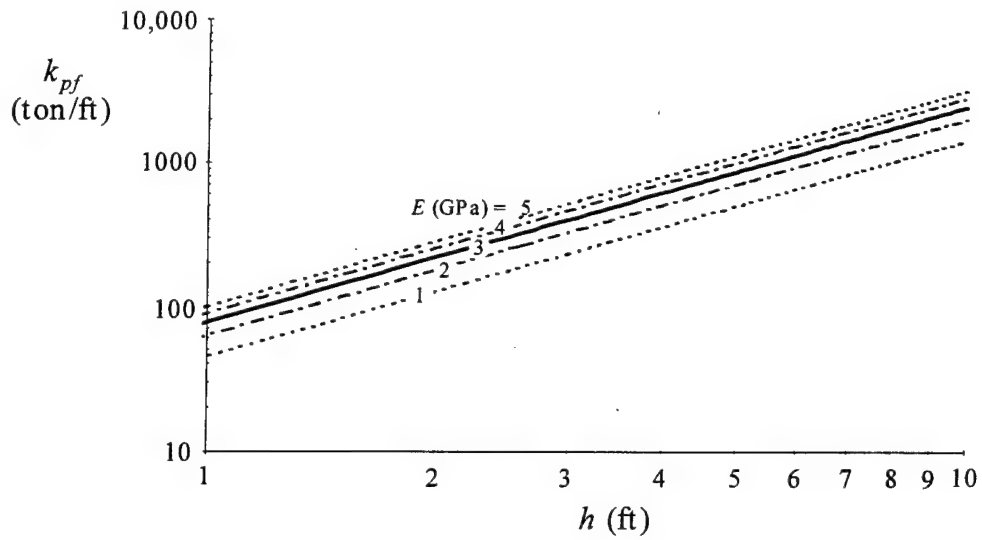
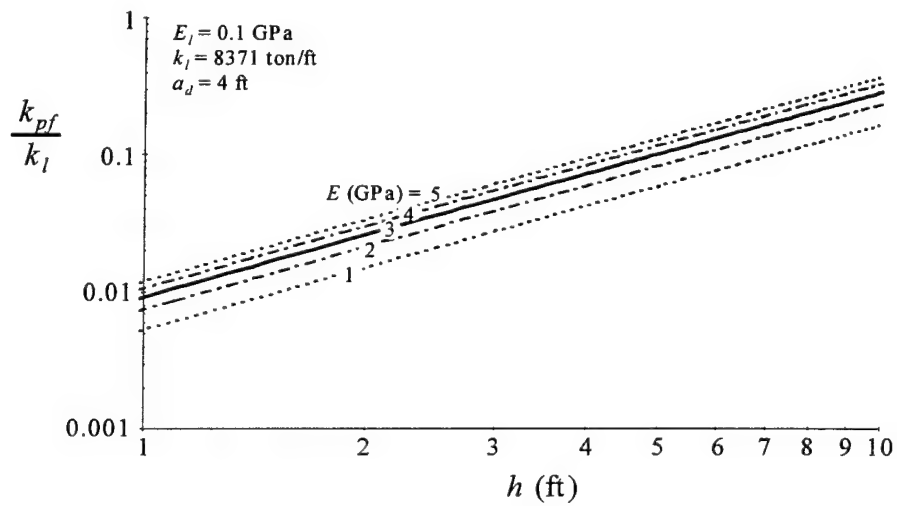Figure 6-2. Stiffness Range for the Plate-fluid System.

Figure 6-3. Comparison of the Plate-fluid Stiffness to that of Local Crushing.

The effective mass, M_{pf}, associated with the plate-fluid system is extremely large due to the "added mass" of the fluid inertia. The influences on M_{pf} are from the same sources as the aforementioned stiffness. See Figure 6-4. However, h has an even greater effect on M_{pf} with a power of more than 2, and the E influence is still under a power of 1, although more than a square root.

An extreme contrast is found when comparing the mass of a given submarine to the effective plate-fluid mass, M_{pf}, see Figure 6-5. Where this particular comparison is limited to a $\Delta = 10$ kton, these particular numbers need only be multiplied by the ratio of a given displacement to 10 kton to ascertain the specific values. However, there doesn't appear to be a submarine on earth that would overcome the odds that exist between M_{pf} and a given impact structure.

This extreme contrast between the masses of the two degree-of-freedom system, as well as the slightly large contrast between the stiffness values for both of the springs, vastly separates the reactions for each of the subsystems. As such, there are essentially two separate systems, as alluded during the last portion of Chapter 5.

The influence of the contrast between the system components is reflected fully in the resulting fundamental frequency values:

$$\omega_1 = \sqrt{\frac{k_{pf}}{M_{pf}}}$$
$$\omega_2 = \sqrt{\frac{k_l}{M_s}}$$

(6-1)

Note that the first frequency, ω_1, is influenced only by the plate-fluid subsystem. The impact mass has no effect on ω_1. Whereas, the second frequency, ω_2, is affected only by the impact mass and the local contact conditions. There is no influence from the ice thickness or global E value on ω_2. These particular influences may be visually observed in Figures 6-6 and 6-7 for ω_1 and ω_2, respectively. Note that there is also an extreme difference in these two frequency ranges. Where one cycle of ω_1 will take multiple minutes to hours for completion, a cycle of ω_2 is complete within a fraction of a second.

The mode shapes also reflect the influence of these contrasts:

$$\beta_1 = 1$$
$$\beta_2 = -\frac{M_{pf}}{M_s}$$

(6-2)
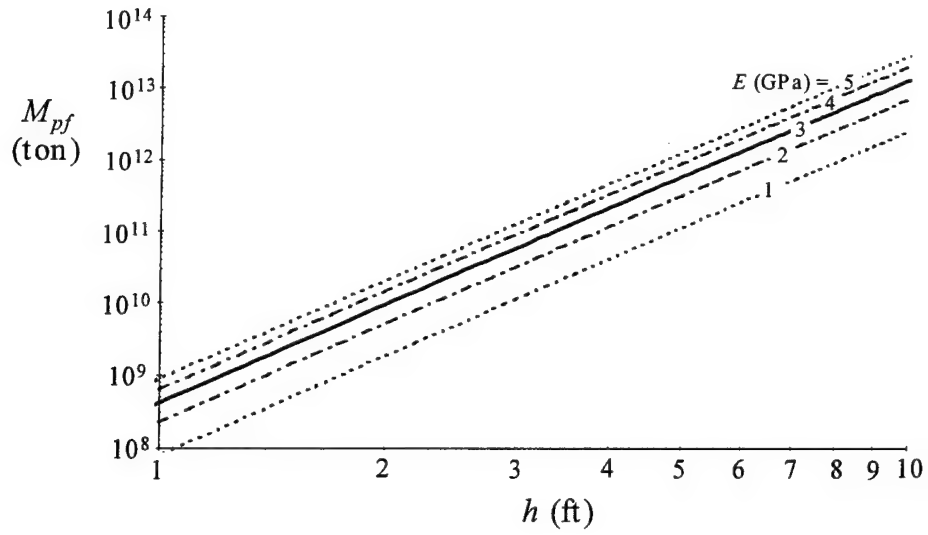
Figure 6-4. The Effective Mass Range for the Plate-fluid System.
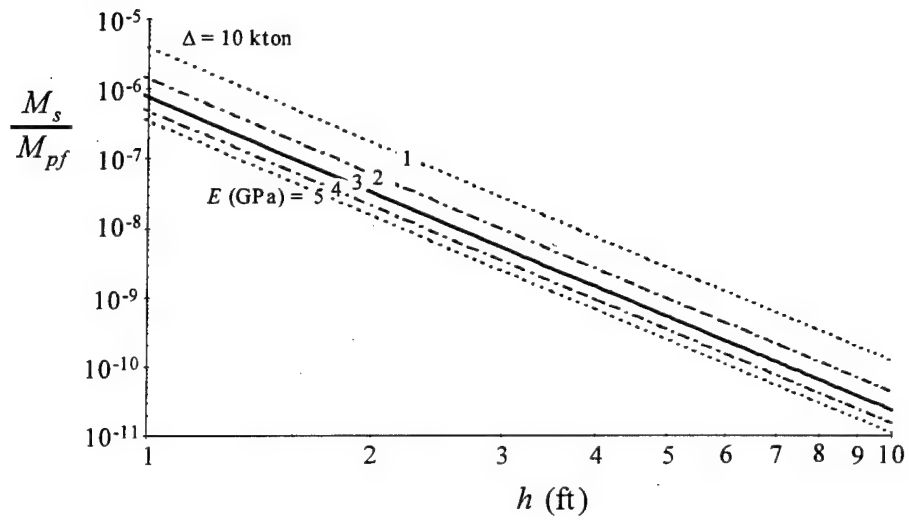
Figure 6-5. Comparison of a Potential Submarine Mass to the Plate-fluid Mass.

$$\omega_1 = \sqrt{\frac{k_{pf}}{M_{pf}}}$$

(hertz)
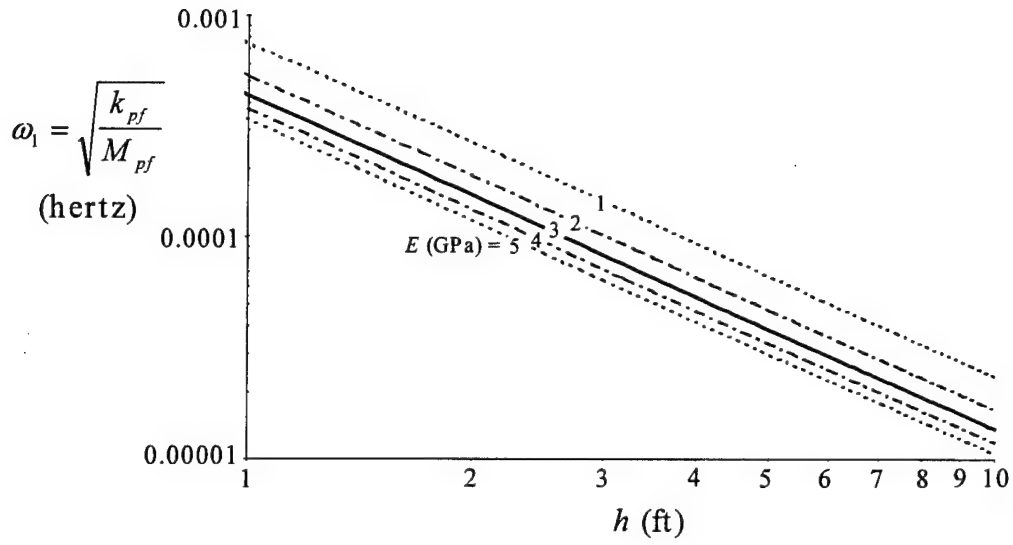
Figure 6-6. The Range of the First Fundamental Frequency.

$$\omega_2 = \sqrt{\frac{k_l}{M_s}}$$

(hertz)
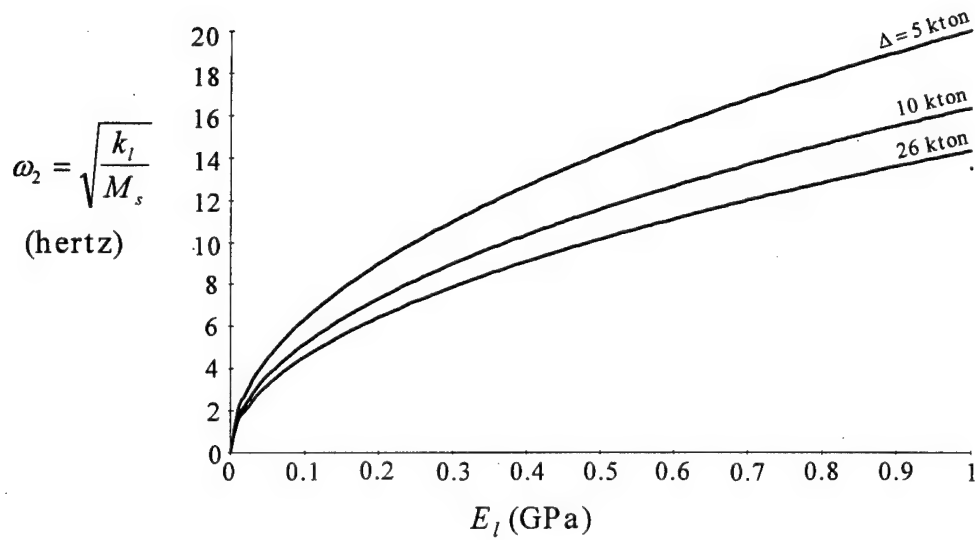
Figure 6-7. The Range of the Second Fundamental Frequency.

The simplifications of ω_1, ω_2, β_1, and β_2, as a result of these component contrasts, lead to more compact expressions for the impact forces as follows:

$$P_{pf} = F_b\left(1 - \cos \omega_1 t\right) - F_b \frac{k_{pf}}{k_l} \frac{M_s}{M_{pf}}\left(1 - \cos \omega_2 t\right)$$

$$+ V_i M_s \sqrt{\frac{k_{pf}}{M_{pf}}}\left(\sin \omega_1 t\right) - V_i k_{pf} \frac{M_s}{M_{pf}} \sqrt{\frac{M_s}{k_l}}\left(\sin \omega_2 t\right) \qquad (6\text{-}3)$$

$$P_s = F_b\left(1 - \cos \omega_2 t\right) + V_i \sqrt{k_l M_s}\left(\sin \omega_2 t\right)$$

These equations have been presented in the manner above, such that a certain interpretation could be made of the transient terms and their respective load amplitudes. Note that there are four different transient terms in total, these are:

1. $(1 - \cos \omega_1 t)$
2. $(1 - \cos \omega_2 t)$
3. $(\sin \omega_1 t)$
4. $(\sin \omega_2 t)$

Since there is such a marked difference between ω_1 and ω_2, the influence of these particular transient terms will also be different, as shown in Figure 6-8.

Figure 6-8. One Cycle of Each of the Transient Terms.

Associated with each of the transient terms is a load amplitude as noted. These factors will dictate the effect that each of the transient terms will have on the maximum value of each perspective impact force. The notation A_{xn} will be assigned to each of the amplitudes, where x refers to either p or s symbolizing the perspective impact force, and n refers to 1, 2, 3, or 4 indicating the specific transient term.
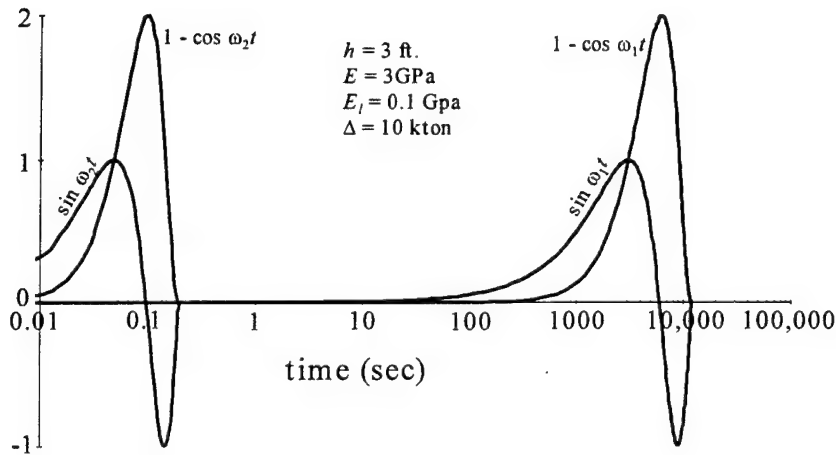
The effect that each of the 4 transients has on the impact load imparted globally on the plate-fluid system may be observed by the amplitude that is associated with each, as shown in Figure 6-9. Each of the amplitudes in the figure is nondimensional due to the buoyancy force. It is obvious from the respective ranges that the only influence on P_{pf} is the buoyancy force of the impacting submarine. Thus, the expression for P_{pf} may be simplified to:

$$P_{pf} = F_b\left(1 - \cos \omega_1 t\right) \tag{6-4}$$

This expression eventually returns a maximum value for $P_{pf(\text{max})} = 2F_b$.
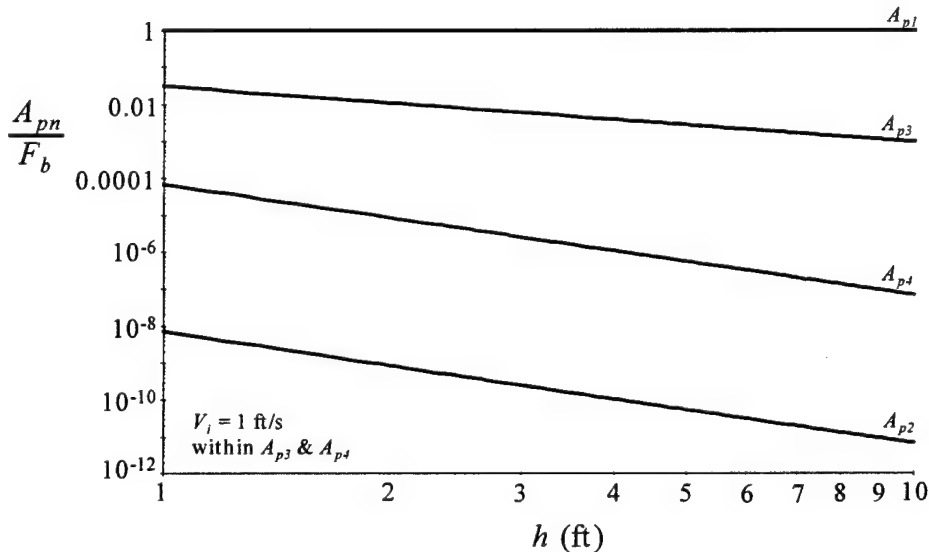
Figure 6-9. Load Amplitude Ranges for P_{pf}.

The same comparison may be made for the load amplitudes that influence the impact force directly imparted on the submarine. However, where the amplitudes for P_{pf} were influenced by the range of ice thickness, the load amplitudes effecting the transient terms remaining in the expression for P_s are influenced by the local Young's modulus, E_l, the mass of the submarine, M_s, and the impact velocity, V_i. Figure 6-10 illustrates the influence of these two load amplitudes.
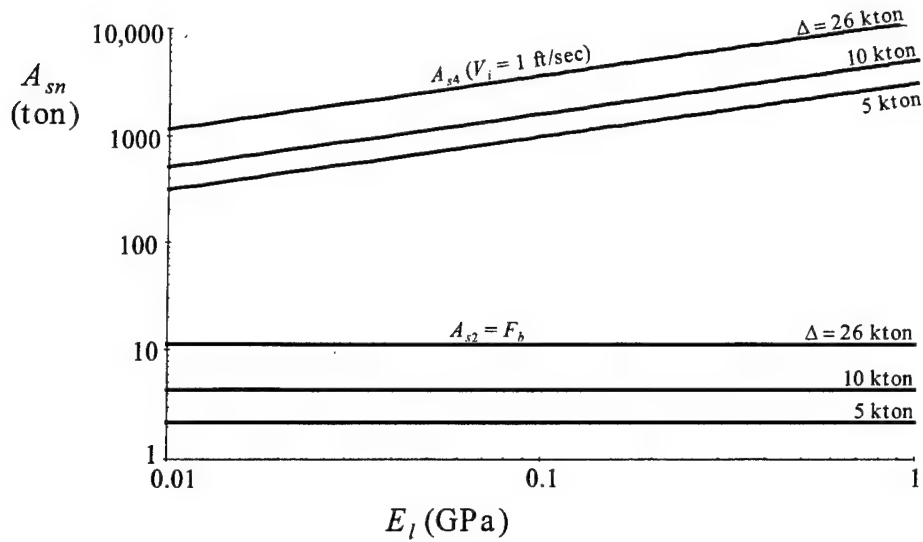
Figure 6-10. Load Amplitude Ranges for P_s.

The effect of the impact velocity is linear on the upper curves, where the lower curves are simply the buoyancy force of the submarine. However, the vast difference between these two sets of load amplitude ranges clearly indicates that the expression for P_s may also be simplified. Figure 6-11 further emphasizes the difference found between the two transient terms in P_s. Therefore, P_s may now be found by:

$$P_s = V_i \sqrt{k_l M_s} \left(\sin \omega_2 t \right) \qquad (6\text{-}5)$$

This expression returns a maximum value for $P_{s(\max)} = V_i \sqrt{k_l M_s}$.
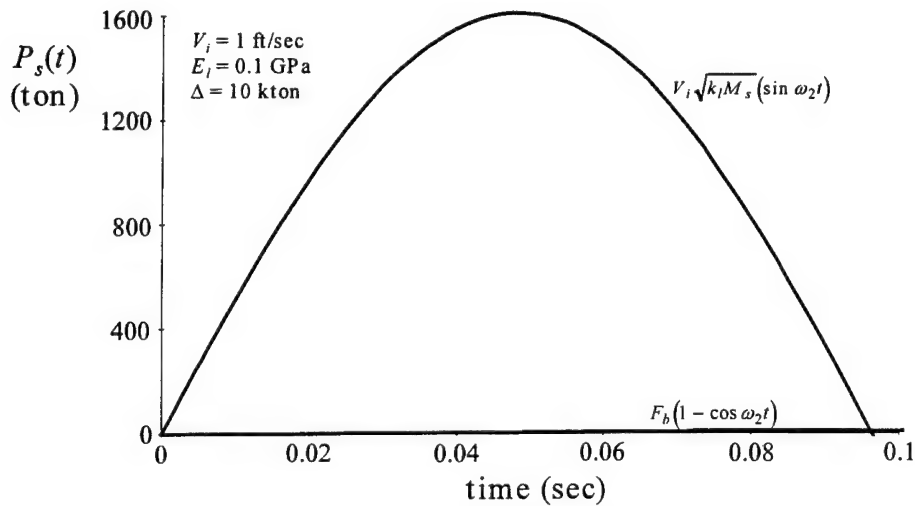
Figure 6-11. Example of the Time-load History for the Impact Structure.

A comparison may now be made of the simplified 2 degree-of-freedom formulation to those from the inelastic collision and to the local crushing incorporating the linear approximation. After incorporating all the same simplifications to the two one degree-of-freedom systems, the formulations are identical to the respective two degree-of-freedom systems. Thus, the only remaining comparison to be made is between the two different local crushing solutions.

Comparison of the Local Crushing Formulations

A comparison of the maximum value obtained for the impact load imparted on both the submarine and locally on the ice plate is shown in Figure 6-12. This Figure shows that, although the same sort of trends appear in both the linear approximation and the Hertz contact solution, the load is consistently less for the Hertz value.

The influence of this local crushing on the underside of the ice plate, itself, is more concisely shown with the maximum deformation, $\alpha_{(mas)}$, occurring into the plate, as shown in Figure 6-13. In this figure, the Hertz contact values are much larger than those found with the linear approximation. However, the deformations are still extremely low in consideration of a multiple foot ice thickness.
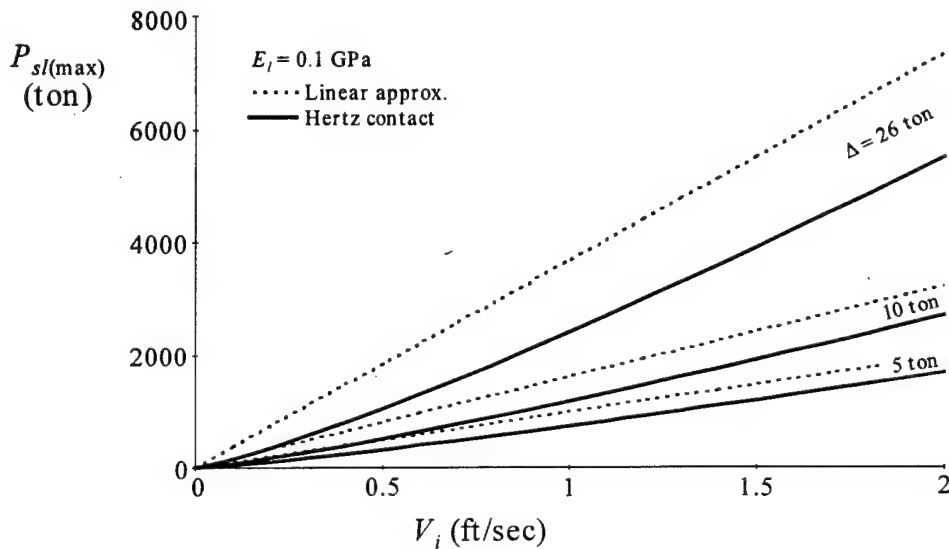
Figure 6-12. Comparison the Maximum Impact Load Obtained by Hertz Contact vs Linear Approximation.
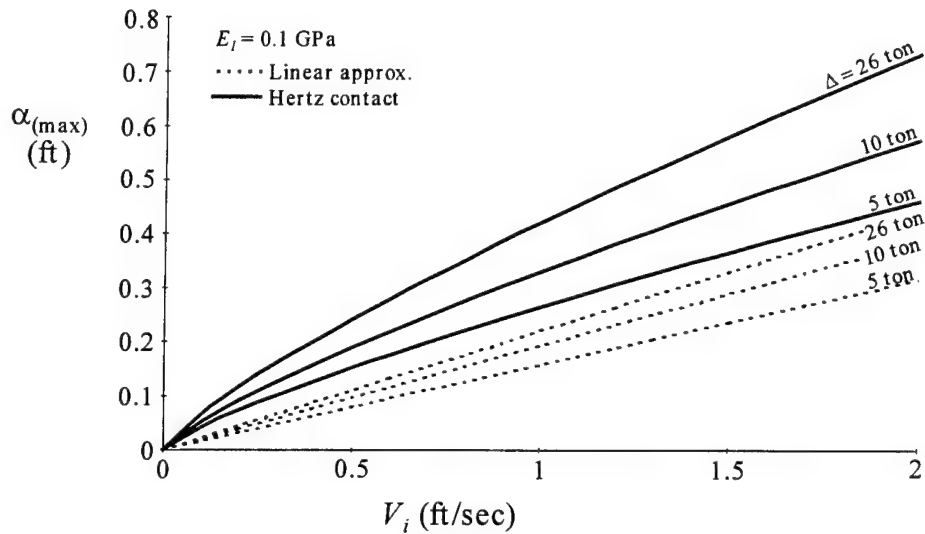
Figure 6-13. Comparison of the Maximum Plate Deformation Obtained by Hertz Contact vs. Linear Approximation.

A final comparison with the fundamental frequency, ω_l, for each of these two formulations will be made to indirectly ascertain the possible influence that the Hertz contact would have on a two degree-of-freedom system. Note that, for the linear approximation, $\omega_l = \omega_2$. A visual comparison is provided in Figure 6-14, showing a range of the frequency with respect to E_l. The frequency associated with the Hertz solution is lower than ω_2. However, the action takes place in a fraction of a second, which is extremely faster than ω_1.
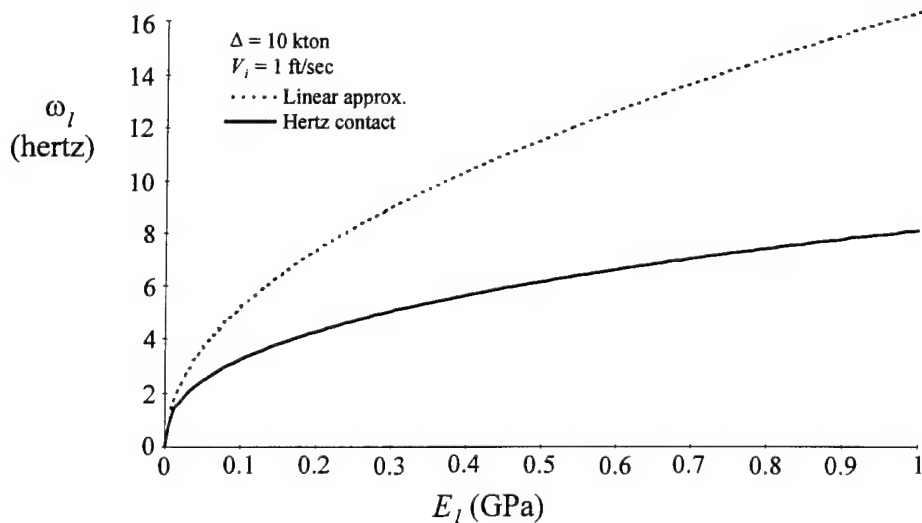
Figure 6-14. Comparison of the Fundamental Frequency Obtained by Hertz Contact vs. Linear Approximation.

The Hertz contact provides an effectively softer spring than does the linear approximation, thus leading to smaller impact loads and larger deformations. However, this effect would not overcome the extreme contrast in the submarine mass to the plate-fluid mass, especially in an ice thickness exceeding 1 ft. Therefore, the effective expression for P_{pf} (6-4) remains valid despite the disparity found between the two methods of modeling the local crushing effect.

Parametric Conclusions

The only influence on the impact force imparted globally on the plate-fluid subsystem, P_{pf}, is the buoyancy force of the impacting submarine. However, the maximum value for the both the impact load imparted directly to the submarine and the ice plate deformation is influenced by the 5 parameters listed in Table 6-5. This list indicates the effective power that is associated with each of the parameters within the determination of either the impact load or local deformation. There is not a specific power of influence associated with ν, however, the difference between using a value of 0.5 as opposed to 0.33 is less than 10%.

Table 6-5. Effective Power Associated with the Local Contact Parameters.

Parameter	$P_{H(max)}$	$\alpha_{H(max)}$
V_i	6/5	4/5
M_s	3/5	2/5
E_l	2/5	-2/5
R_s	1/5	-1/5
ν	N/A	N/A

Both the initial velocity and submarine mass influence the impact load slightly more than the deformation; however, both directly relate to an increase or decrease. The initial velocity influence is slightly more than linear upon the impact load and slightly less than linear in determining the deformation. The submarine mass effect is slightly greater than a square root on the impact load and slightly less than a square root on the deformation.

Both E_l and R_s provide opposite effects on the impact load as on the deformation. An increase in either one will increase the impact load, however, that same increase will decrease the deformation. Thus, for the initial impact to cause greater damage to the ice with less load imparted on the submarine, E_l and R_s should both be decreased.

·· The Young's modulus values that are found on the underside of the ice plate are not constant. There is a huge variation of E_l in this area and an "effective" value may not do justice to the accuracy of obtaining either an impact load on the submarine or deformation the underside of the ice. The typical value used in all the numerical calculations probably provides a very conservative result for both the impact load and the ice plate deformation. A more accurately modeled value for this parameter would most likely soften the local crushing effect, thus, providing a smaller impact load on the submarine with greater deformation imparted on the underside of the ice.

Chapter 7

Conclusions

This dissertation has characterized the influence of various parameters on the structural dynamics of a floating ice sheet due to the initial impact of a large mass. The most obvious conclusion is that the fluid inertia influence completely dominates the dynamic behavior of the ice plate. The huge disparity between the two masses, due entirely to the "added mass" of the fluid inertia, effectively splits the *two* degree-of-freedom spring-mass system into two separate *one* degree-of-freedom systems. Each of these systems provides solutions for different issues of the study.

An inelastic collision between the effective plate-fluid mass and that of the impact structure, a submarine, expresses the global impact loading that will effect the general bending of the ice plate; whereas, the influence of the local crushing deformation on the underside of the ice plate defines the impact load that will be imparted on the submarine. Note that this local deformation may also help define the amount of initial damage that is imparted on the ice due to the impact. Both of these results are valuable in generally characterizing the effect that an initial impact has upon both the submarine and the ice plate.

The global impact load on the ice plate was found to be 2 F_b, regardless of any other factor. This is twice the amount of net buoyancy realized to attain an upward velocity and will most likely be a relatively small value. In addition, the time between the impact and maximum response is on the order of hours for an ice thickness exceeding 2 ft. Note that this load is basically the equivalent of a static load that would bring about the maximum displacement. This load is directly associated with the pure bending behavior of the plate as a result of the impact. Where the failure mechanism of the ice plate during an ice-surfacing maneuver is governed by bending, the initial impact will most likely have little effect on the result. Therefore, the general conclusion is that, with regard to the global impact result, an initial impact has no influence on the eventual penetration of the ice plate, especially for an ice thickness exceeding 2 ft.

The impact load that is imparted directly on the submarine is also a localized load on the underside of the ice plate. Thus, two specific results need to be considered when reviewing this loading: the magnitude of the impact load on the submarine and the amount of deformation imparted on the underside of the ice plate.

The results addressed will be solely those associated with the Hertz contact solution in the interest of clarity. The linear approximation served a major role in primarily facilitating a formulation for the two degree-of-freedom system and secondarily providing a step in the indirect comparison of that system to the solitary local contact solution. The Hertz contact provides an effectively softer spring than does the linear approximation, thus, leading to smaller impact loads and larger deformations. However, this effect would not overcome the extreme contrast in the submarine mass to the plate-fluid mass, especially in an ice thickness exceeding 1 ft.

Both the initial velocity and submarine mass influence the impact load slightly more than the deformation; however, both directly relate to an increase or decrease. The initial velocity influence is slightly more than linear upon the impact load and slightly less than linear in determining the deformation. The submarine mass effect is slightly greater than a square root on the impact load and slightly less than a square root on the deformation.

Both the local Young's modulus, E_l, and spherical radius of contact, R_s, provide an opposite effect on the impact load as on the deformation. An increase in either one will increase the impact load, however, that same increase will decrease the deformation. Thus, for the initial impact to cause greater damage to the ice with less load imparted on the submarine, E_l and R_s should both be decreased.

Impact load magnitudes on the submarine appear to be substantial with respect to the parametric ranges provided for this study, especially considering that there may be no benefit toward final penetration. The specific values for an initial impact velocity of 30 fpm range from 320 ton to 1046 ton for submarines with displacements of 5 to 26 kton, respectively. These amounts were obtained with $E_l = 0.1$, where a tenth of this value would lessen the impact load by 0.4 or an increase of 10 times would increase the values by a factor of 2.5. Another aside is that a sharper or smaller R_s will decrease these impact loads while increasing the deformation imparted on the underside of the ice plate.

The amount of deformation into the plate will serve to indicate how much this loading will influence the eventual penetration. The deformation values that obtained in this study are only in the range of a couple of inches. Compared to an ice plate with a thickness greater than 2 ft, this deformation range is less than 10% of the total and may not affect the overall ice strength. A more detailed study involving the shear effects of the plate would be required at the very least to ascertain the actual effect this magnitude of deformation would have toward complete penetration.

The Young's modulus values that are found on the underside of the ice plate are not constant. There is a huge variation of E_l in this area and an "effective" value may not do justice to the accuracy of obtaining either an impact load on the submarine or deformation the underside of the ice. The typical value used in all the numerical calculations probably provides a very conservative result for both the impact load and the ice plate deformation. A more accurately modeled value for this parameter would most likely soften the local crushing effect, thus, providing a smaller impact load on the submarine with greater deformation imparted on the underside of the ice.

The final conclusions of this study are that the global impact load on the ice plate is not going to have an effect on the flexural failure mechanism that may define the requirements to penetrate a floating ice sheet. The initial impact imparted on the submarine could be seen as a substantial load to that structure, where an increase in velocity will only increase that load by a 6/5 power. The deformation imparted on the ice due to an initial impact does not appear to be substantial, especially when compared to an ice thickness that exceeds 2 ft. All in all, the relative advantage of an initial impact is not ascertained with respect to the range of values used in this study.

References

Ackermann, N.L. and A. Arbhabhirama [1964] Viscous and boundary effects on virtual mass. *J. Eng. Mech. Div., Am. Soc. Civil Engrs*. 90, EM4, p. 123-130.

Assur, A. [1962] Surfacing Submarines Through Ice. *Proceedings of the 1962 Army Science Conference*, U.S.Military Academy, West Point, N.Y., 20-22 June 1962. Washington, D.C., [U.S.] Army Research Office, Vol. I, p. 11-20.

Assur, A. [1967] Flexural and other properties of sea ice sheets. Proceedings Physics of snow and ice: international conference on low temperature science, Vol. I, Pt. I. [Sapporo], *Institute of Low Temperature Science*, Hokkaido University, p. 557-67.

Babbitt, F.G. [1970] A Submarine for the Tsar. U.S.Naval Institute *Proceedings*, April, p. 47-55.

Bedel, John and Jerome Feldman [1991] Investigation of the motions of the SSN 751 submarine after impact with ice from free-running model experiments. DTRC, Ship Hydromechanics Departmental Report, 0386-122, p. 6.

Bernshteyn, S. [1929] Ledyanaya zheleznodorozhnaya pereprava [The railway ice crossing]. *Trudy Nauchno-Tekhnicheskeogo Komiteta Narodnogo Komissariata Putei Soobshcheniya*, Tom 84, p. 36-82.

Birkhoff, G. [1950] *Hyrodynamics, a study in logic, fact and similitude*. Princeton University Press, p. 151-154.

Blevins, Robert D. [1979] *Formulas for Natural Frequency and Mode Shape*. p. 415.

Boresi, Arthur P., Omar M. Sidebottom, Fred B. Seely, and James O. Smith [1978] *Advanced Mechanics of Materials*. Third Ed., John Wiley & Sons, Inc., p. 405.

Bourke, R.H. and Garrett, R.P. [1987] Sea Ice Thickness Distribution in the Arctic Region. *Cold Regions Science and Technology*, 13(3): p. 259-280.

Calvert, CDR James F. [1959] Up Through the Ice of the North Pole. *The National Geographic Magazine*, Vol. CXVI, No. 1, p. 1-41, July.

Conway, Harry D. [1956] The pressure distribution between two elastic bodies in contact. *Zeitschrift für angewandte Mathematik und Physik*, Vol. 7, p. 460-465.

Cox, G.F.N., and W.F.Weeks [1986] On the profile properties of undeformed first-year sea ice. *Second Workshop on Ice Penetration Technology*, Naval Postgraduate School, Monterey, CA, CRREL Special Report 86-30, p. 257-330.

Craig, Roy R. Jr. [1981] *Structural Dynamics*. John Wiley & Sons, Inc., p 217.

Dane, Abe [1993] Ice Station X. *Popular Mechanics*, November, pp. 30-34, 132.

Dempsey, J.P., Z.G.Zhao, L.Minnetyan, and H.Li [1990] Plane contact on an elastic layer supported by a Winkler foundation. *Journal of Applied Mechanics*, Vol. 57, No. 4, p. 974-980.

Dempsey, J.P. and Z.G.Zhao [1992] Elastohydrodynamic response of an ice sheet to forced sub-surface uplift. *Journal of the Mechanics and Physics of Solids*, Vol.?.

Gabler, Ulrich [1986] *Submarine Design*. Bernard & Graefe Verlag, Koblenz.

Gellman, Barton [1992] The 'Silent Service' Breaks the Ice; Submariners Test Waters for New Role as Soviet Threat Dries Up. *The Washington Post*, 19 April. p.A1.

Getler, Michael [1982] Lehman Sees Norwegian Seas as a Key to Soviet Naval Strategy. *The Washington Post*, 29 December, p.4.

Goldsmith, Werner [1960] *Impact*. Edward Arnold Ltd., London, p. 82-91.

Gossett, J. [1996] Arctic Research Using Nuclear Submarines. *Sea Technology*, March, p. 33-40.

Hentényi, [1946] *Beams on Elastic Foundation*. University of Michigan Studies, Scientific Series, XVI.

Hertz, H. [1884] Über das Gleichgewicht schwimmender elastischer Platten. Wiedemann's Annalen der Physik und Chemie, Vol. 22, pp. 449-55. [English translation: "On the equilibrium of floating elastic plates," in Miscellaneous papers by H. Hertz. London, MacMillan, 1896, p. 266-72.]

Holl, D.L. [1950] Dynamic loads on thin plates on elastic foundations. *Proceedings 3rd AMS Symposium in Applied Mathematics*, McGraw-Hill, New York, N.Y., III, p. 107-116.

Hutter, K. [1974] Significance of Poisson's ratio for floating sea ice. *Mitteilung der Versuchsanstalt für Wasserbau*, Hydrologie und Blaziologie, ETH Zurich.

Jane, Fred T. [1989/90] *Jane's Fighting Ships*. Edited by Richard Sharpe, Jane's Information Group Inc., Alexandria, Virginia.

Jordan, John [1989] *Soviet Submarines*. Arms & Armour Press, London.

Kennedy, John B. and K.J.Iyengar [1981] Rigid-plastic analysis of floating ice sheets under impact loads, *Canadian Journal of Civil Engineering*, Vol. 8, p. 409-415.

Kerr, A.D. and W.T. Palmer [1972] The deformations and stresses in floating ice plates. *Acta Mechanica*, Vol. 15, Nos. 1-2, p. 57-72.

Kerr, A.D. [1976] The bearing capacity of floating ice plates subjected to static and quasi-static loads. *Journal of Glaciology*, Vol. 17, no. 76.

Kheisin, D.Y. [1967] Dynamics of the Ice Cover. Gigrometeorolicheskoe, Izdat-et'stvo, Leningrad (U.S. Technical Translation FSTC-HT-458-69)

Kobeko, P.P., N.I.Shishkin, F.I.Marey, and N.S.Ivanova [1946] Prolom I gruzopod"yemnost' l'da [The break-through and carrying capacity of a floating ice cover] *Zhurnal Tekhnicheskoy Fiziki*, Tom 16, No. 3, p. 273-76.

Lake, R.A. and E.L.Lewis [1970] Salt rejection by sea ice during growth. *Journal of Geophysical Research*, 75(3), p. 583-597.

Lamb, H. [1921] On the vibrations of an elastic plate in contact with water. *Proc. Royal Soc.* (London), Series A 98, p. 205-216.

Likhomanov, V.A. and D.E.Kheisin [1971] Experimental investigation of solid body impact on ice. *Problemy Arktiki I Antarktiki*, Vol. 38, p105-111.

Lyon, W.K. [1952] An Approach to Submarine Warfare in Sea Ice. Report 353, U.S.Navy Electronics Laboratory, San Diego, CA.

Lyon, W.K. [1959] Polar Submarine and Navigation of the Arctic Ocean. Report 88, U.S.Navy Electronics Laboratory, San Diego, CA.

Lyon, Waldo K. [1984] The Navigation of Arctic Polar Submarines. *Journal of Navigation*, Royal Institute of Navigation, May, vol. 37, no. 2, p. 155-179.

Lyon, Waldo K. [1992] Submarine Combat in the Ice. Naval Institute *Proceedings*, February 1992, p. 33-40.

Marguerre, K., and Hans-Theo Worrnle [1969] *Elastic Plates*. Blaisdell, Division of Ginn, Waltham, Mass.

McConnell, K.G. and D.F.Young [1965] Added mass of a sphere in a bounded viscous fluid. *J. Eng. Mech. Div.*, Am. Soc. Civil Engrs. 91, EM4, p 147-164.

McGilvary, W.R., D.S.Sodhi, and J.H.Lever [1990] Dynamic analysis of a floating ice sheet undergoing vertical indentation. *Proceedings 9th International OMAE Conference*, Houston, Texas, IV, p. 195-203.

McLachlan, N.W. [1932] The accession to inertia of flexible discs vibrating in a fluid. *Proc. Phys. Soc.* (London) 44, p. 546-555.

McLaren, Captain Alfred S. [1981] Under the Ice in Submarines. Naval Institute *Proceedings*, July, p. 105-109.

McLaren, A.S. [1989] The under-ice Thickness Distribution of the Arctic Basin as recorded in 1958 and 1970. *Journal of Geophysics Research*, 94(C4): p. 4971-4983.

Mintz, John [1993] Sweating Out The 'Sunburn'; U.S. Firms Seek Deals With Russia, Ukraine for Missile Pentagon Wants. *The Washington Post*, 13 June, p. H1.

Murat J.R. and L.M.Lainey [1982] Some experimental observations on the Poisson's ratio of sea-ice. *Cold Regions Science and Technology*, Vol. 6.

Naval Undersea Center, Arctic Submarine Laboratory (NUC, ASL) [1974] Submarine Arctic Operation. San Diego, CA.

Neidraur, T.M. and S.Martin [1979] An experimental study of brine drainage and convection in young sea ice. *Journal of Geophysical Research*, 84 (C3), p. 1176-1186.

Nevel, D.E. [1970] Vibration of a floating ice sheet. CRREL Research Report 281, Hanover N.H.

Newman, M. and M.Forray [1962] Thermal stresses and deflections in thin plates with temperature dependent elastic modulus. *Journal Of Aerospace Sciences*, Vol. 29, No. 3, p. 372-73.

ONI Review [1951] German U-Boats in the Arctic.

Panfilov, D.F. [1960] Priblizhennyy mehod rascheta gruzopod"yemnosti ledyanogo pokrova [Approximate method to analyze the bearing capacity of an ice cover] *Izvestiya Vsesoyuznogo Nauchno-Issledovatel'skogo Instituta Bidrotekhniki*, Tom 65, p. 221-24.

Panfilov, D.F. [1961] K raschetu gruzopod"yemnosti ledyanogo pokrova pri stoyanke gruzov na l'du [On the determination of the carrying capacity of an ice cover for loads of long duration] *Izvestiya Vysshikh Uchebnykh Zavedeniy Ministerstva Vysshego i Srednego Spetsial'nogo Obrazovaniya SSSR.* Stroitel'stvo i Arkhitektura, No. 6, p. 47-57.

Panfilov, D.F. [1960] Raschet nesushchey sposobnosti ledyanogo pokrova s uchetom neodnorodnosti yego po tolshchine [Analysis of the bearing capacity of an ice cover taking into consideration its nonhomogeneity with thickness*]* *Izvestiya Vysshikh Uchebnykh Zavedeniy Ministerstva Vysshego i Srednego Spetsial'nogo Obrazovaniya SSSR.* Stroitel'stvo i Arkhitektura, No. 2, p. 3-8.

Peake, W.H. and E.G.Thurston [1954] The lowest resonant frequency of a circular plate. *J. Acoust. Soc. Am.*, vol. 26, p. 166-168.

Polmar, Norman [1984] The U.S. Navy: Sailing Under the Ice. Naval Institute *Proceedings*, June, p. 121-123.

Polmar, Norman [1986] The Soviet Navy: The Submarine Enigmas. Naval Institute *Proceedings*, January, p. 128-129.

Polmar, Norman [1991] The U.S. Navy: Submarines in Ice. Naval Institute *Proceedings*, August, p. 105-106.

Polmar, Norman [1993] *The Naval Institute Guide To The Ships And Aircraft Of The U.S. Fleet.* Fifteenth Ed., Naval Institute Press, Annapolis, Maryland.

Rayleigh, Lord [1906] On the Prediction of Vibrations by Forces of Relatively Long Duration, with Application to the Theory of Collisions. *Philosophical Magazine*, Series 6, Vol. 11, p. 283-292.

Reismann, H. and Y.C.Lee [1968] ?. Journal of Hydronautics, Vol. 2, p. 108.

Rockwell, Theodore [1992] *The Rickover Effect: How One Man Made a Difference.* Naval Institute Press, Annapolis, MD, p. 245-255.

Ross, Bernard [1969] Perforation of the Arctic sea-ice cover by projectile impact. *Journal of Hydronautics*, Vol. 3, No. 3, July.

Sears, Zemansky, and Young [1977] *University Physics.* Fifth Ed., Third Printing, Addison-Wesley Publishing Company, Inc. Philippines.

Shivakumar, K.N., W.Elber, and W.Illg [1985] Prediction of impact force and duration due to low-velocity impact on circular composite laminates. *Transactions of the ASME*, Vol 52, p. 674-680.

Sodhi, D.S. [1989] Interaction forces during vertical penetration of floating ice sheets with cylindrical indenters. *Proceedings 8th International OMAE Conference*, The Hague, The Netherlands, IV, p. 377-382.

Stelson, T.E. and F.T.Mavis [1955] Virtual mass and acceleration in fluids. *Proc. ASCE 81*, p. 670-1-670-9.

Streeter, Victor L. and E.Benjamin Wylie [1979] *Fluid mechanics*. Seventh ed., McGraw-Hill Book Company, p. 311-313.

Strutt, John W., Lord Rayliegh [1937] *Theory of Sound*. Vol. 1, 2nd Rev. Ed., New York: Dover Publications, p. 109-110.

Thomson, William T. [1981] *Theory of Vibration with Applications*. Second Ed., Prentice-Hall, Inc., Englewood Cliffs, N.J.,

Timco, G.W. and R.M.W.Frederking [1993] Laboratory impact tests on freshwater ice. *Cold Regions Science and Technology*, Vol. 22, p. 77-97, Elsevier Science Publishers B.V., Amsterdam.

Timoshenko, S.P. and J.N.Goodier [1951] *Theory of Elasticity*. McGraw-Hill Book Company, New York, p. 108.

Timoshenko, S. and S. Woinowsky-Krieger [1959] *Theory of Plates and Shells*. 2nd ed. McGraw Hill, New York, N.Y.

Tunik, Alfred L.[1994] Route-Specific Ice Thickness Distribution In The Arctic Ocean During A North Pole Crossing In August 1990. *Cold Regions Science and Technology*, 22: p. 205-217.

Ugural, A.C. [1981] *Stresses in Plates and Shells*. McGraw-Hill, Inc., p 22, 43.

Vlasov, V.Z. and U.N.Leont'ev [1960] Balki, plity I obolochki na uprugom osnovanii (Beam, plates and shells on elastic foundations) *Gosudarstvennoe Izdatel'st vo Fiziko-Matematicheskoi Literatury, Moskva*. Translated from Russian, Israel Program for Scientific Translations, Jerusalem, 1966.

Welsh, James P., et al [1986] A Compendium of Arctic Environmental Information. Naval Ocean Research and Development Activity, Report 138, March.

Wen, T., et al [1989] Environmental measurements in the Beaufort sea, spring 1988. APL-UW TR 8822, Applied Physics Laboratory, University of Washington, Seattle.

Wendel, K. [1950] Hydodynamische massen und hydrodynamische massentrapheitmomente. Jahrbuch Schiffbautechnisches Gesellschaft 44, p 207. (Available in English as, Wendel, K., Hydrodynamic masses and Hydrodynamic moments of inertia. David Taylor Model Basin Translation No. 260.)

Wilkins, H. [1931] *Under the North Pole*. New York: Brewer, Warren & Putnam.

Winkler, E. [1867] Die lehre von der Elastizität and Festigkeit, Praga Dominicus.

Wyman, M. [1950] Deflections of an infinite plate. *Canadian Journal of Research*, Ser. A, Vol.28, p. 293-302.

Zhao, A.G. and J.P.Dempsey [1990] Low-velocity rigid sphere vertical impact on a floating ice sheet. *Proceedings of the Tenth International Association for Hydrodynamic Research Symposium on Ice*, Espoo, Finlan, August.

Zubov, N.N. [1942] Osnovy ustroystva dorog na ledyanom pokrove [The basis of road construction on the ice cover] Moscow, Gidrometeoizdat.

Zubrin, Robert [1983] What Ever Happened to Our Nuclear Merchant Marine? Naval Institute *Proceedings*, August, pp. 119-121.

Nomenclature

a	Radius of an finite plate
a_d	Radius of the circular contact area for a linear approximation to contact stiffness
A_{pn}	Load amplitude for transient terms ($n = 1, 2, 3, 4$) of P_{pf} expression (5.3)
A_{sn}	Load amplitude for transient terms ($n = 2, 4$) of P_s expression (5.3)
A_s	Amplitude of r_{eff} to distribute hemispherical volume of fluid mass by each individual shape function
A_v	Amplitude of vibration in given direction relative to the plate
B_s	Amplitude constant of l for inclusion of the added mass due to fluid inertia determined for each individual shape function
$\cos(x)$	Trigonometric function cosine of x
D	Flexural rigidity of the ice plate
e	Base of the natural system of logarithms (2.71828…)
e_c	Eccentric distance from the mass center to the impact point
E	Young's modulus of sea ice
E_{av}	Averaged Young's modulus of sea ice
E_b	Energy due to bending deformation of the plate
E_c	Energy due to contact deformation of the plate underside
E_{eff}	Effective Young's modulus of sea ice
E_K	Kinetic energy
E_{Kf}	Kinetic energy of the fluid
E_{Kp}	Kinetic energy of the ice plate
E_{Ks}	Kinetic energy of the impact structure
E_l	Local Young's modulus from the underside of the ice plate
E_p	Potential energy
E_{ps}	Potential energy of the impact structure
$E(z)$	Young's modulus as a function of the transverse axis z
F_b	Buoyancy force of impact structure
g	Acceleration due to gravity

Nomenclature (continued)

h	Thickness of the ice plate
$\mathrm{Im}(x)$	Imaginary portion of x
i	square root of -1
$J_o(x)$	Bessel function of x
k	Modulus of the foundation
$\mathrm{kei}(x)$	Kelvin function of x, a modified Bessel function
k_l	Spring stiffness associated with the local crushing deformation
k_{ls}	Effective spring stiffness of the impact structure and local contact
k_{pf}	Spring stiffness associated with the plate and fluid together
k_s	Spring stiffness associated with the impacting structure
K	Hertz material parameter incorporated in the stiffness parameter
K_l	K value for plate underside material properties
K_s	K value for impact structure contact area.
l	Characteristic length of the floating ice plate
L	Half length of a finite beam
m_f	Equivalent mass magnitude added due to fluid inertia
M_a	Failure moment
M_{end}	Moment at the end of a finite beam
M_{eff}	Effective mass
M_f	Added mass due to the fluid inertia
M_o	Moment at the origin of the beam
M_p	Plastic moment
M_{pf}	Effective mass of the plate and fluid together
M_s	Mass of the impacting structure
P	Concentrated lateral load
P_a	Allowable load
P_{cr}	Load at which the first crack occurs in the ice plate
P_f	"break-through load" for the ice plate
P_{pf}	Impact force imparted globally on the plate-fluid system
P_s	Impact force imparted on the impact structure
$P_{sH(max)}$	Maximum impact force imparted on the impact structure found by Hertz contact
P_{sl}	Impact force imparted on the impact structure found by a linear approximation of the local contact deformation
$P(w)$	Load as a function of transverse displacement

Nomenclature (continued)

q	Laterally distributed force
r	Radial (horizontal) distance from the center of an infinite plate
r_{eff}	Effective radius of the infinite plate
r_p	Rotational radius of a submarine
R_s	Spherical radius of contact associated with the impact structure
$\mathrm{Re}(x)$	Real portion of x
$\sin(x)$	Trigonometric function sine of x
t	Time
t_f	"time to failure" for P_f
U_f	Strain energy owing to the deformation of the elastic foundation
U_p	Strain energy in the plate
V_d	Velocity of a dropped object
V_{end}	Shear at the end of a finite beam
V_i	initial velocity of the impacting structure at contact with the plate
V_o	Velocity resulting from an inelastic collision
w	Transverse deflection of the ice plate
w_f	Critical deflection
w_o	Maximum vertical plate deformation at the origin
$w(r)$	Vertical plate deformation as function of radius
$w(r,t)$	Vertical plate deformation as function of r and t`
$\dot{w}(r,t)$	First time derivative of $w(r,t)$
W	Work
x	Horizontal distance from the center of an infinite beam
X_a	Constant multiplier for k_{pf} and M_{pf} when considering shape function (3.33a)
X_b	Constant multiplier for k_{pf} and M_{pf} when considering shape function (3.33b)
y	Vertical deflection
y_{end}	Vertical deflection at the end of a finite beam
y_{max}	Maximum vertical deflection at the center of beams
y_p	Displacement of the plate-fluid system
y_{pm}	Maximum displacement of the plate
$\dot{y}_p$	First time derivative of y_p
$\ddot{y}_p$	Second time derivative of y_p
y_{ps}	Displacement of the plate-impact structure amalgam

Nomenclature (continued)

$\dot{y}_{ps}$	First time derivative of y_{ps}
$\ddot{y}_{ps}$	Second time derivative of y_{ps}
y_s	Displacement of the impact structure
$\dot{y}_s$	First time derivative of y_s
$\ddot{y}_s$	Second time derivative of y_s
$Y_o(x)$	Weber's function of x
Y_p	Amplitude of the assumed harmonic solution for y_p
Y_s	Amplitude of the assumed harmonic solution for y_s
z	Vertical distance from the origin of a floating plate
α	Deformation at the contact point of the underside of the ice plate
$\alpha_{H(\max)}$	Maximum deformation defined by a Hertz contact solution at the contact point of the underside of the ice plate
α_l	Local contact deformation defined by a linear approximation of the ice plate underside crushing
$\dot{\alpha}_l$	First time derivative of α_l
$\ddot{\alpha}_l$	Second time derivative of α_l
β	Characteristic of the beam on elastic foundation system
β_1	Mode shape associated with ω_1
β_2	Mode shape associated with ω_2
Δ	Weight displacement of a submarine
ϕ	Potential function of the fluid
γ	Euler's constant (0.5772157)
η	Hertz contact stiffness parameter
$\varphi(z)$	Dimensionless linearly independent function for z-distribution of the vertical displacements
ν	Poisson's ratio
π	3.14159...
ρ_f	Mass density of the fluid foundation
ρ_p	Mass density of the ice plate
σ_f	Flexural strength of ice
$\sigma_{\max}$	Maximum strength of ice
ω_1	First fundamental frequency of a system
ω_2	Second fundamental frequency of a system

Nomenclature (continued)

ω_l Frequency associated with the local contact deformation

ω_n Natural frequency of the axisymmetric plate on an elastic foundation

ω_{Rn} Fundamental frequency approximation found by Rayleigh method

$\omega_{Rn}^{\bullet}$ Fundamental frequency approximation found by Rayleigh method neglecting additional foundation kinetic energy

∇^2 Laplace operator